Naval Surface Warfare Center
Carderock Division
West Bethesda, MD 20817-5700

NSWCCD-61-TR–2006/18 November 2006

Survivability, Structures, and Materials Department

Technical Report

Characterization of Surface Film Growth During Electrochemical Process: Nickel/Nickel Alloys in Seawater

by

A. Srinivasa Rao

NSWCCD-61-TR–2006/18 Characterization of Surface Film Growth During Electrochemical Process: Nickel/Nickel Alloys in Seawater

Naval Surface Warfare Center
Carderock Division
West Bethesda, MD 20817-5700

NSWCCD-61-TR–2006/18 November 2006

Survivability, Structures, and Materials Department
Technical Report

Characterization of Surface Film Growth During Electrochemical Process: Nickel/Nickel Alloys in Seawater

by
A. Srinivasa Rao

This page intentionally left blank

REPORT DOCUMENTATION PAGE

Form Approved
OMB No. 0704-0188

1. REPORT DATE *(DD-MM-YYYY)*	2. REPORT TYPE	3. DATES COVERED *(From - To)*
October 2006	Research and Development	

4. TITLE AND SUBTITLE

Characterization of Surface Film Growth during Electrochemical Process: Nickel/Nickel Alloys in Seawater.

5a. CONTRACT NUMBER

5b. GRANT NUMBER

5c. PROGRAM ELEMENT NUMBER

6. AUTHOR(S)

A. Srinivasa Rao

5d. PROJECT NUMBER

5e. TASK NUMBER

5f. WORK UNIT NUMBER

7. PERFORMING ORGANIZATION NAME(S) AND ADDRESS(ES) AND ADDRESS(ES)

NAVAL SURFACE WARFARE CENTER,
CARDEROCK DIVISION
CODE 612 (METALS ENGINEERING BRANCH)
9500 MACARTHUR BLVD
WEST BETHESDA MD 20817-5700

8. PERFORMING ORGANIZATION REPORT NUMBER

NSWCCD-61-TR-2006/18

9. SPONSORING / MONITORING AGENCY NAME(S) AND ADDRESS(ES)

Electric Power Research Institute, Palo Alto, CA
Office of Naval Research

10. SPONSOR/MONITOR'S ACRONYM(S)

11. SPONSOR/MONITOR'S REPORT NUMBER(S)

12. DISTRIBUTION / AVAILABILITY STATEMENT

Distribution unlimited; approved for public release.

13. SUPPLEMENTARY NOTES

14. ABSTRACT

In order to better understand the formation of films during corrosion processes, an analytical technique using x-ray diffraction was developed to examine the structure of compounds in closest proximity to the metal / liquid interface. The in-situ structure at the metal liquid interface was examined for pure nickel, 90-10 and 70-30 Cu-Ni alloy in seawater solution at room temperature. The nickel-seawater system was investigated at potentiostatically controlled potentials of -800 mV and + 450 mV (versus Ni/NiO). Both the 90-10 Cu-Ni and the 70-30 Cu-Ni alloys seawater systems were investigated at -500 mV, -100 mV, +500 mV and +100 mV versus Ni/NiO. The chemical changes at the metal interface were studied over a period of 48 hours. The inner and outer oxide structure of pure nickel in seawater at -800 mV is NiOOH and $Ni(OH)_2$. Similarly the structure of inner and outer layers at +450 mV (versus Ni/NiO) contains both NiO/Ni_2O_3 and Ni_2O_3. The results for 90-10 Cu-Ni and 70-30 Cu-Ni alloys in seawater indicated that the structure of outer passive layers at -500 mV and -100 mV (versus Ni/NiO), comprises $Ni(OH)_2$, $Cu(OH)_2$, NiOOH and Cu_2O.NiO and the structure of inner passive layer is NiOOH and Cu_2O·NiO. Similarly, the structure of outer interface at + 500 mV and + 100 mV (versus Ni/NiO) contains NiO, Ni_2O_3, Cu_2O·NiO and Ni_2CuO_3; and the inner passive layer contains Cu_2O·NiO and Ni_2CuO_3.

15. SUBJECT TERMS

Electrochemical process	Nickel/Nickel Alloys	Inner passive layer
Outer passive layer	Seawater	XRD and XPS analysis

16. SECURITY CLASSIFICATION OF:			17. LIMITATION OF ABSTRACT	18. NUMBER OF PAGES	19a. NAME OF RESPONSIBLE PERSON
a. REPORT	b. ABSTRACT	c. THIS PAGE			DR A SRINIVASA RAO
UNCLASSIFIED	UNCLASSIFIED	UNCLASSIFIED	SAR	92	19b. TELEPHONE NUMBER *(include area code)* 301-227-5141

This page intentionally left blank

Contents

FIGURES

Tables

Executive Summary

In order to better understand the formation of films during corrosion processes, an analytical technique using x-ray diffraction was developed to examine the structure of compounds in closest proximity to the metal/liquid interface. The in-situ structure at the metal liquid interface was examined for pure nickel, 90 % copper and 10 % nickel alloy (90-10 Cu-Ni) and 70 % copper and 30 % nickel (70-30 Cu-Ni) alloy in seawater solution at room temperature. The nickel -seawater system was investigated at potentiostatically controlled potentials of -800 mV and +450 mV (versus Ni/NiO), while both the 90-10 and 70-30 Cu-Ni alloys in seawater systems were investigated at four potentials (- 500 mV, -100 mV, +500 mV and +100 mV versus Ni/NiO).

The results indicated that two different passive oxide layers were present. While the outer passive layer was in contact with the seawater, the inner passive layer is in contact with the metal surface. The results also suggest that as prepared metal/alloy foils are associated with an oxide layer. During the electrochemical reaction, the oxide layer continued to be associated with the metal surface and became the main constituent of the inner passive layer.

The x-ray diffraction and XPS analysis results conclude that growth of the oxide film on the surface under an applied potential follows typical electrochemical (cathodic and anodic reaction) processes.

These results provide direct evidence of the existence of inner and outer passive layers during an electrochemical reaction.

Introduction

A key to the extension of equipment life is the reduction of material degradation or the failure rate. The use of thin films, e.g. oxides, has been the first line of defense in protecting machinery systems from the onset of corrosion. When these films are passive to the environment, they can impart excellent corrosion resistance. It is believed that a fundamental, electrochemical understanding of how and which passive films will provide better corrosion resistance will provide a means to improve or extend the operational life of machinery components or structure. However, there is disagreement regarding existence of several zoned passive oxide layers. While some of the basic corrosion scientists argue that the passive oxide films consist of more than one passive oxide layer, the others disagree on the existence of different passive layers with a distinct interface boundary. The proponents of different passive oxide layers suggest that one oxide layer must be in close contact with the metal phase while the other passive layer will be in contact with the liquid phase. Since the experimental determination of the inner passive layer is difficult, no detailed studies were reported in the literature prior to

the current investigations. This investigation was undertaken to examine in-situ the corroded oxide interface and to provide an analytical answer of the structure of passive oxide layer (i.e., whether more than one passive layer exists or not).

Background

The seawater corrosion processes are controlled by the chemical reactions that take place at the metal/liquid interface. In general, this is often studied with analytical techniques that look through the liquid to see the interface. Although it is more difficult, it may be far more revealing to view this interface by looking at it from the other side - through the metal. By doing this, new information can be gained concerning the manner in which a passive film resists the action of a liquid corrodent. This information is important because if the inner passive layer (i.e. the oxide layer that is in contact with the metal) is responsible for progression of the electrochemical reaction at the solid-liquid interface, it is possible that designing a suitable protection against the migration of the inner passive layer into the bulk of the metal may extend the life of the system.

In the recent past, a number of in-situ and structure-sensitive studies were made of electrochemical processes within the confines of conventional and ultra-high vacuum systems (uhv) systems [1-3]. Most of these earlier studies involved the emission and/or the scattering of photons or charged particles as a part of the analysis technique. These techniques could provide only indirect information regarding the structure of the corrosion products and interfaces.

In the open literature, there have been reports on the elucidation of structure during electrochemical processing using neutron diffraction [4]. However, the neutron diffraction studies required an elaborate and complex experimental set up. Recently, a few investigators have suggested the feasibility of experiments using analytical techniques such as the surface extended x-ray adsorption fine structure (SEXAFS), x-ray adsorption near edge structure (XANES), and total external reflection Bragg diffraction (TRBD) [5-8]. However, these studies often ignored the near-metal side of the metal/liquid interface because the extent of the reaction product is so much broader on the liquid side than the metal side (1-10 μm versus l-20 nm) of the metal/liquid interface.

Nickel/Nickel Alloy System

The electrochemistry of nickel and nickel alloy systems warrants study by the scientific community because these systems are pertinent to many machinery components or structures that are widely used in seawater environment. During corrosion, nickel and its alloys undergo the formation of passive oxyhydrates and/or hydroxides. In the literature, it has been reported that the identification of the formation of nickel hydroxides and or oxyhydrates has been difficult because these compounds often have highly disordered and/or have an amorphous crystal structure. Several earlier researchers used analytical techniques such as the EXAFS [5-6] and XAS [7- 9] to study nickel compounds. However, these researchers focused their attention on understanding the oxidation state of the nickel (Ni^{4+}) during the electrochemical process instead of examining the nucleation and growth of new compositions at the interface.

Two earlier studies [10 -11] that have focused their attention on understanding the structure of the near metal side of the metal-liquid interface; however, no other reports were cited in the open literature. One study [10], reported that the in-situ x-ray diffraction study is the key to understanding the electrochemical processes at the nickel electrode solution interface. These researchers designed and developed an electrochemical cell for x-ray reflection mode experiments. They reported that they found a 0.75-μm thick layer of $Ni(OH)_2$ after 40 hours of chemical reaction of nickel in 5 M KOH at 1 mV/s. However, their x-ray diffraction data showed very broad peaks. They concluded that the broadening was due to a mixture of phases in incompletely-aged electrodes.

Another in-situ x-ray diffraction analysis [12] involved the study of the structure of nickel electrodes during hydrogen evolution in sulfuric acid electrolysis. Those investigators reported that by x-ray diffraction they observed the formation of β-NiH. They also reported that they resolved the structure of β-NiH by x-ray diffraction. The peaks were very sharp and the 2θ values corresponding to β-NiH (111), (200), and (220) were at 41.9, 48.8, and 71.1, respectively.

Passive Layer Degradation

The passive oxide films/layers on many corrosion resistant alloys (e.g. stainless steels and copper/nickel alloys) are what distinguish them from alloys that readily corrode in aqueous environments. However, even these alloys can corrode and their passive layers degrade in many

applications. The mechanism of passive layer degradation has been extensively studied from the perspective of the aqueous side of the process. It has not been studied for the most part from the perspective of the metal side of the process, due to the complexity of the interface region. As the electrochemical reaction starts, the metal at the interface will be converted to its corresponding oxide/hydroxide. This oxide layer then may act as a passive barrier thus retarding progression of the electrochemical process.

The intriguing question is whether the passive film extends from the solution to the reacting interface of the metal, or whether it forms a transient inner passive layer. Assuming that such a process exists, the electrochemical process can be represented schematically as follows. Figure 1 is a schematic diagram of the metal-solution interface region during an electrochemical reaction process. The metal interface region can be divided into four possible regions: (a) bulk metal, (b) inner passive layer, (c) outer passive layer, and (d) solution. The existence of an inner passive layer (~ 10 - 20 nm thick) has been accepted widely by the scientific community. Most of the earlier conventional experiments have studied the degradation of the passive layers by observing the interface region from the solution side (Figure 1(A)). The current approach investigated the structure of the inner passive layer from the metal side of the metal solution interface (as shown in Figure 1(B)). The motivation for the present approach is the desire to establish whether the inner passive layer can be detected by the present experimental analytical technique.

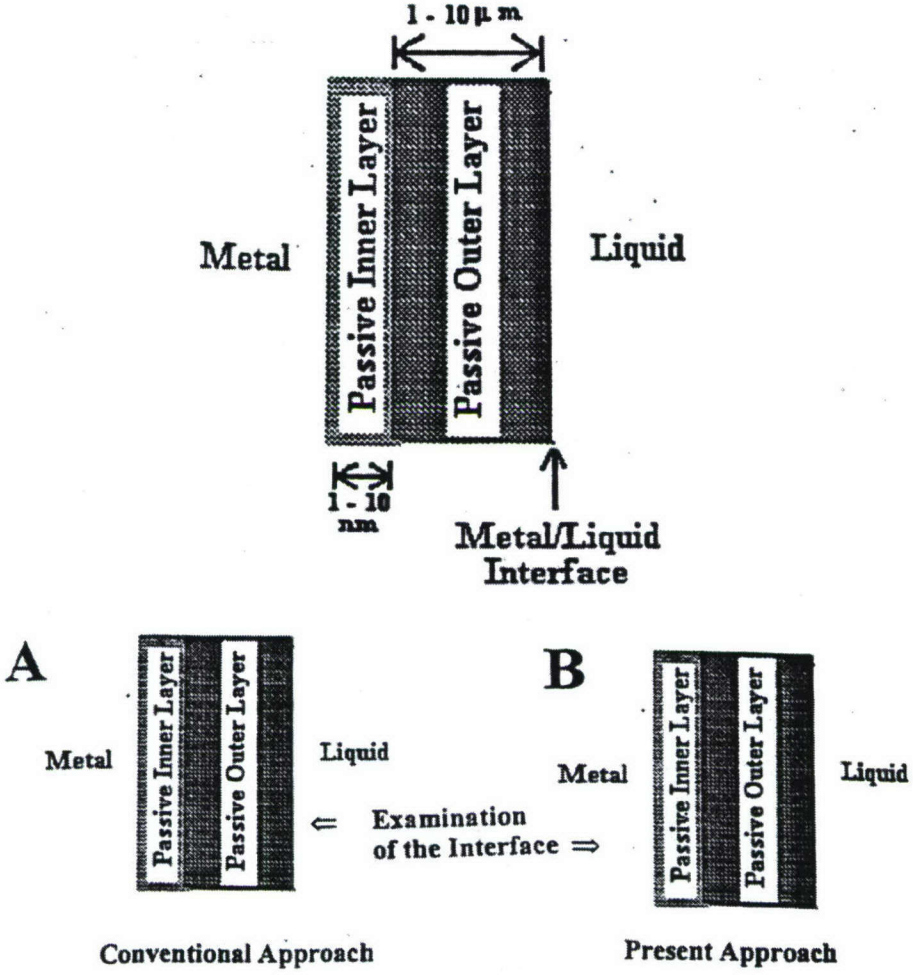

Figure 1. Schematic Diagram of the metal/solution interface region during electrochemical reaction process (A) Conventioanl and (B) present approach to study the inner passive layer.

Objectives

The present investigation was conceived to conduct a systematic study of the near metal interface structure in the nickel/nickel oxide system during alkaline hydrolysis. The overall goals of this program are: (1) to develop an experimental method to ascertain basic scientific information of the chemical and electrochemical interactions at the near metal - chemical reagent interface during electrochemical process, and (2) to characterize the changes in the surface oxide composition of nickel, and nickel alloys during cathodic and anodic electrochemical reaction. Consequently, the objectives of this investigation can be summarized as:

1. To develop an analytical method to study the reaction of metal/liquid interfaces from the metal side.

2. To apply this technique to follow in-situ, the oxide formation at the nickel/seawater interface during cathodic and anodic electrochemical reaction.

3. To apply this method to a more complicated metal alloy system, e.g. 90-10 Cu-Ni and/or 70-30 Cu-Ni utilized for the naval seawater piping applications.

Experimental Procedure

An experimental electrochemical cell was designed, fabricated, and tested. This cell was designed to allow for the use of x-ray diffraction as a method to study the corrosion process from the metal side of the metal/liquid interface. The nickel-seawater interface was studied in conjunction with the electrochemical characteristics of the corrosion process in the cell.

Materials

Pure nickel foil of 25 μm thick was obtained from commercial sources. The foils were cold rolled and annealed. The surface was cleaned first by using nitric acid followed by distilled water. The thin foils were then dried in a vacuum desiccator. No special care was taken to remove the air oxide film on any of the foils prior to electrochemical testing.

Commercial grade alloys of 90 % copper and 10 % nickel, (known as Alloy 706), and 70 % copper and 30 % nickel, (known as Alloy 715), were procured from the Eagle Brass

Companay, Leesport, PA as 0.003 in.-thick sheets (90-10 Cu-Ni) and 0.0071 in.-thick sheets (70-30 Cu-Ni) of Annealed Deep Draw Quality. The chemical composition and the mechanical properties are given in Table 1 and Table 2 respectively. At present the role of the minor elements (viz. Fe, Sn, Zn etc.) was not investigated.

Table 1. Alloy Composition and Properties of As Received 90-10 Cu -Ni Alloys

Chemical Composition	89.22 % Cu; 8.77 % Ni; 1.94% Sn; 0.002% Fe; 0.020 % Zn and < 0.002% Pb
Alloy Sheet Thickness After Rolling	~ 0.003 inch
Tensile Strength	~ 69 –70 ksi
% Elongation	~ 5 -8 %
Sheet Quality	Annealed Deep Draw Quality

Table 2. Alloy Composition and Properties of As Received 70-30 Cu -Ni Alloys

Chemical Composition	68.06 % Cu; 29.91 % Ni; 0.008 % Sn; 0.740 % Fe;0.966 % Zn, 0.305 % Mn; 0.004 % P, 0.003 % S and < 0.002% Pb.
Alloy Sheet Thickness After Rolling	~ 0.0071 inch
Tensile Strength	~ 55 ksi
% Elongation	~ 21 -23 %
Sheet Quality	Annealed Deep Draw Quality

The details of the rolling method and procedures to make the sheets were unavailable. The as-procured 90-10 and 70-30 Cu-Ni sheets were cut into 6 in.x 6 in. samples, and were chemically thinned using nitric acid. The samples were placed in a plastic tray containing 1 M nitric acid solution. The tray was gently shaken in order to obtain a uniform thinning. Once the samples were thinned to ~ 0.001 in.-thick, they were cleaned using distilled water and were placed in a second tray containing 0.1 M nitric acid. The sample thinning was continued until the thickness was reduced to 0.0005 in. The foils were then thoroughly cleaned in a distilled water bath where the water was circulated continuously for 30 minutes. The foils were then air-dried.

Electrochemical Cell Design

Figure 2 (A) shows the schematic diagram of electrochemical cell reported in the open literature [11] for in-situ examination of the changes in the structure of the interface region. The principle behind the cell design is the application of Bragg-configured reflection mode x-ray

measurement of the interface. The design incorporates a window that is provided with a complex arrangement for the placement of a thin metal foil facing the incoming x-ray source. The x-ray beam is transmitted through the foil and diffracted to a detection system. Although this type of cell arrangement can provide satisfactory information, the resolution can be poor because the angle between the incident and reflected x-ray beam is small. As a result, interference between the incident and reflected x-rays increases and such an increase in interference decreases the resolution. The second disadvantage is that this cell design requires a complex metal foil assembly.

In order to increase the angle between the incidence and reflection and to maximize the Bragg reflection without interference, an x-ray diffraction unit in which the detector system moves vertical to the plane of the sample foil and the x-ray source was used in this investigation. Additionally, a new cell was designed for ease of metal foil mounting.

Figure 2 (B) shows a schematic diagram of the electrochemical cell designed for this test. It was designed to be easily attached to and detached from the x-ray unit. A noteworthy feature of this cell design is that the top surface of the electrochemical cell was kept at an inclined angle of 5^{o} to the plane of the x-ray beam. At the mid point of the cell width, the cell surface is in plane with the incident x-rays. The inclination of the cell surface provides for strong and sharp Bragg reflections, thus resolving sharp x-ray peaks. The need for the 5^{o} inclination of the top surface of the cell was discovered by a process of trial and error.

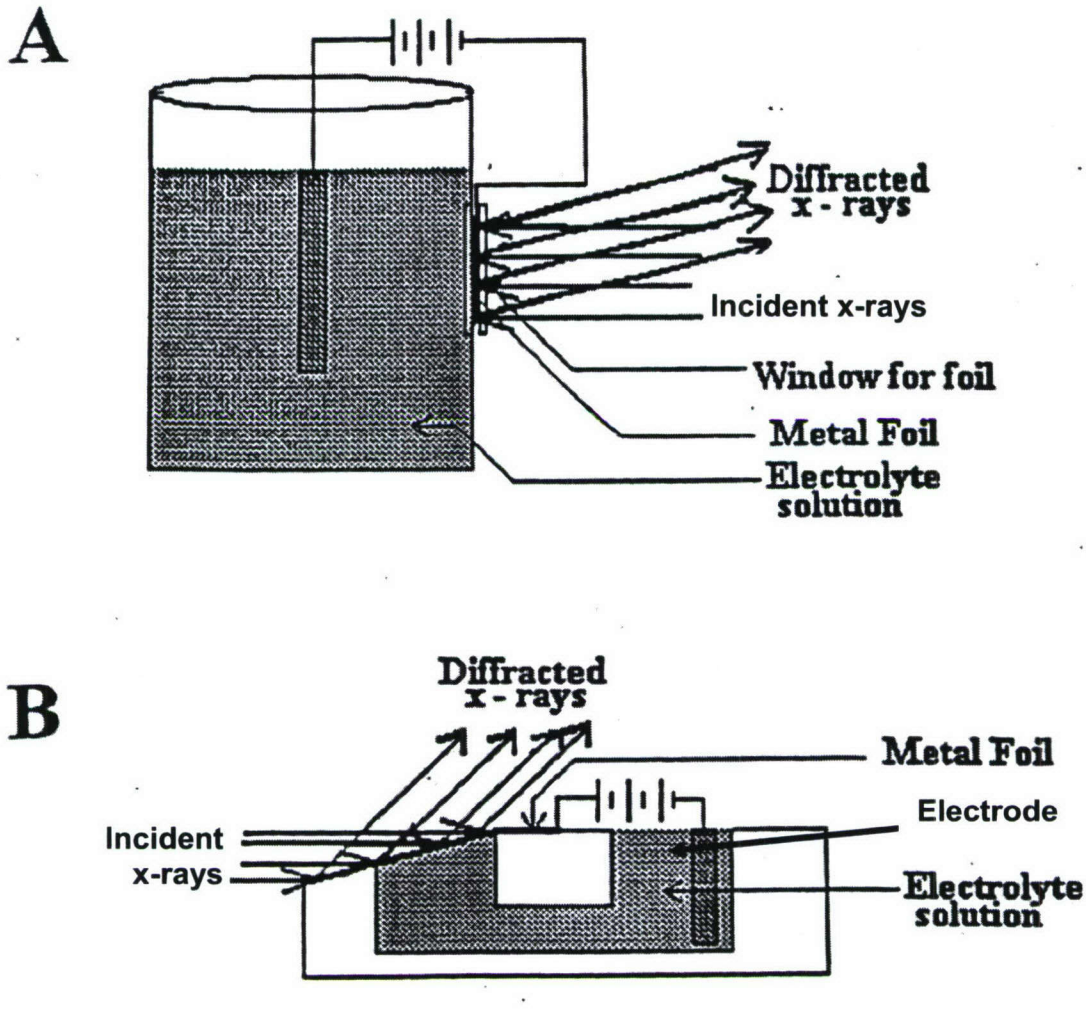

Figure 2. Schematic diagram of the design of the electrochemical cell (A) reported in the literature and (B) designed during this investigation.

Electrochemical Parameters

In order to establish electrochemical parameters, a reference nickel/nickel oxide (Ni/NiO) electrode system was fabricated. The system was calibrated in 20 wt.% seawater solution. The nickel/nickel oxide (Ni/NiO) electrode was constructed on an 80X80 nickel mesh screen consisting of a screen flag 2.5 x 1 cm with a connection piece 10-cm long. The final form of the electrode is a basket with 0.8-cm diameter x 1-cm depth.

The Ni/NiO electrode was placed in a beaker consisting of seawater solution. Two 90-10 Cu-Ni strips were used as the working electrodes of the electrochemical cell. The electrodes were connected to a computer-controlled potentiostatic analyzer. The analyzer system consists of a Princeton Applied Research (PAR) PARC Model 273 potentiostat, and an EG&G 5206 Lock-in Amplifier with a conventional PC, utilizing the PARC M 388 Software for system control and data accumulation.

A Sintag XDS-2000 x-ray diffractometer with a CuKα1 source at 8048 eV, -2.5 FWHM was used during this investigation. To ensure x-rays penetrated the test foil to the metal/solution interface, x-ray energy, current and foil thickness values of 35 KV, 30 mA and 12.5 μm (0.0005 in.), respectively, were necessary.

Test Procedure

The current versus applied potential plots were determined for pure nickel, 90-10, and 70-30, copper nickel foils in seawater at room temperature. The cyclic voltametric curves were plotted. The voltage that corresponds to the critical current values for both nickel and copper - nickel foils were determined. It was found that the critical current for cathodic and anodic reaction for pure nickel foils occur around -800 mV and + 450 mV, respectively. For the copper-nickel alloy, the transition from cathodic to anodic reaction was found to be very sharp and the change in the electrochemical behavior occurred in a very narrow potential range (viz. -5 to + 5 mV). Since no polarization was observed at a potential of zero volts, and it was difficult to maintain +5 or –5 mV on the electrochemical test cell fitted to the x-ray diffraction unit, it was decided to conduct the electrochemical tests for copper nickel alloys at two potentials (-500mV, -100 mV and +100 mV and +500 mV). The selection of the potential values was arbitrary. The detailed results are shown in the later section.

The seawater solution was aerated in order to control the oxygen content and was later pre-electrolyzed to remove any cationic impurities. The test cell was filled with the seawater solution. Due care was taken during the filling of the test cell to ensure that no air bubbles were trapped between the metal foil and the solution. The test cell was attached to the x-ray unit and the electrochemical testing was initiated. The nickel-seawater system was investigated at -800 mV and +450 mV. The 90-10 Cu-Ni and 70-30 Cu-Ni foils were investigated at four pre-selected constant potentials (-500 mV, -100 mV, +500 mV, and +100 mV). The potentials were applied continuously during each electrochemical study period of nearly 48 hours. (Only one specimen at one potential was investigated at a time). The interface study was made on 5 different thin foils for each material in order to establish the composition of both the inner and outer passive layers. The results were evaluated by analyzing the x-ray and XPS data obtained on all five foils.

X-ray diffraction patterns were obtained after 1, 1.5, 2, 4, 6, and 24 hours in order to follow the structural changes during the electrochemical process. Each x-ray diffraction run took 20 minutes. For convenience, we have labeled the x-ray diffraction patterns as those obtained after 1, 1.5, 2, 4, 6, and 24 hours only.

X-Ray Photoelectron Spectroscopy (XPS)

X-ray photoelectron spectroscopy (XPS) was used to examine the nature of the surface reactions that were the subject of this research effort. It was also used to study the nature of the initial oxides formed on the test foils. XPS involves exposing the surface of interest to x-rays of a discrete energy. In the Kratos model XSAM 800 surface analyzer used in these experiments, AlKα (1486.6 eV, -0.85 FWHM) was the radiation source. This radiation interacts with the specimen, causing the material to emit electrons with an energy that is characteristic of the atoms from which they were emitted. The XPS equipment has an electron energy analyzer that measures the kinetic energy of the emitted electrons. This measurement was made with a hemispherical analyzer having an aberration-compensated input lens (ACIL). The analyzer superimposes different voltages on the inner and outer hemispheres which then allow only electrons with energies between these two values to pass through to the detector at the opposite end of the analyzer. The equipment scans the voltages on the two hemispheres through an energy range in steps and during its dwell time at each step, it keeps track of the counts per

second, or intensity of electrons. This information can then be graphed as electron energy versus intensity. The major limit on the energy-resolving capabilities of the instrument is the width of the exciting radiation, e.g. 1.0 eV at full-width half maximum for Al K_α radiation.

The XPS spectrometer and specimen were contained within an ultra-high vacuum. This prevented the electrons from being scattered by gas molecules before they reached the analyzer and allowed experiments to be conducted and data acquired in reasonable times before the specimen surfaces were excessively contaminated with unwanted gases and carbon from the atmosphere. This latter point is important since the XPS method analyzes for elements on the surface and within several atomic layers of the surface. The surface sensitivity of the XPS method arises from its ability to measure the energy of emitted electrons. These electrons have a very short mean free path in solid matter. Typically, this distance is on the order of 5 to 10 angstroms. Therefore, the emitted electrons represent elements present in the outer layer or several atomic layers below the surface.

The concentration of a given element in the surface is represented by the intensity of electrons (counts per second) emitted at a given characteristic binding energy. The area under these peaks in the XPS spectrum was used as a measure of the intensity. The experimental procedure adopted for obtaining the XPS spectrum and for the spectral analysis was as follows: First, a sample surface analysis survey scan in the binding energy range 0 -1200 eV was made in order to ensure that all the relevant elements are identifiable. A series of regional scans for required elements (viz. Cu, Ni, O, and C) was made. The range of the scan was within $\pm$10 eV of the corresponding binding energy. Computer-aided routines were used to perform the necessary background subtraction around the peak of interest and to calculate the area under the peak. If peaks partially overlap, a peak synthesis routine was used to extract the peak of interest. All intensities were then corrected by a multiplication factor representing the spectrometer efficiency and the probability of emission from a particular electron energy level in a given atom. These correction factors were determined by the analyzer's manufacturer. The peak locations for the various identified compounds were obtained from the hand book of x-ray photoelectron spectroscopy [13-15]. To assist in identifying the chemical state of the metal foils after corrosion testing, XPS spectra were obtained from standards of pure nickel. The nickel foil may have a nonconductive oxide layer charging up during the spectra acquisition. This can cause the peaks to shift from the normal locations. To correct for this, the adventitious carbon peak found on

these standards was referenced to the carbon peak at 284.6 eV and all other peak locations were corrected accordingly. The details of the analysis parameters used to acquire the XPS data are shown in Table 3.

Table 3. XPS Analysis Parameters

Al excitation (1486.6 eV)	Fixed analyzer transmission	True time averaging
Low magnification	Start energy of scan, 1200 eV	Step size, 0.5 eV
Low resolution	Channels, 2400	Dwell, 0.5 s.

In order to minimize any chemical changes that may result due to surface heating, no sputter cleaning of the surface was made prior to the acquisition of the XPS spectra. Sputter cleaning may induce some chemical changes (viz. oxidation) due to local heating. The maximum information for all elements at a minimum time was obtained by taking the data for one energy sweep per element. Once the XPS spectra were obtained, a peak synthesis routine was used to match the binding energy to the real data peaks of the elements so that a better correlation between the XPS spectra and the binding energy of the element of interest could be obtained.

Interface Structure Identification Procedure

For the foil thickness used in this investigation, it is reasonable to suggest that the x-ray diffraction patterns represent the cumulative structure of metal and the metal/liquid interface. Since the interface region is composed of both the inner passive layer and the outer passive layer, it is reasonable to assign the x-ray diffraction data to represent the structure of the base metal and the inner and outer passive layers.

The information acquired in the XPS data represents the structure of the top few layers of the electrochemically reacted surface. Since the top few layers are contained in the outer passive layer (Figure 1), the XPS analysis can be suggested to provide information on the outer passive layer without being obscured with the information from the inner passive layer or the bulk material. By subtracting the structure of the outer passive layer (obtained from XPS data) from the XRD structural information, the inner passive layer structure can be established.

Results

Nickel -Seawater System

Figure 3 shows a typical x-ray diffraction pattern obtained from a 12.5 μm-thick (0.0005 in.) nickel foil mounted on the test cell. In order to eliminate any interference to the diffraction pattern from the cell material (Lucite), the x-ray measurement program was modified to eliminate the background information on the final x-ray diffraction pattern. For example, Figure 4 shows a typical x-ray diffraction pattern obtained from the test cell material. Figure 5 shows the x-ray diffraction pattern of nickel foil shown in Figure 3 wherein the contribution due to the cell material (lucite) was removed. The x-ray diffraction pattern obtained from 12.5 μm-thick (0.0005 in.) thick nickel foils is shown in Figure 6. Although the peaks for nickel foil in Figures 3 and 6 appear to be different, they are the same. The apparent difference is due to the fact that the two results are obtained from two different foils that were subjected to different rolling conditions. It is possible that both foils have two different grain orientations. For the in-situ electrochemical study, one foil that was started with no potential was continued until the end of the experiment. Therefore, the all XRD results obtained for a foil with specific grain orientation continued until the end.

The observed two diffraction peaks correspond to the two standard diffraction peaks (44.6 and 51.9; d spacing of 20.3, and 17.6 nm, respectively). Some of the nickel samples also showed an additional peak (at 29 ~ 41 corresponding to d-spacing of 23 nm).

In order to make sure that the samples were thin enough to resolve the structure of the under-side of the metal foil, a calibration was carried out with a second foil. This was done with a 12.5 m-thick (0.0005 in.) nickel foil glued onto a silver foil. The sandwich of nickel and silver foils was then glued onto the test cell. The direct exposure of silver foil to the incident x-ray beam was avoided by covering the edges with a copper shielding plate. Figure 7 shows a typical x-ray diffraction pattern of nickel/silver laminate. The results demonstrate that at the x-ray incident energy studied, the x-ray penetrated through the nickel foil and into the silver foil.

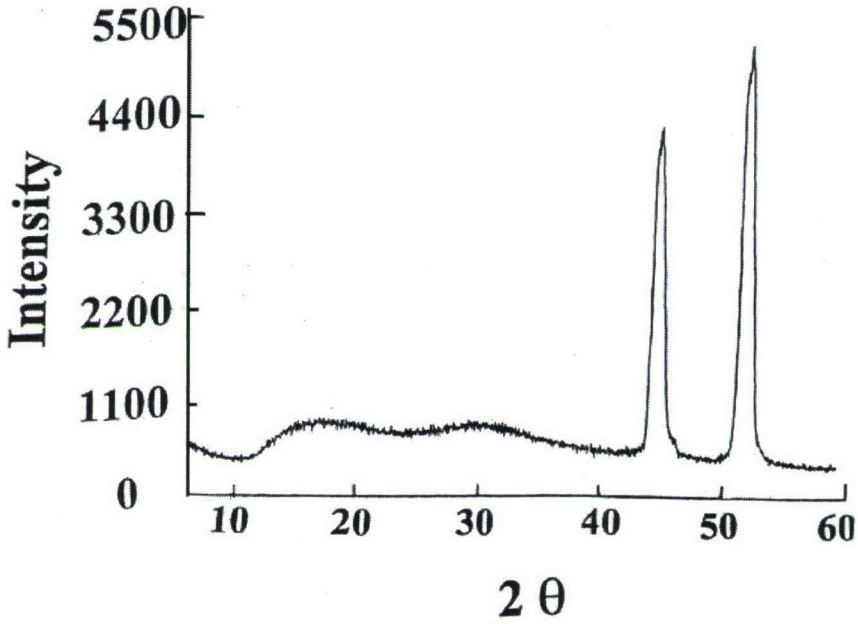

Figure 3. Typical x-ray diffraction pattern obtained from nickel foil mounted on the electrochemical test cell.

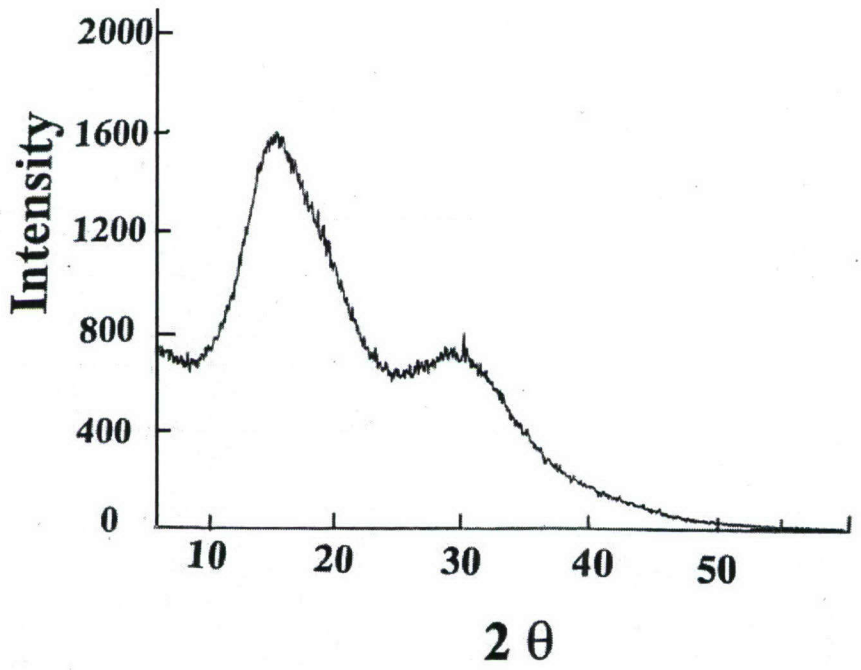

Figure 4. X-ray diffraction pattern obtained from the electrochemical test cell material.

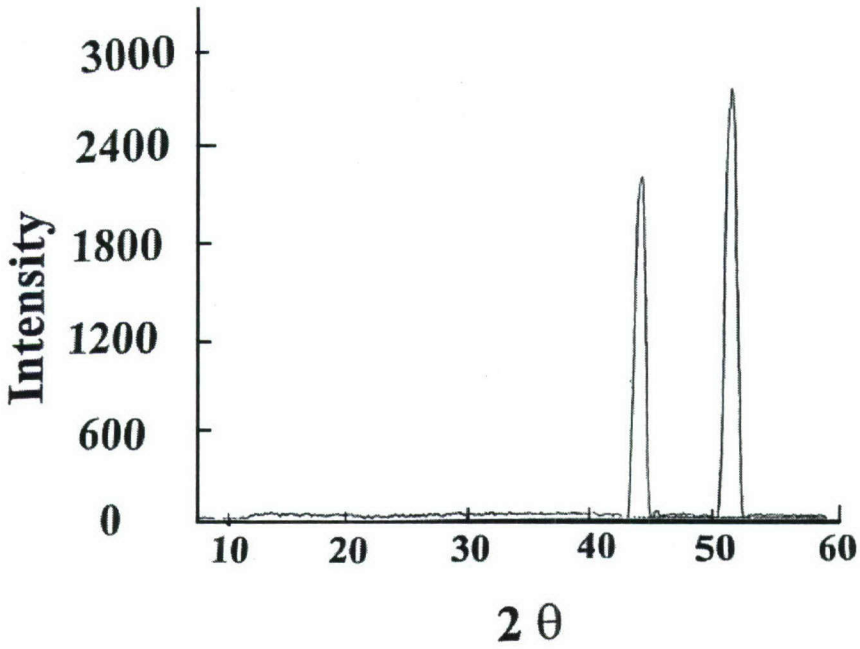

Figure 5. X-ray diffraction of nickel foil after subtracting the contribution due to the cell material.

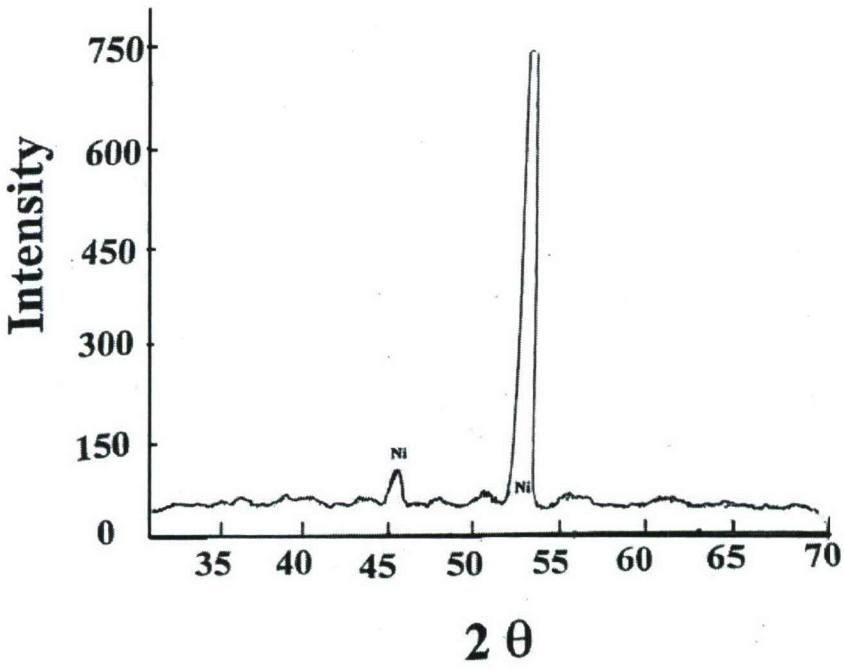

Figure 6 . Typical x-ray diffraction pattern obtained from 12.5 μm-thick (0.0005 in.) nickel foil mounted on the electrochemical test cell.

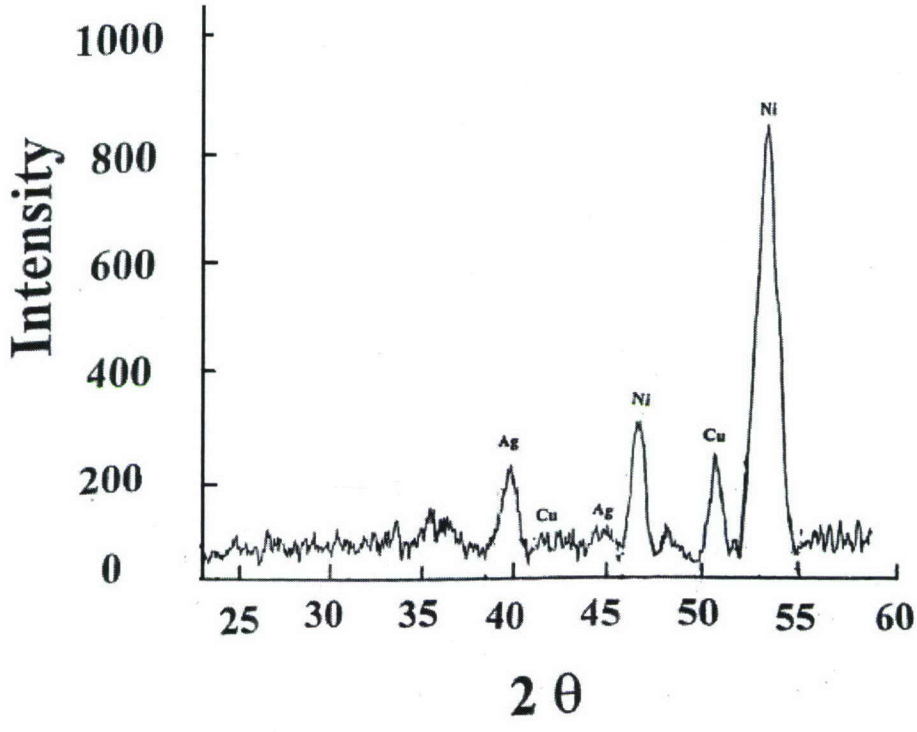

Figure 7. X-ray diffraction pattern of thin nickel foil and silver foil composite laminated on a copper back plate.

Figure 8 shows a typical current versus applied potential plot of nickel foil in seawater solution as it cycles once through -1000 mV → +800 mV→ -1000 mV. A similar plot, with applied potential (-1000 mV → +300 mV) as a function of log current density is shown in Figure 9. The results (shown in Figures 8 and 9) suggest that as the applied potential is increased from 0 -100 mV, no change in the cell current is noticeable. As the applied potential is increased above 100 mV, initially, the current increases slightly. Above 200 mV, the cell current increases significantly with increase in potential. Above +450 mV, the trend is reversed. Similarly, as the applied potential is increased from 0 to -600 mV, no changes in the cell current are observed. For applied potential in the range -600 mV to -800 mV, an increase in the applied potential increases the cell current.

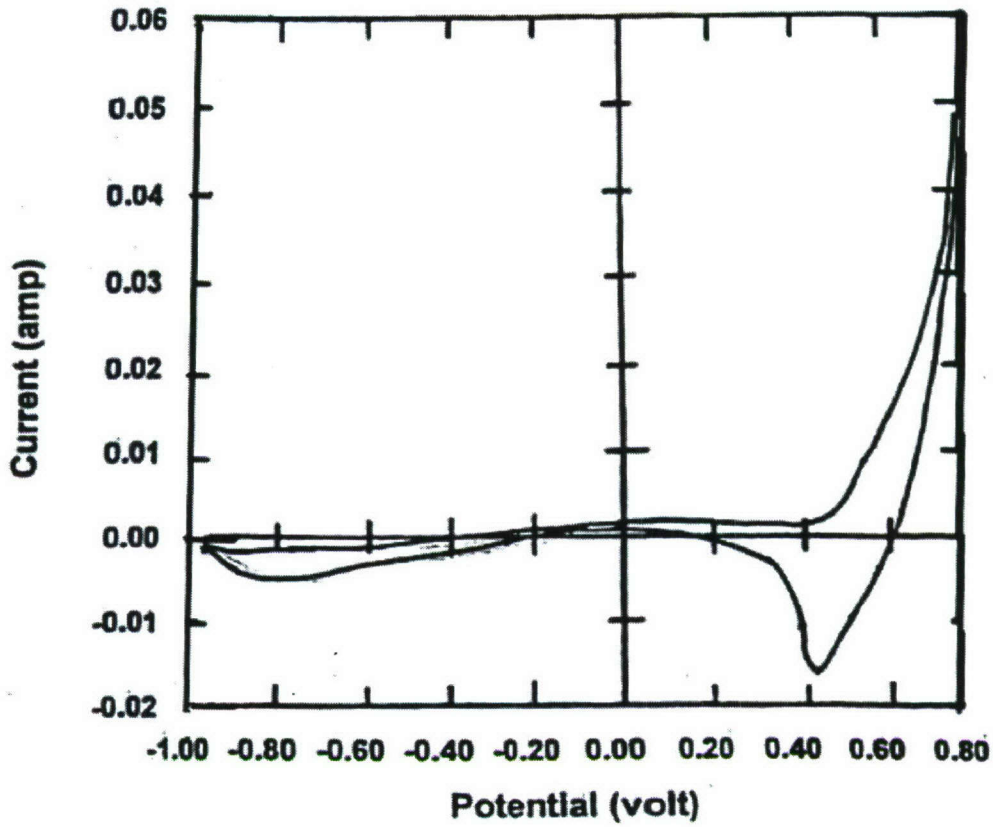

Figure 8. Potential versus current plot of nickel in seawater at room temperature.

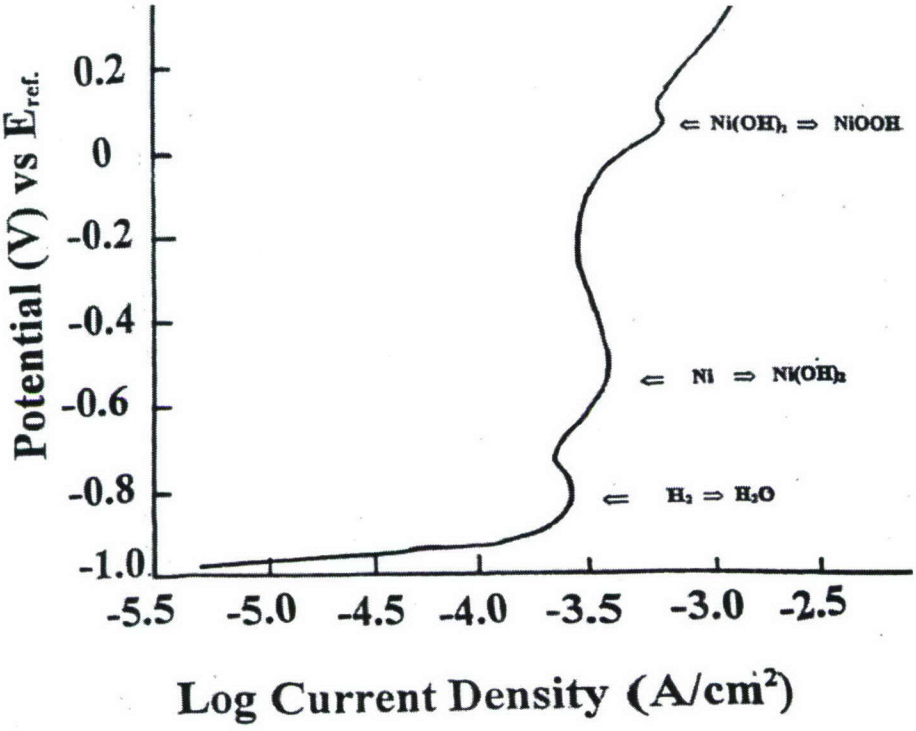

Figure 9. Log current density versus applied potential (versus reference potential) plot of nickel/seawater at room temperature.

XRD Results for Potential of -800 mV

It was found that when a cathodic potential of - 800 mV was applied, during the first 60 minutes, no significant changes were observed in the diffraction pattern. However, a careful examination of x-ray scans acquired later revealed that the possible changes were masked by the system's background noise. After one hour, significantly measurable differences in the diffraction patterns were observed. Figures 10 thru 15 show typical x-ray diffraction patterns obtained after 0.5, 1, 2, 4, 6, and ~24 hours of exposure to seawater at -800 mV, respectively. The results in Figure 10 thru 15 suggest that the electrochemical reaction at -800 mV produced significant amounts of NiOOH. During the first 2 hours, the formation of NiOOH increases with increasing reaction time. After 2 hours, there appears to be a decrease in the amount of NiOOH. However, it was found that after 24 hours, the concentration of NiOOH has increased. The

results also suggest that the electrochemical reaction also produced a small amount of $Ni(OH)_2$. Although, the x-ray diffraction peaks are not well defined, the above conclusions are based on several examinations of metal samples that were exposed to the electrical potential both in simulated seawater, and concentrated KOH solution. The detailed analysis of our electrochemical studies in KOH medium was discussed in our earlier reports [13-15].

When - 800 mV was continuously applied, the cathodic reaction progressed with the accumulation of OH at the cathode, and the reaction from the nickel interface can be represented as,

$$NiOOH \Rightarrow Ni(OH)_2 \Rightarrow H_2 \uparrow$$

However, it is surprising to notice from the present results that there is a significant formation of NiOOH at this negative potential (-800 mV).

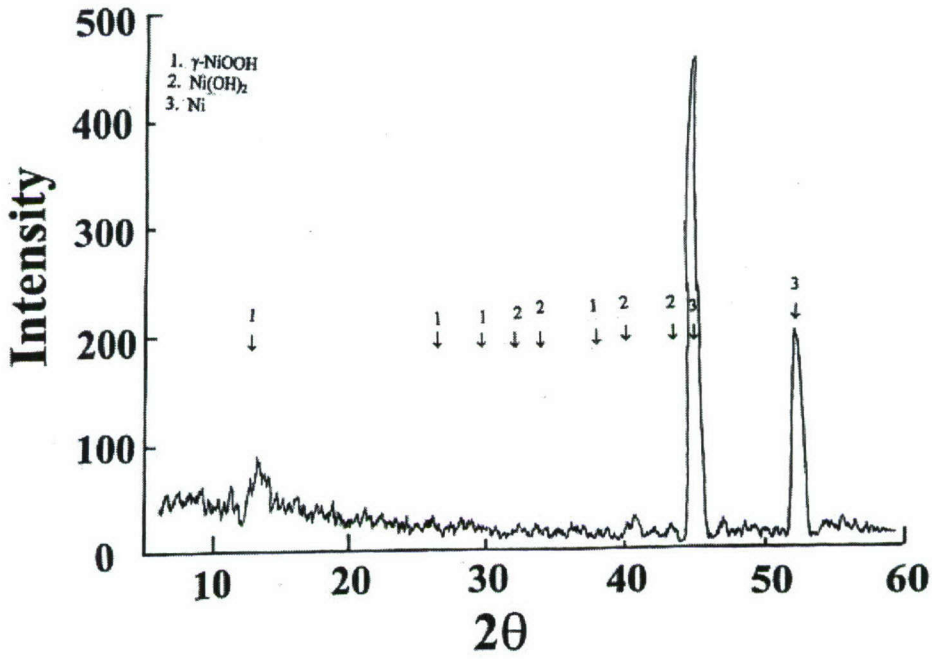

Figure 10. In-situ x-ray diffraction pattern obtained from 12.5 μm-thick (0.0005 in.) nickel foil mounted on the electrochemical test cell, at -800 mV versus Ni/NiO in seawater after 30 minutes.

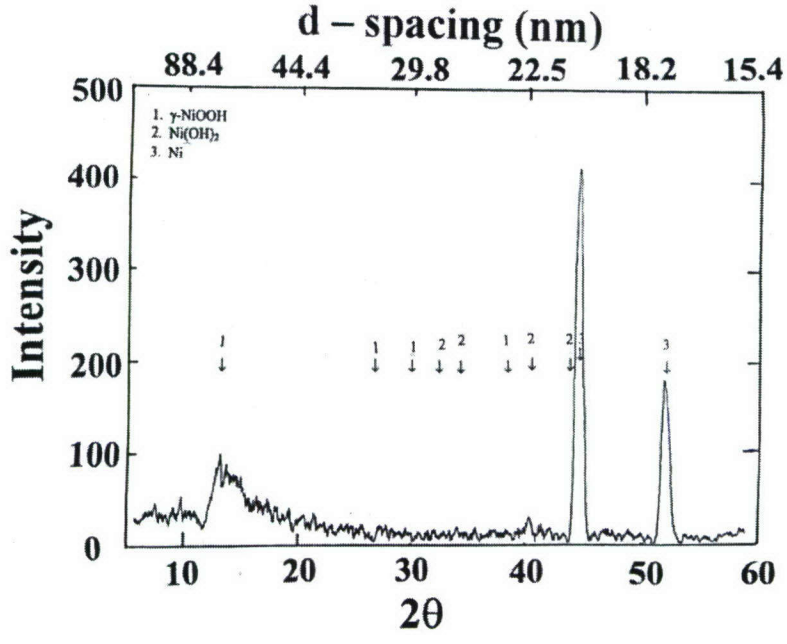

Figure 11. In-situ x-ray diffraction pattern obtained from 12.5 μm-thick (0.0005 in.) nickel foil mounted on the electrochemical test cell, at -800 mV versus Ni/NiO in seawater after 1.0 hour.

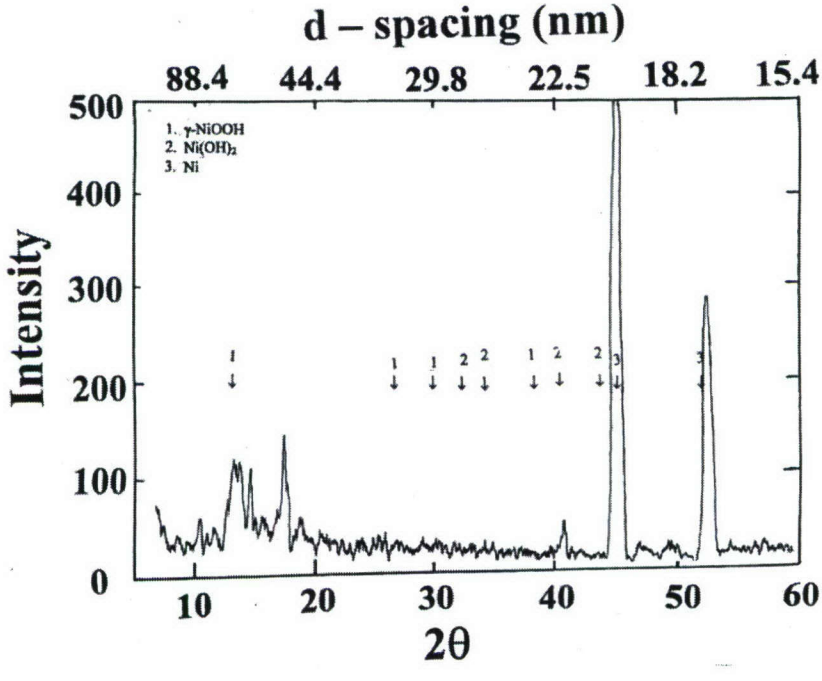

Figure 12. In-situ x-ray diffraction pattern obtained from 12.5 μm-thick (0.0005 in.) nickel foil mounted on the electrochemical test cell, at -800 mV versus Ni/NiO in seawater after 2.0 hours.

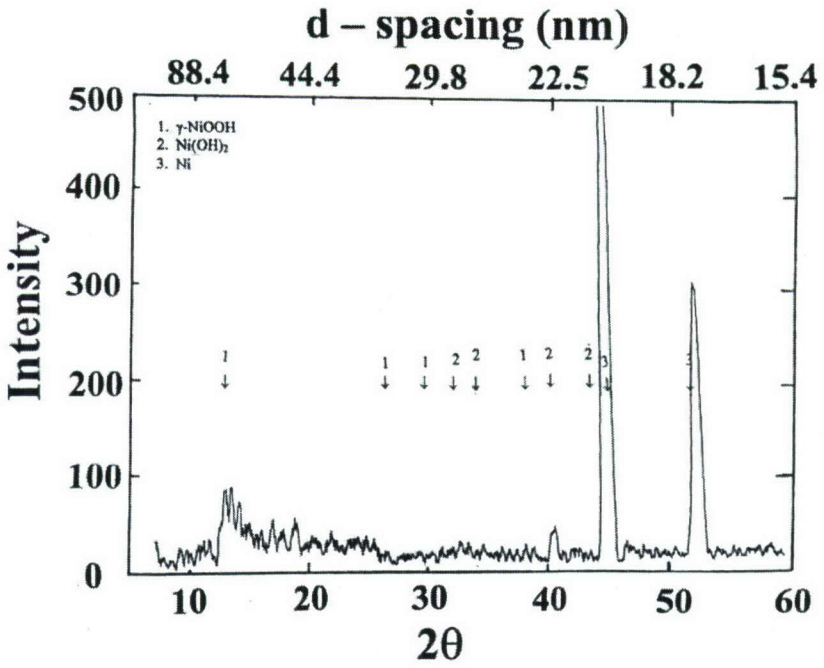

Figure 13. In-situ x-ray diffraction pattern obtained from 12.5 μm-thick (0.0005 in.) nickel foil mounted on the electrochemical test cell, at -800 mV versus Ni/NiO in seawater after 4.0 hours.

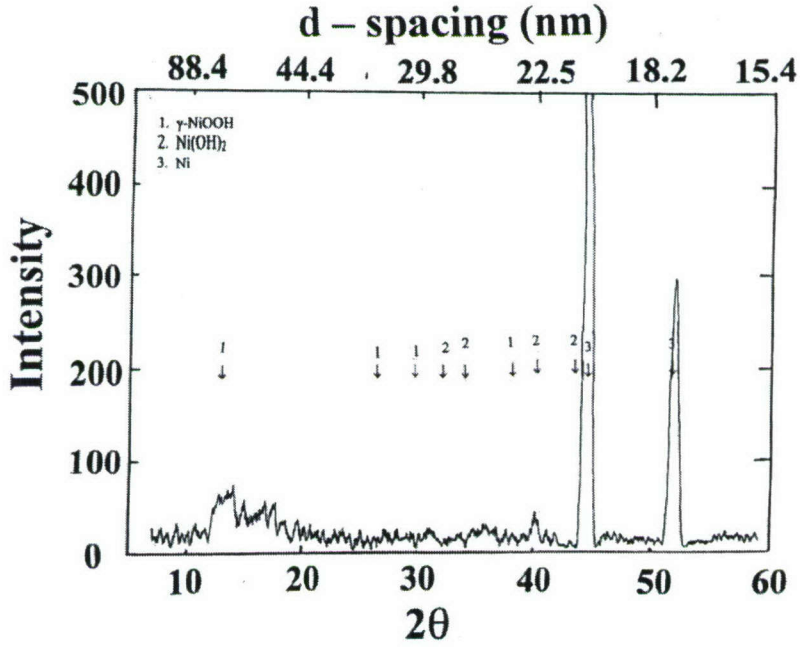

Figure 14. In-situ x-ray diffraction pattern obtained from 12.5 μm-thick (0.0005 in.) nickel foil mounted on the electrochemical test cell, at -800 mV versus Ni/NiO in seawater after 6.0 hours.

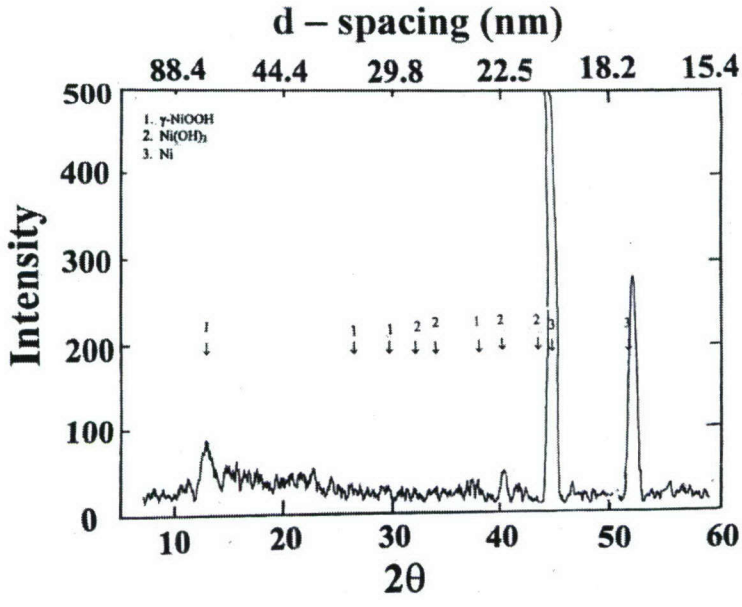

Figure 15. In-situ x-ray diffraction pattern obtained from 12.5 μm-thick (0.0005 in.) nickel foil l mounted on the electrochemical test cell, at -800 mV versus Ni/NiO in seawater after 24.0 hours.

XPS Results for Potential of -800 mV

Figures 16 and 17 show typical XPS spectra for nickel and oxygen obtained from the test foil subjected to -800 mV in seawater solution. The XPS analysis results shown in Figures 16 and 17 indicate that the chemical composition of outer surface layers is $Ni(OH)_2$.

XRD Results for Potential of + 450 mV

The results from the nickel foils subjected to +450 mV following the in-situ x-ray diffraction studies are shown in Figures 18-23. The figures correspond to the measurements made after exposures of 0.5, 1, 2, 4, 6, and 24 hours, respectively. The results suggest that the x-ray diffraction patterns for the +450 mV potentials are more complicated than the earlier patterns (potential - 800 mV). The results verify that the surface is oxidized with nickel oxidation states of both Ni^{+3} and Ni^{+2} in addition, the results also show that the surface of the nickel foil contains $Ni(OH)_2$. At + 450 mV, the reaction of nickel in seawater can be postulated as:

$$\text{Ni} \Rightarrow Ni(OH)_2 \Rightarrow Ni(OH)_2 \cdot 0.75\ H_2O \Rightarrow 3Ni(OH)_2 \cdot 2\ H_2O$$
$$\Rightarrow NiOOH \Rightarrow Ni_2O_3 \Rightarrow NiO$$

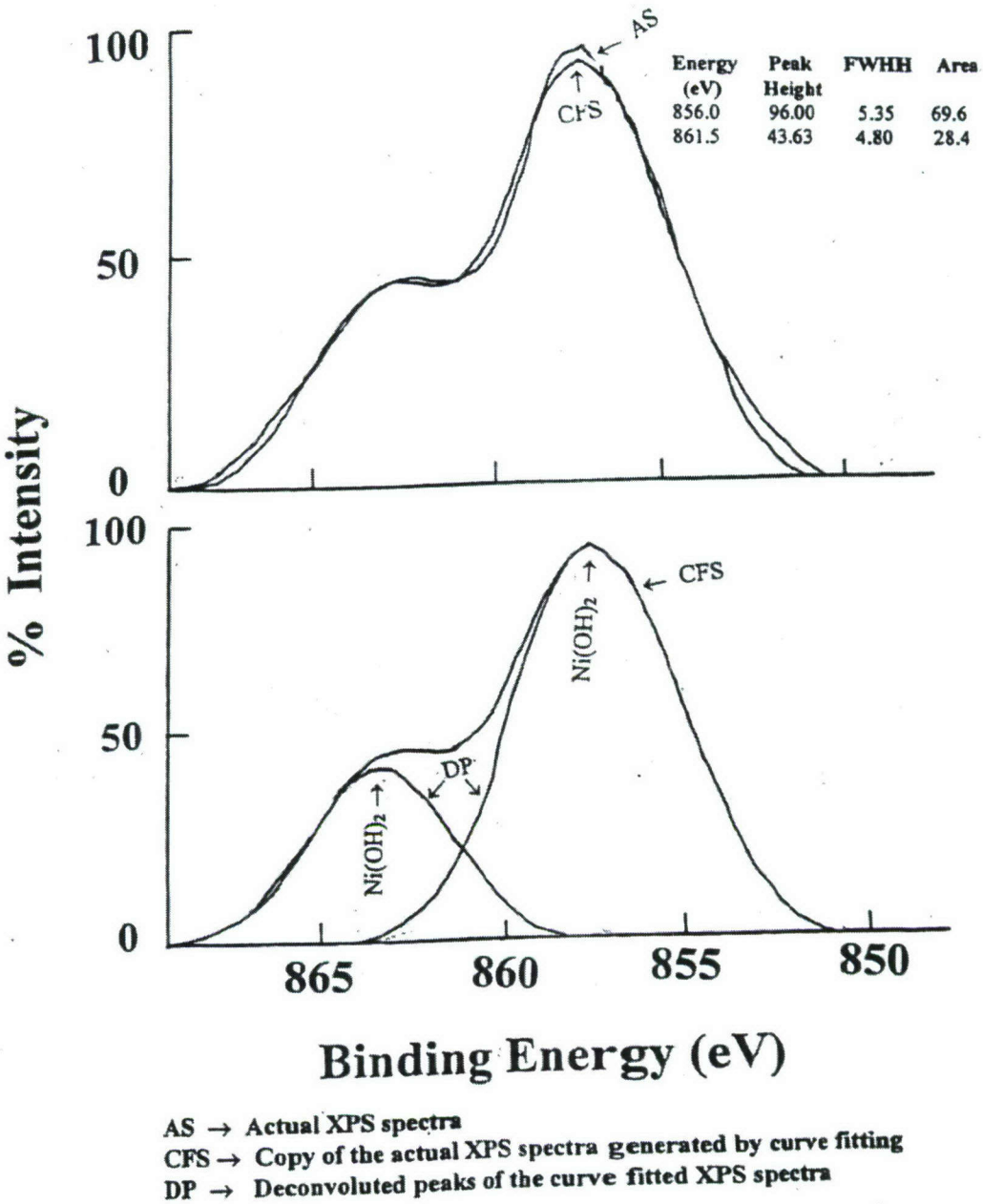

Figure 16. Nickel peaks obtained from XPS analysis of 12.5 μm-thick (0.0005 in.) nickel foil surface exposed to seawater at -800 mV for 24 hours.

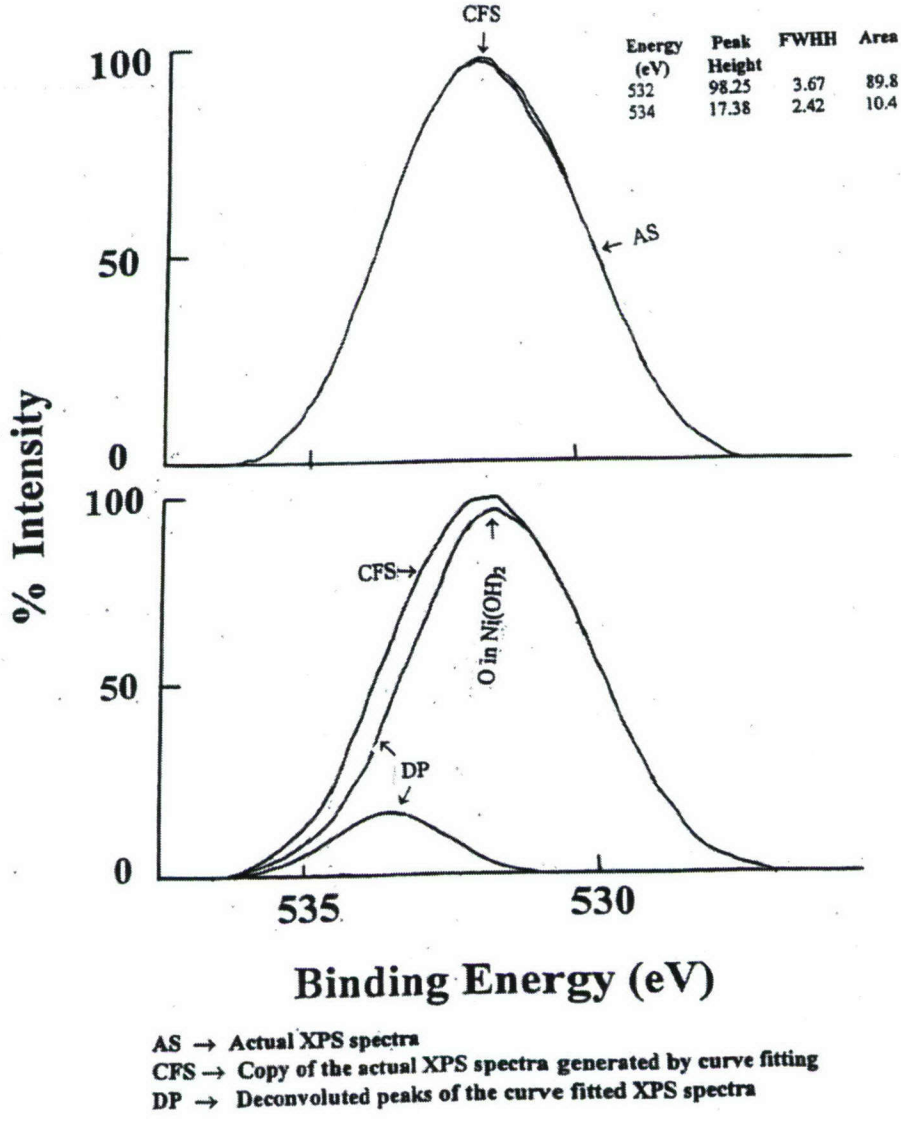

Figure 17. Oxygen peaks obtained from XPS analysis of 12.5 μm-thick (0.0005 in.) nickel foil surface exposed to seawater at -800 mV for 24 hours.

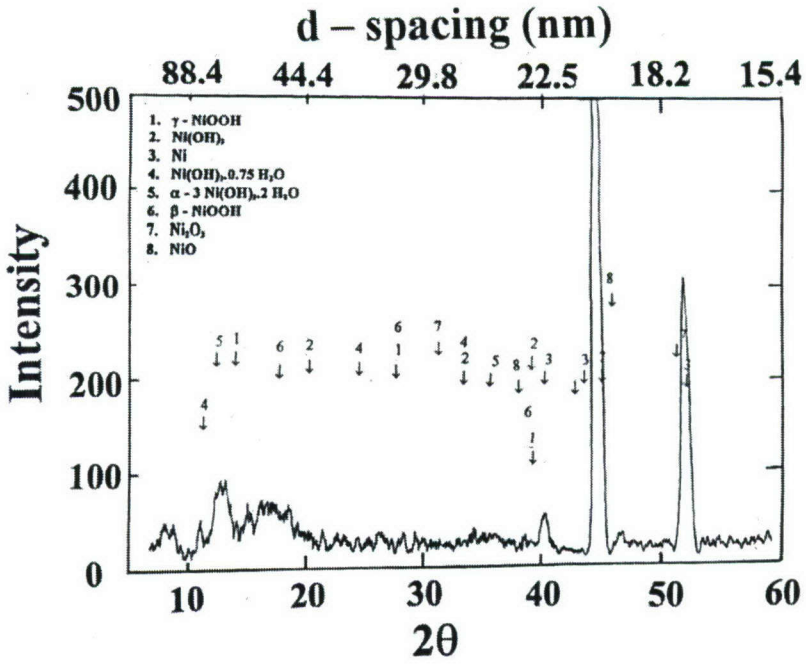

Figure 18. In-situ x-ray diffraction pattern obtained from 12.5 μm-thick (0.0005 in.) nickel foil mounted on the electrochemical test cell at +450 mV versus Ni/NiO in seawater after 0.5 hour.

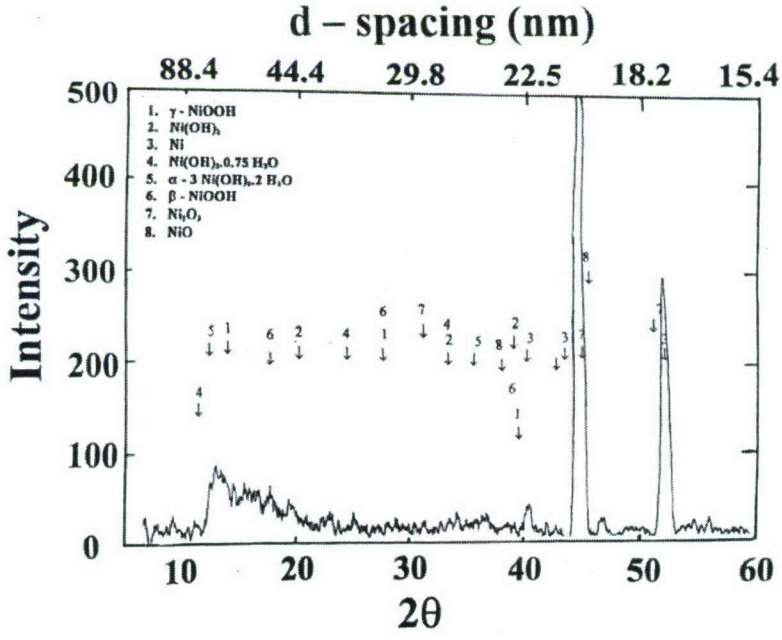

Figure 19. In-situ x-ray diffraction pattern obtained from 12.5 μm-thick (0.0005 in.) nickel foil mounted on the electrochemical test cell at +450 mV versus Ni/NiO in seawater after 1 hour.

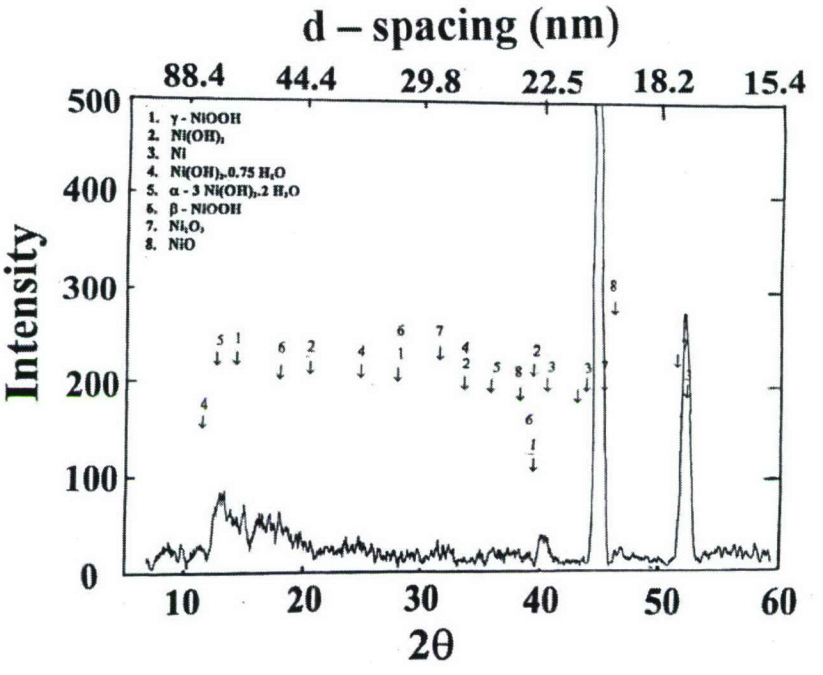

Figure 20. In-situ x-ray diffraction pattern obtained from 12.5 μm-thick (0.0005 in.) nickel foil mounted on the electrochemical test cell at +450 mV versus Ni/NiO in seawater after 2 hours.

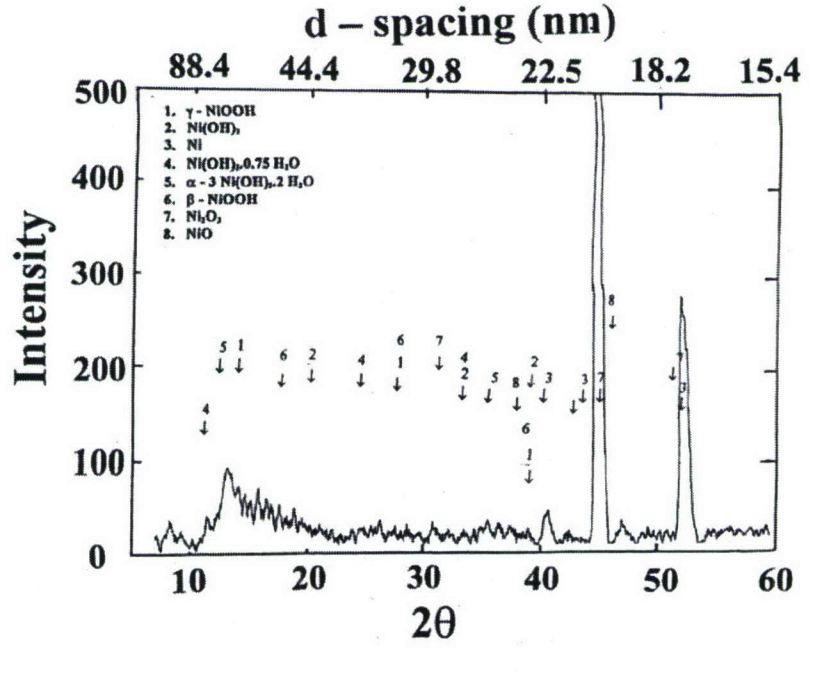

Figure 21. In-situ x-ray diffraction pattern obtained from 12.5 μm-thick (0.0005 in.) nickel foil mounted on the electrochemical test cell at +450 mV versus Ni/NiO in seawater after 4 hours.

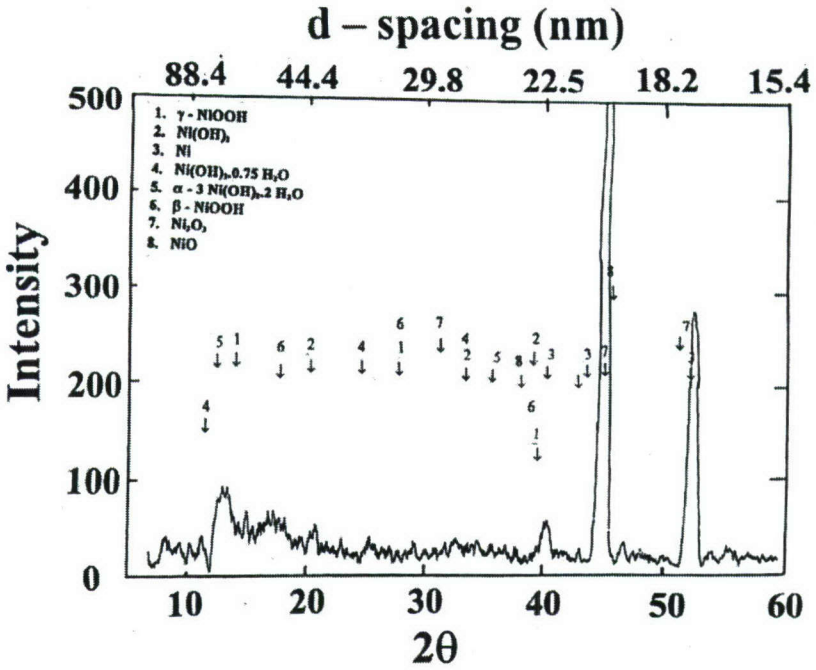

Figure 22. In-situ x-ray diffraction pattern obtained from 12.5 μm-thick (0.0005 in.) nickel foil mounted on the electrochemical test cell at +450 mV versus Ni/NiO in seawater after 6 hours.

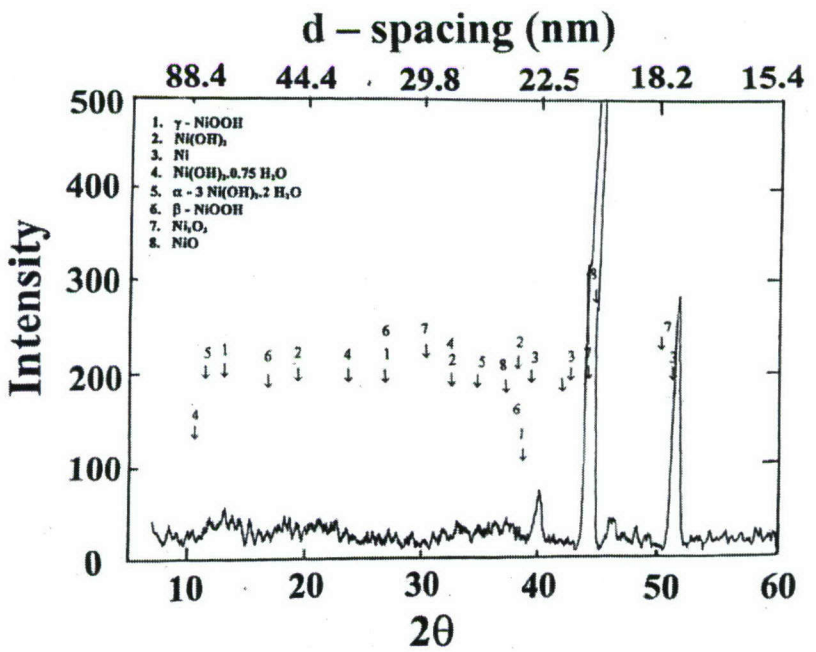

Figure 23. In-situ x-ray diffraction pattern obtained from 12.5 μm-thick (0.0005 in.) nickel foil mounted on the electrochemical test cell at +450 mV versus Ni/NiO in seawater after 24 hours.

XPS Results for Potential of + 450 mV

Figures 24 and 25 show typical XPS spectra for nickel and oxygen obtained from the test foil subjected to +450 mV in seawater solution. The XPS analysis results shown in Figures 24 and 25 indicate that the chemical composition of outer surface layers is Ni_2O_3.

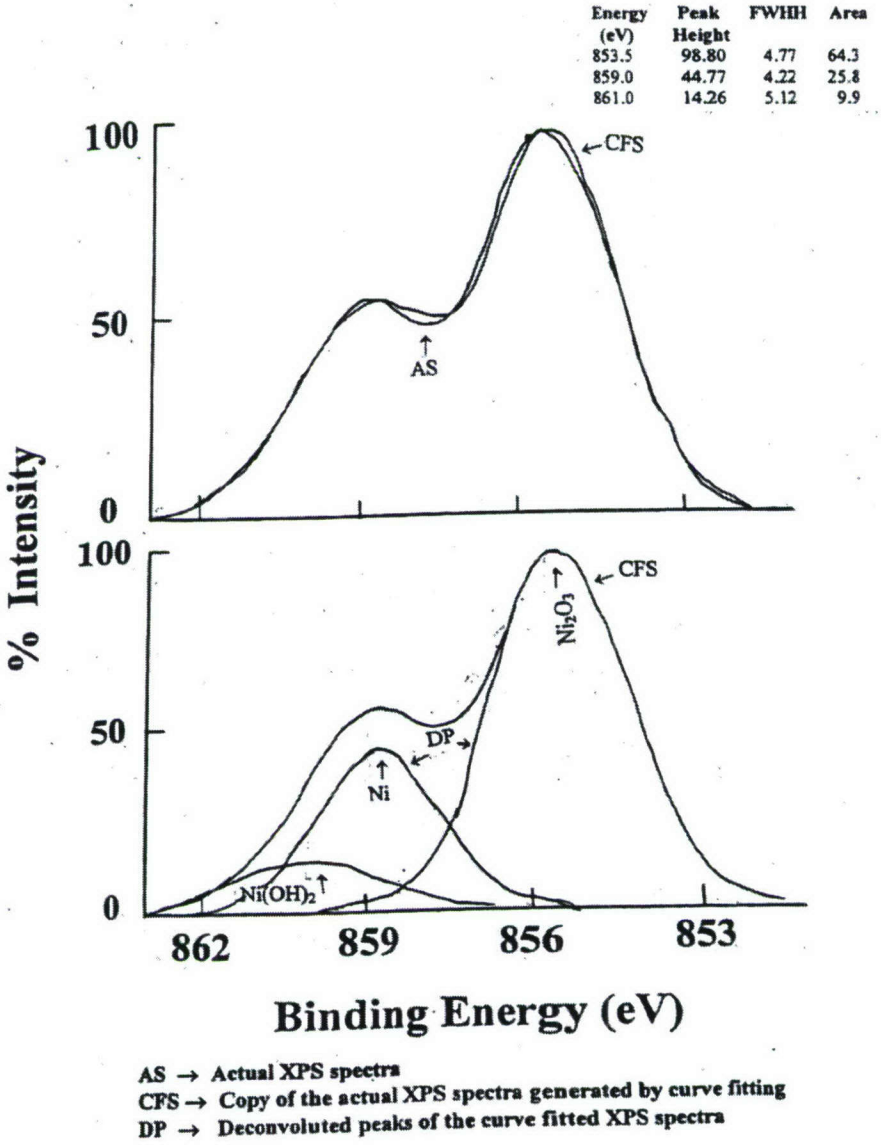

Figure 24. Nickel peaks obtained from XPS analysis of 12.5 μm-thick(0.0005 in.) nickel foil surface exposed to the seawater at +450 mV for 24 hours.

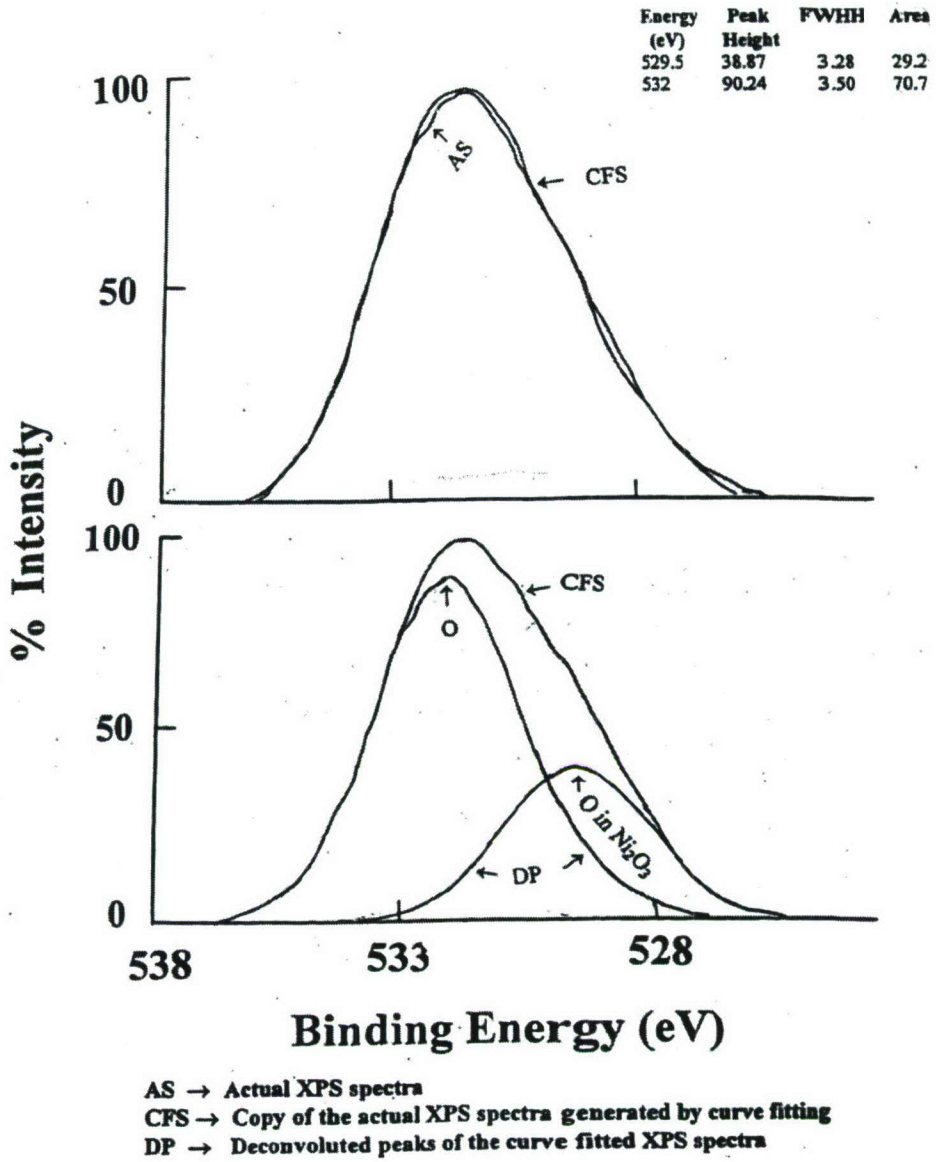

Figure 25. Oxygen peaks obtained from XPS analysis of 12.5 μm-thick(0.0005 in.) nickel foil surface exposed to the seawater at +450 mV for 24 hours.

90% Copper - 10 % Nickel -Seawater System

Figure 26 shows a typical x-ray diffraction pattern obtained from a 12.5 m-thick (0.0005 in.) 90 % copper-10 % nickel foil mounted on the test cell. The results suggest that the test sample surfaces are slightly oxidized.

Figure 27 shows a typical current versus applied potential plot of the 90-10 Cu-Ni foil in seawater solution as it cycles once through from -1.0 V → +1.0 V→ -1.0 V. The results suggest that the transition between a cathodic and anodic chemical reaction occurs over a very narrow potential range (-10 mV → +10 mV). The current remains independent of potential over the potential range investigated (i.e., 10 to 1000 mV and/or -10 to -1000 mV).

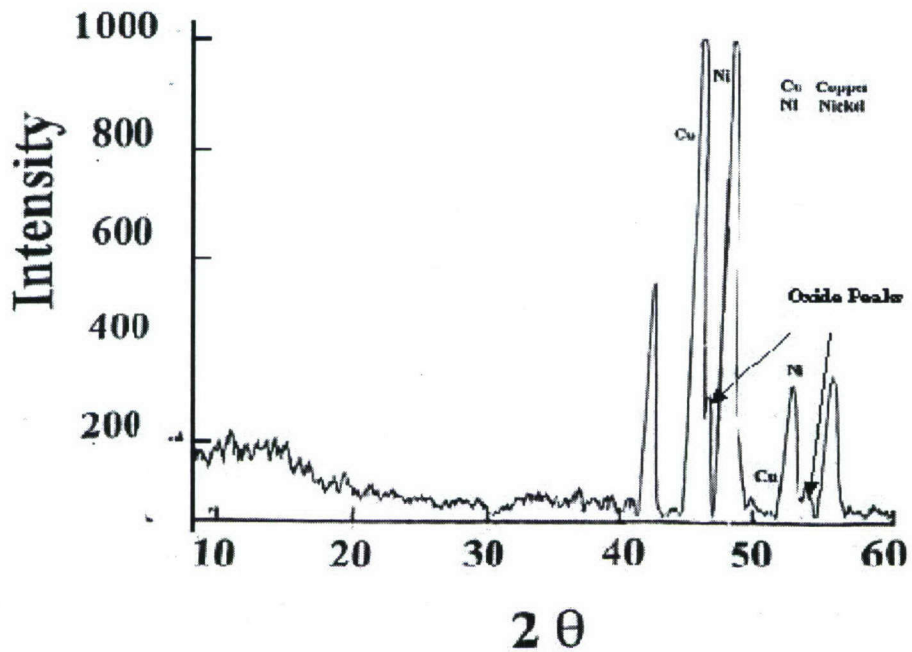

Figure 26. Typical x-ray diffraction pattern obtained from 90 % copper - 10 % nickel foil mounted on the electrochemical test cell.

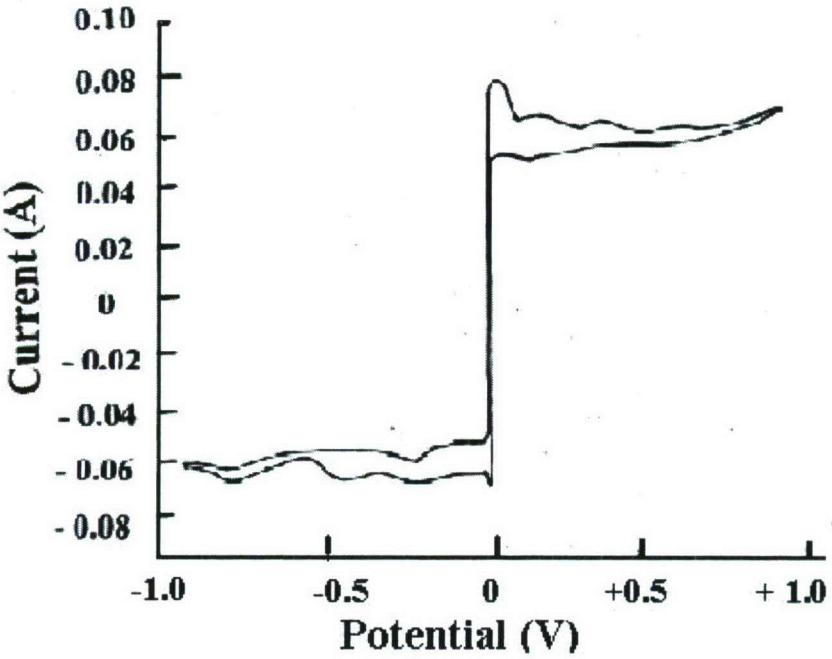

Figure 27. Current versus applied potential (versus reference potential (Ni/NiO)) plot of 90% copper -10% nickel/seawater system at room temperature.

XRD Results for Potentials of -500 mV and -100 mV

The in-situ XRD results for 90-10 copper-nickel foil in seawater are shown in Figures 28 thru 35. It was found that when a cathodic potential of either - 500 mV or -100 mV was applied, during the first 60 minutes, no significant changes were observed in the diffraction pattern. However, a careful examination of x-ray scans acquired for longer electrochemical reaction times (> 60 minutes exposure) revealed that the possible changes were masked by the system's background noise. After two hours, significantly measurable differences in the diffraction patterns were observed. Figures 28 thru 32 show x-ray diffraction patterns obtained after 1, 2, 4, 6, and ~ 24 hours of exposure to a constant potential of -500 mV, respectively. The clear electrolyte solution developed a light blue color after approximately 4 hours. Figures 33 thru 35 show x-ray diffraction patterns obtained after 2, 4, and 6 hours of exposure to a constant potential of -100 mV, respectively.

From the above x-ray diffraction results, a progression of the chemical reaction can be suggested as follows. When a constant negative potential (-500 or -100 mV) was continuously applied, the cathodic reaction progresses with the accumulation of OH at the cathode and the reaction at the alloy/seawater interface can be represented as follows:

$$NiOOH \Rightarrow Ni(OH)_2 \Rightarrow H_2 \uparrow, + Cu \Rightarrow Cu(OH)_2 \Rightarrow H_2 \uparrow$$

The x-ray diffraction results obtained during the present investigation indicate that, at negative potential (-500 mV and -100 mV) in addition to the presence of $Ni(OH)_2$, $Cu(OH)_2$ and $Cu_2O{\cdot}NiO$, there is a significant formation of NiOOH and CuO. Although the formation of $Ni(OH)_2$, $Cu(OH)_2$ are expected during electrochemical reaction at -500 and -100 mV, the observed presence of NiOOH, $Cu_2O{\cdot}NiO$, and CuO would not be expected.

The presence of NiOOH and CuO can be explained only if one assumes that immediately after the introduction of seawater into the electrochemical cell, the top layers of the 90-10 Cu-Ni that are in contact with the seawater underwent oxidation and formed NiOOH and CuO. As soon as the negative potential was applied, the cathodic reaction began. As a result, the NiOOH and CuO were reduced to form $Ni(OH)_2$ and $Cu(OH)_2$.

Thus, the reaction for nickel (oxide) is:

$$NiOOH \Rightarrow Ni(OH)_2 \Rightarrow H_2O \Rightarrow \tfrac{1}{2}\, H_2 \text{ gas} \uparrow + (OH)^-$$

$$NiO \Rightarrow Ni(OH)_2 \Rightarrow H_2O \Rightarrow \tfrac{1}{2}\, H_2 \text{ gas} \uparrow + (OH)^-$$

$$NiOOH \Rightarrow Ni(OH)_2 \Rightarrow H_2O \Rightarrow \tfrac{1}{2}\, H_2 \text{ gas} \uparrow + (OH)^-$$

Similarly, the reaction for copper (and copper oxide) can be suggested as:

$$Cu \Rightarrow Cu(OH)_2 \Rightarrow H_2O \Rightarrow \tfrac{1}{2}\, H_2 \text{ gas} \uparrow + (OH)^-$$

$$Cu_2O \Rightarrow Cu(OH)_2$$

$$CuO \Rightarrow Cu(OH)_2 \Rightarrow H_2O \Rightarrow \tfrac{1}{2}\, H_2 \text{ gas} \uparrow + (OH)^-$$

$$Cu_2O + NiO \Rightarrow Cu_2O{\cdot}NiO$$

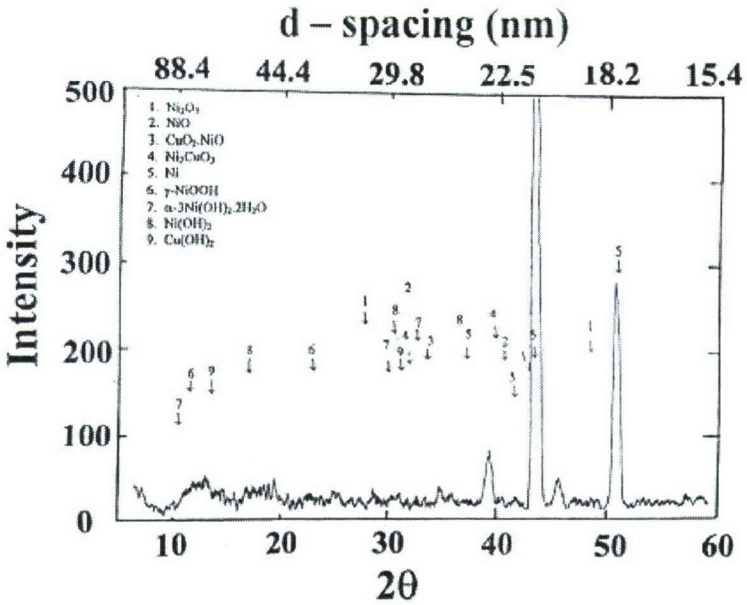

Figure 28. In-situ x-ray diffraction pattern obtained for 12.5 μm-thick (0.0005 in.) 90 -10 Cu - Ni foil mounted on the electrochemical test cell, after exposure to seawater for 1 hour at -500 mV versus a Ni/NiO electrode.

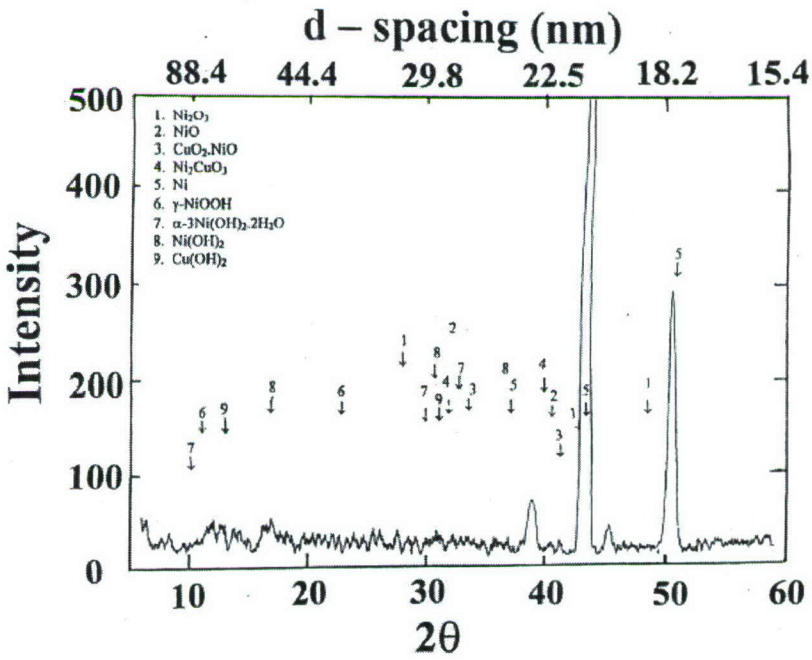

Figure 29. In-situ x-ray diffraction pattern obtained for 12.5 μm-thick (0.0005 in.) 90-10 Cu - Ni foil mounted on the electrochemical test cell, after exposure to the seawater for 2 hours at - 500 mV versus a Ni/NiO electrode.

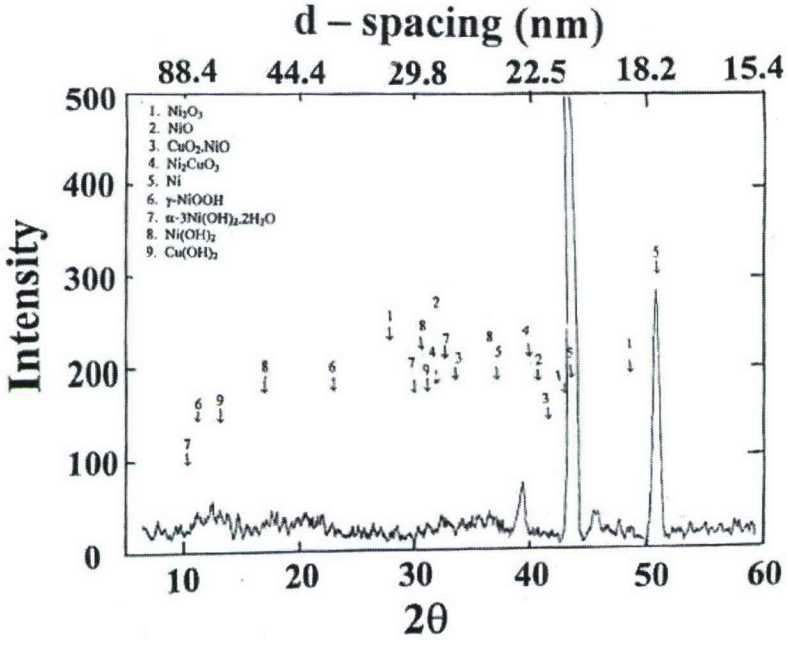

Figure 30. In-situ x-ray diffraction pattern obtained for 12.5 μm-thick (0.0005 in.) 90 - 10 Cu - Ni foil mounted on the electrochemical test cell, after exposure for 4 hours in seawater at - 500 mV versus a Ni/NiO electrode.

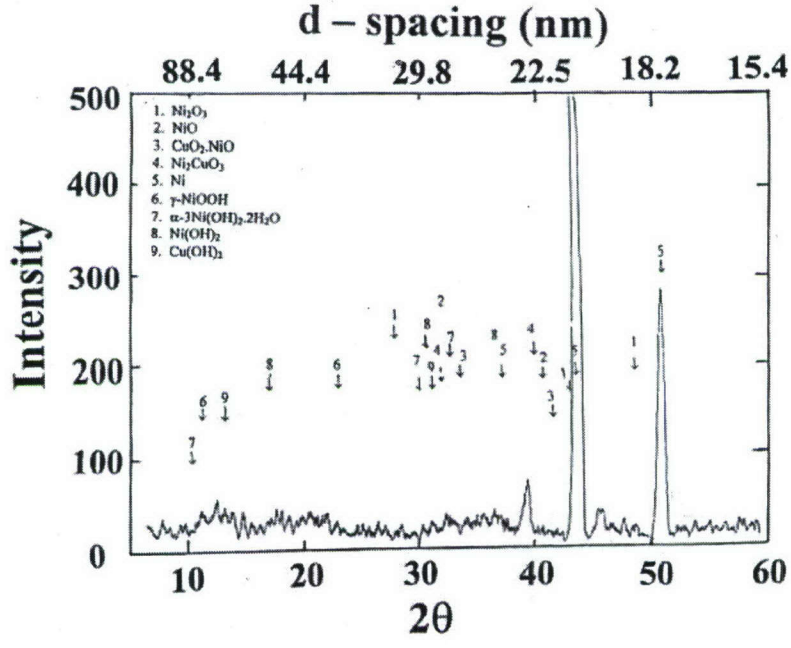

Figure 31. In-situ x-ray diffraction pattern obtained for 12.5 μm-thick (0.0005 in.) 90 - 10 Cu - Ni foil mounted on the electrochemical test cell, after exposure for 6 hours in seawater at - 500 mV versus a Ni/NiO electrode.

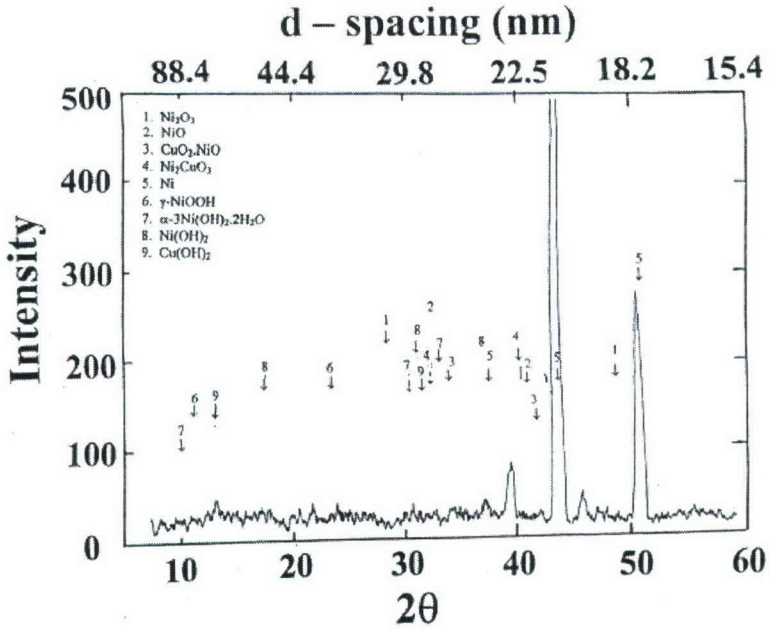

Figure 32. In-situ x-ray diffraction pattern obtained for 12.5 μm-thick (0.0005 in.) 90 - 10 Cu - Ni foil mounted on the electrochemical test cell, after exposure for 24 hours in seawater at - 500 mV versus a Ni/NiO electrode.

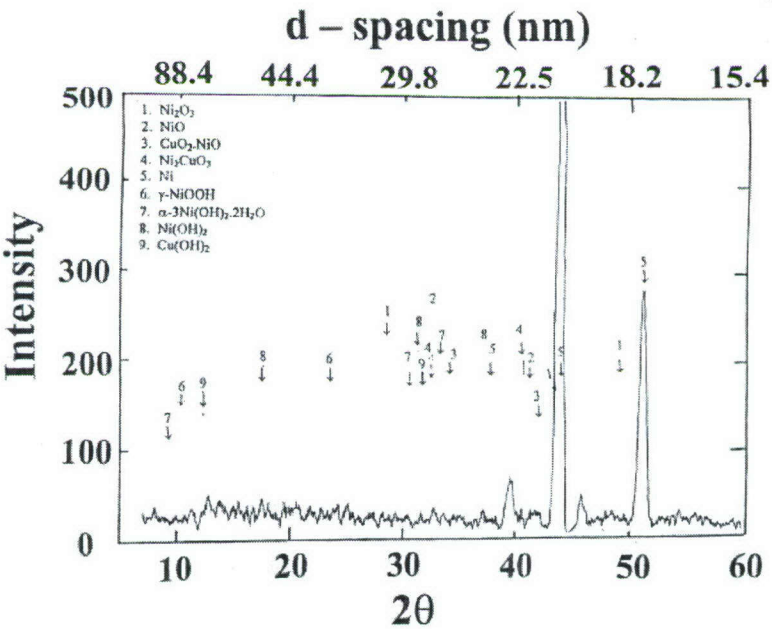

Figure 33. In-situ x-ray diffraction pattern obtained for 12.5 μm-thick (0.0005 in.) 90 - 10 Cu - Ni foil mounted on the electrochemical test cell, after exposure for 2 hours in seawater at -100 mV versus a Ni/NiO electrode.

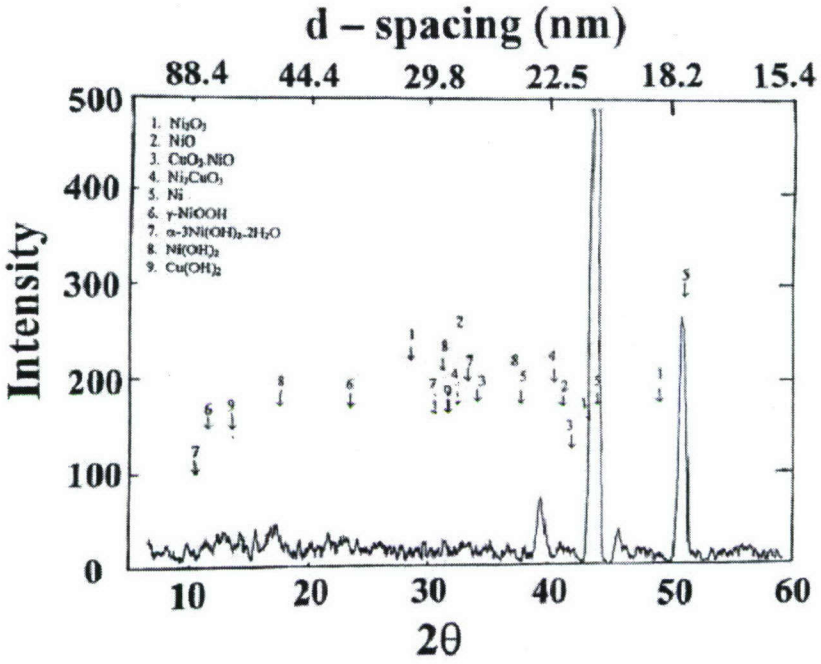

Figure 34. In-situ x-ray diffraction pattern obtained for 12.5 μm-thick (0.0005 in.) 90 -10 Cu - Ni foil mounted on the electrochemical test cell, after exposure for 4 hours in seawater at - 100 mV versus a Ni/NiO electrode.

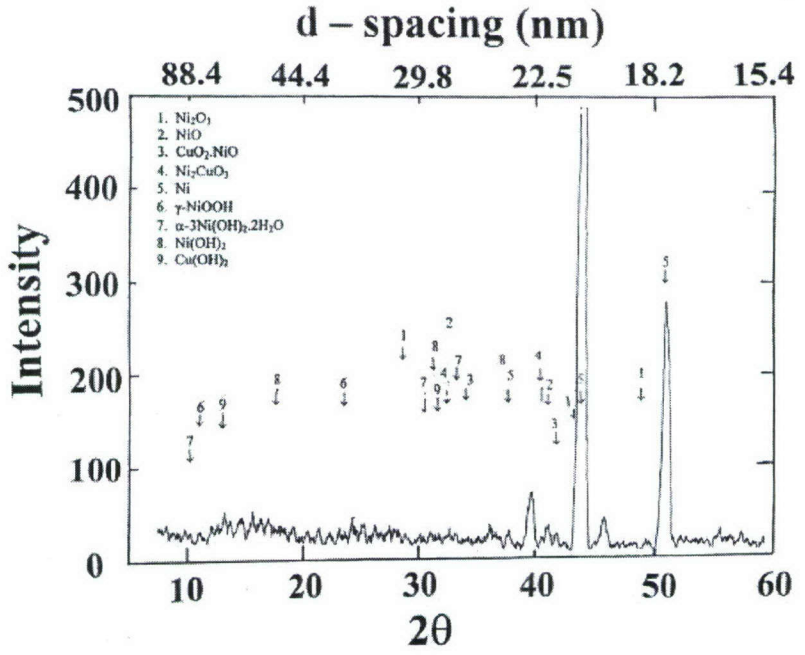

Figure 35. In-situ x-ray diffraction pattern obtained for 12.5 μm-thick (0.0005 in.) 90 - 10 Cu - Ni foil mounted on the electrochemical test cell, after exposure for 6 hours in seawater at -100 mV versus a Ni/NiO electrode.

XPS Results for Potential of -500 mV

Figures 36, 37, and 38 show typical XPS spectra for copper, nickel, and oxygen obtained from the test foil that had been subjected to -500 mV in seawater solution. The results in Figures 36 and 37 suggest that $Cu(OH)_2$, and $Ni(OH)_2$ are present in the outer passive layer along with CuO and NiO. The detected structure of oxygen at 528.5 and 531.5 eV in Figure 38 corresponds to the oxygen associated with $Ni(OH)_2$ and NiO respectively.

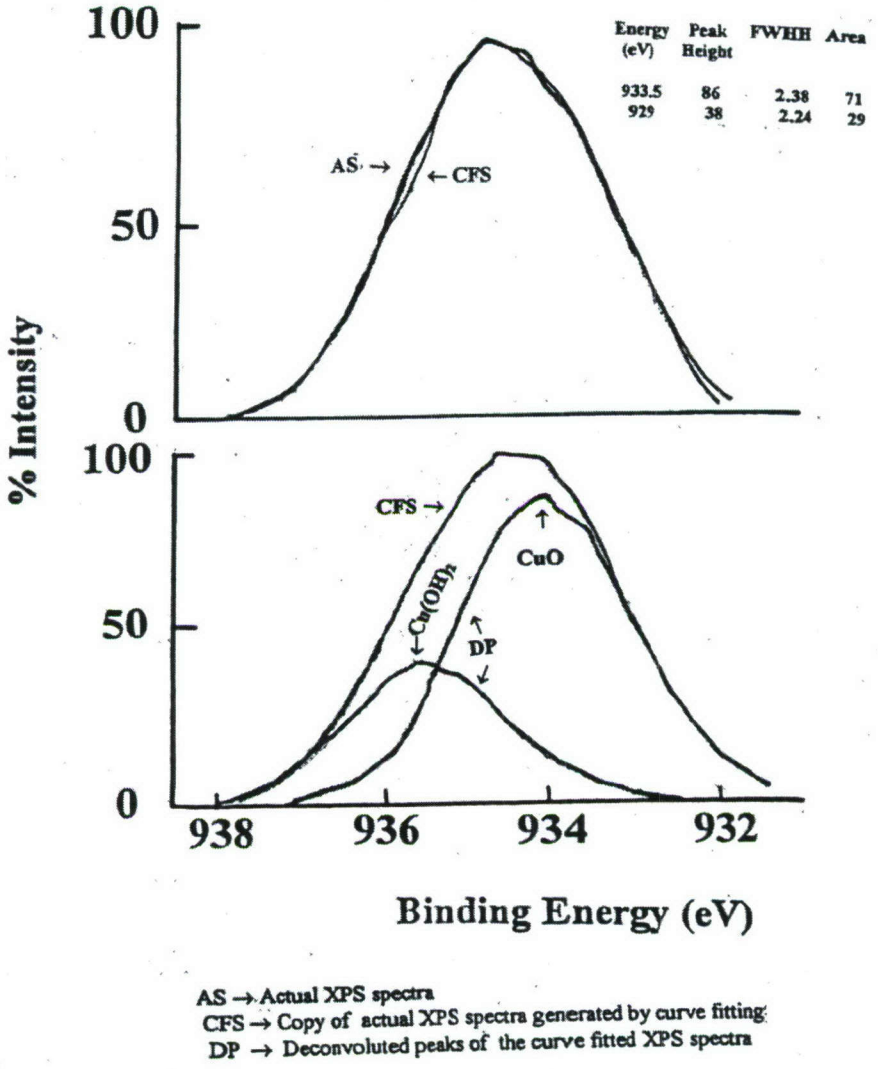

Figure 36. Copper peaks obtained from XPS analysis of 12.5 μm-thick (0.0005 in.) 90 -10 Cu - Ni foil surface exposed to the seawater at -500 mV for 24 hours.

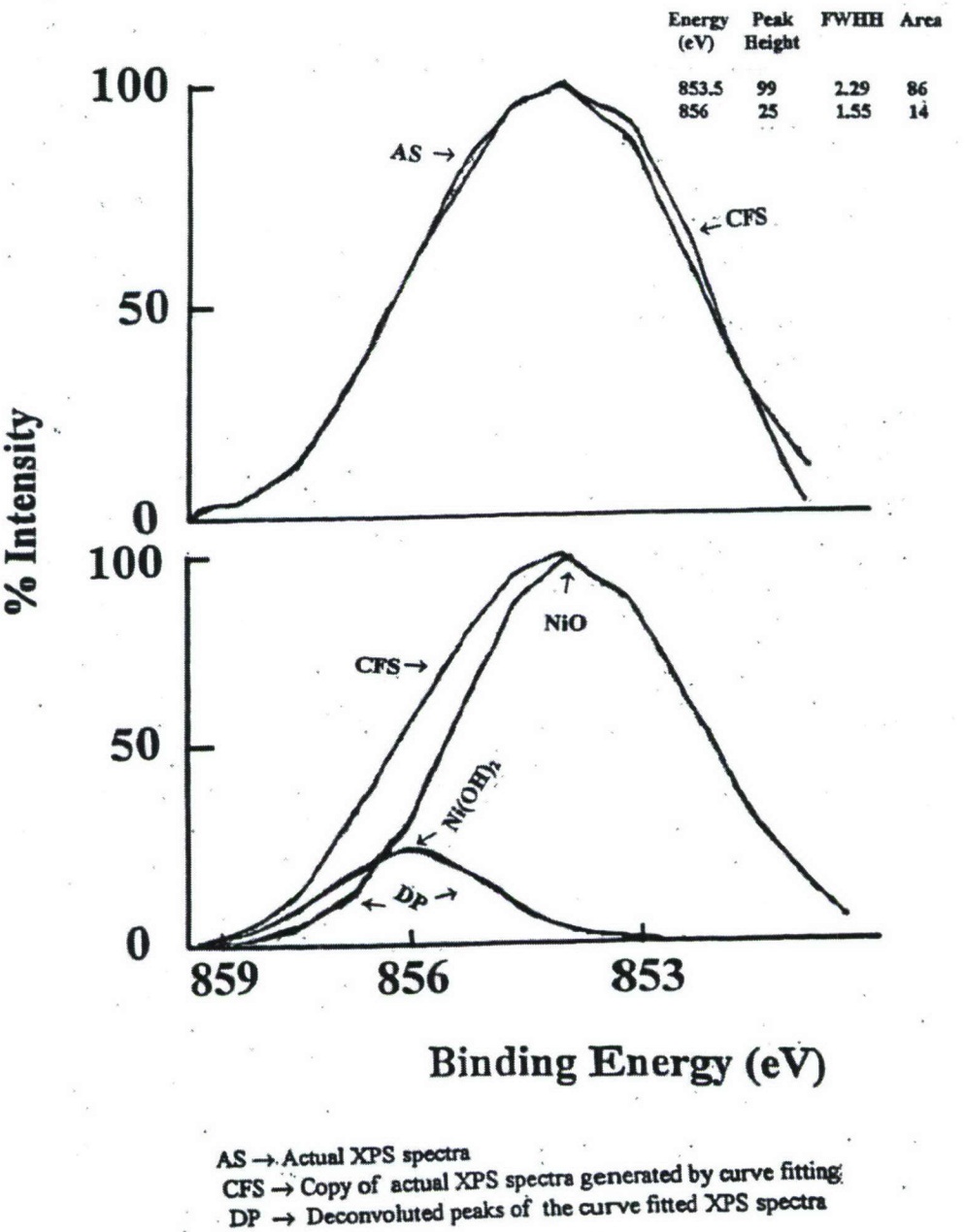

Figure 37. Nickel peaks obtained from XPS analysis of 12.5 μm-thick (0.0005 in.) 90 - 10 Cu - Ni foil surface exposed to the seawater at -500 mV for 24 hours.

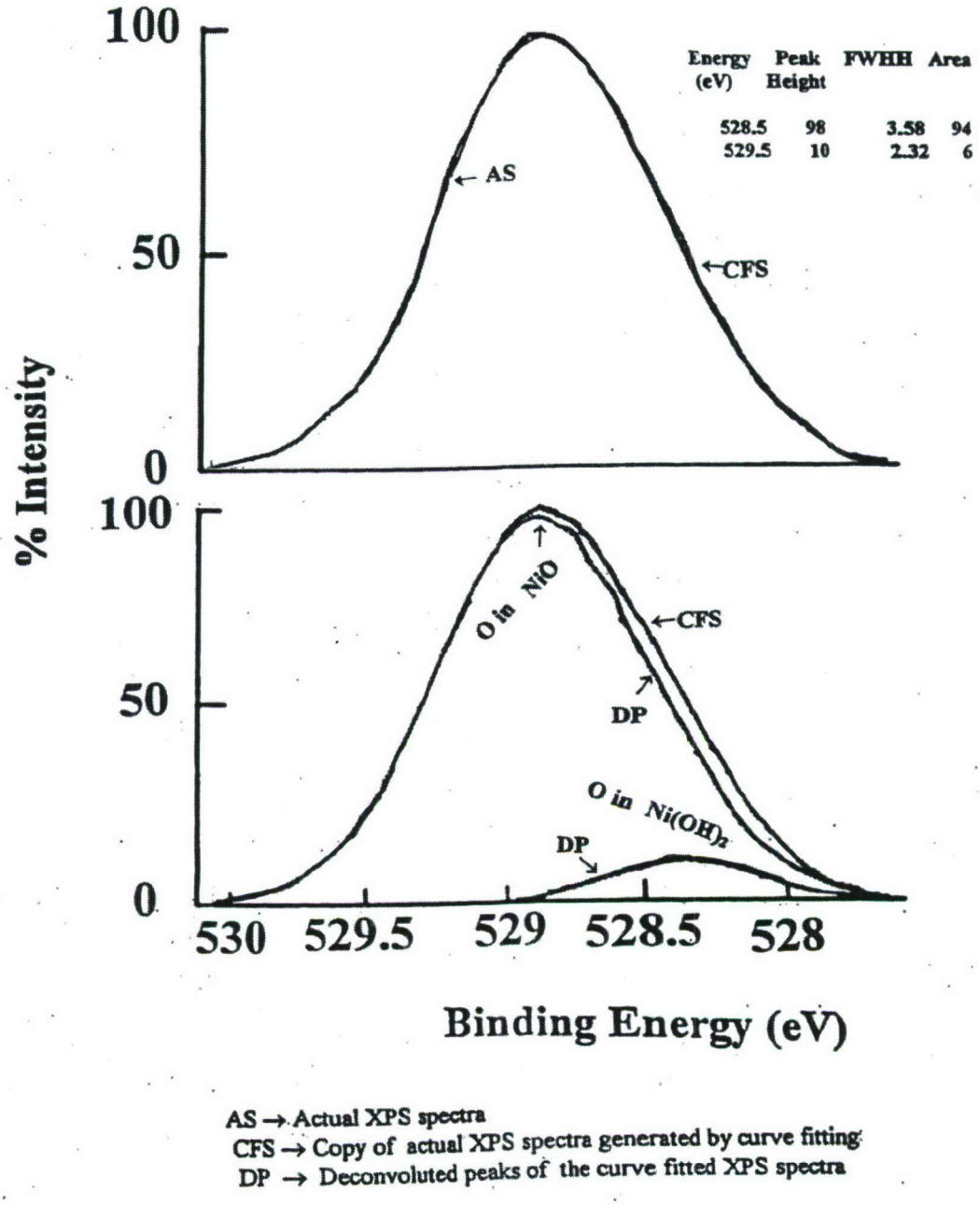

Figure 38. Oxygen peaks obtained from XPS analysis of 12.5 μm-thick (0.0005 in.) 90 - 10 Cu - Ni foil surface exposed to the seawater at -500 mV for 24 hours.

XRD Results for Potentials of + 500 mV and +100 mV

The results on the 90-10 Cu-Ni foils subjected to +500 mV and +100 mV following the in-situ x-ray diffraction studies are shown in Figures 39 to 43 and 44 to 46, respectively. The figures correspond to the measurements made at time intervals of 1 hour (Figure 39), 2 hours (Figure 40), 4 hours (Figure 41), 6 hours (Figure 42), and 24 hours (Figure 43) hours in seawater at +500 mV and 2 hours (Figure 44) , 4 hours (Figure 45) and 6 hours (Figure 46) at +100 mV hours exposure to seawater at +100 mV. The x-ray diffraction results indicate that the interface of 90 -10 Cu-Ni/seawater consists of NiO, Ni_2O_3, Ni_2CuO_3, NiOOH, $Ni(OH)_2$, NiO, $Cu(OH)_2$ and CuO. From the above results, it can be suggested that the 90-10 Cu-Ni foil is oxidized, and both Ni^{+3} and Ni^{+2} states of nickel and Cu^{+1} and Cu^{+2} states of copper are present at the interface.

Therefore, it can be postulated that the electrochemical anodic reaction for 90-10 Cu-Ni in seawater at +500 mV and +100 mV follow the typically expected steps:

The reaction for nickel at +500 and +100 mV is:

$$Ni \Rightarrow Ni(OH)_2 \Rightarrow NiOOH \Rightarrow Ni_2O_3 \Rightarrow NiO$$

and for copper (and or oxide) the reactions can be expressed as:

$$Cu \Rightarrow Cu(OH)_2 \Rightarrow CuO$$

$$Cu_2O \Rightarrow CuO$$

$$CuO + NiO \Rightarrow Cu_2 \cdot NiO$$

XPS Results for Potential of + 500 mV

Figures 47 to 49 show XPS spectra for copper, nickel and oxygen obtained from test foils after corrosion testing at +500 mV in seawater solution for 24 hours. The results for the electrochemical reaction of 90-10 Cu-Ni foil at +500 mV in seawater suggest that the copper close to the surface is chemically transformed to $Cu(OH)_2$ and CuO.

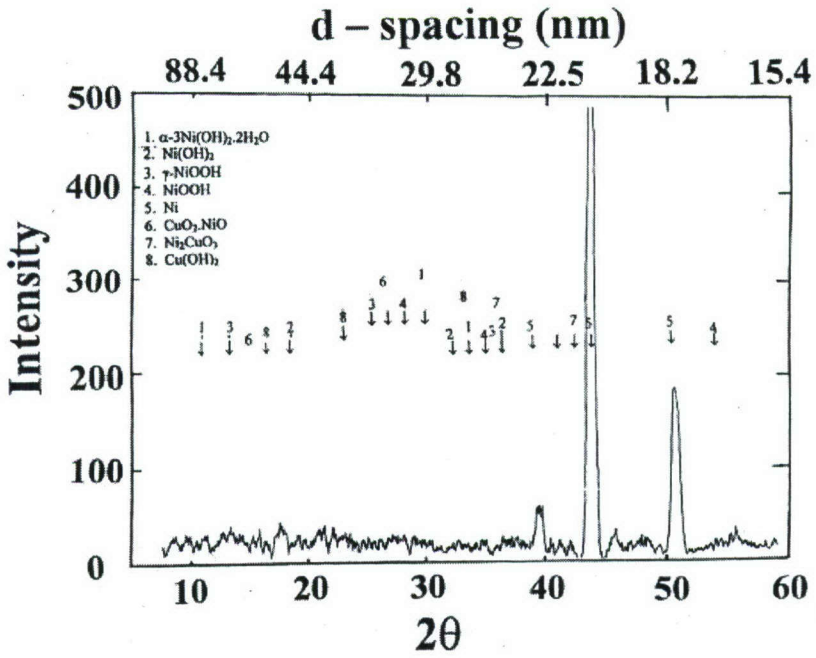

Figure 39. In-situ x-ray diffraction pattern obtained for 12.5 μm-thick (0.0005 in.) 90 - 10 Cu - Ni foil mounted on the electrochemical test cell, after exposure for 1 hour in seawater at + 500 mV versus a Ni/NiO electrode.

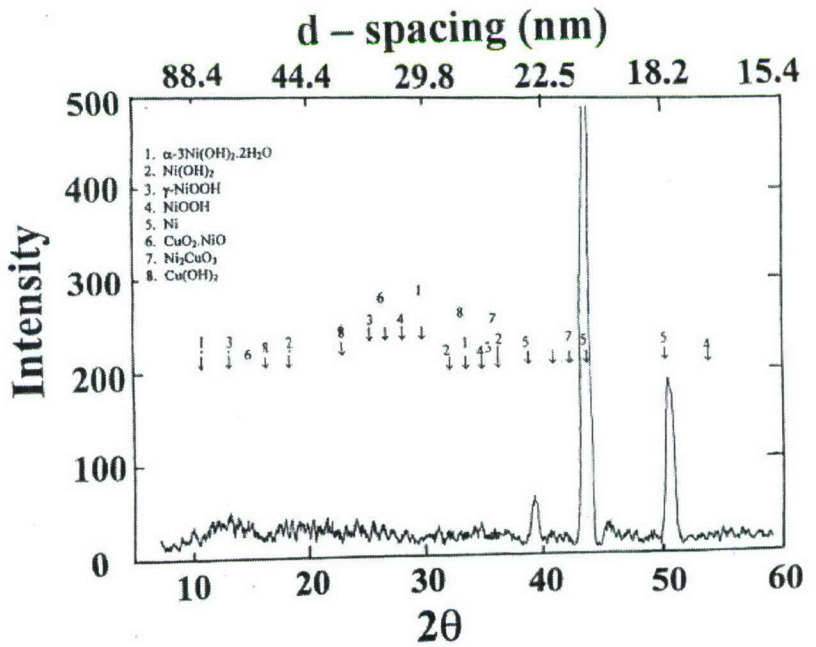

Figure 40. In-situ x-ray diffraction pattern obtained for 12.5 μm-thick (0.0005 in.) 90 -10 Cu - Ni foil mounted on the electrochemical test cell, after exposure for 2 hours in seawater at + 500 mV versus a Ni/NiO electrode.

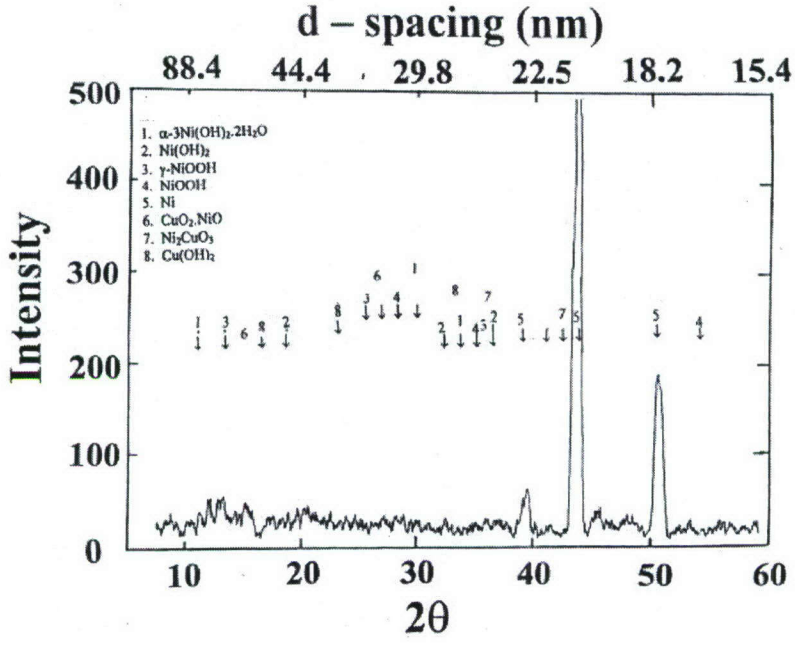

Figure 41. In-situ x-ray diffraction pattern obtained for 12.5 μm-thick (0.0005 in.) 90 - 10 Cu - Ni foil mounted on the electrochemical test cell, after exposure for 4 hours in seawater at + 500 mV versus a Ni/NiO electrode.

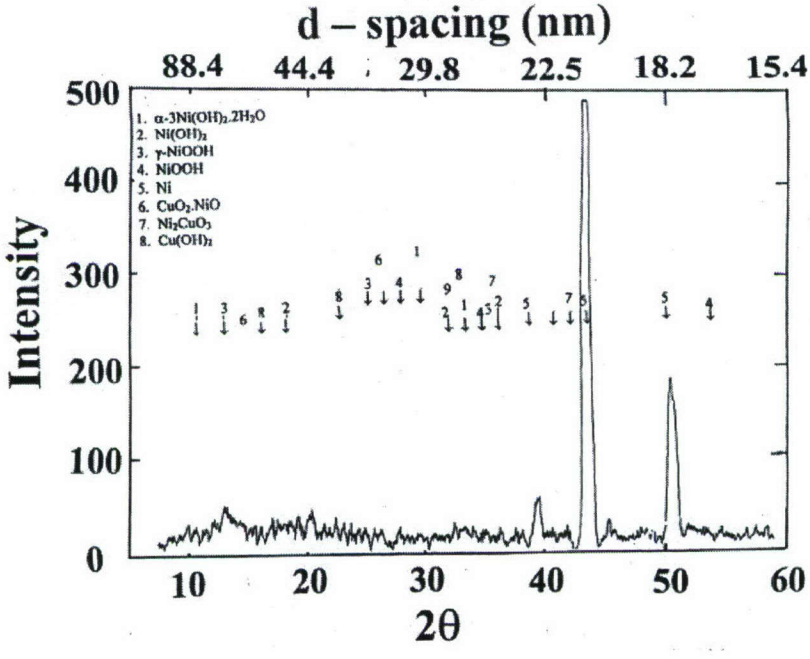

Figure 42. In-situ x-ray diffraction pattern obtained for 12.5 μm-thick (0.0005 in.) 90 - 10 Cu - Ni foil mounted on the electrochemical test cell, after exposure for 6 hours in seawater at +500 mV versus a Ni/NiO electrode.

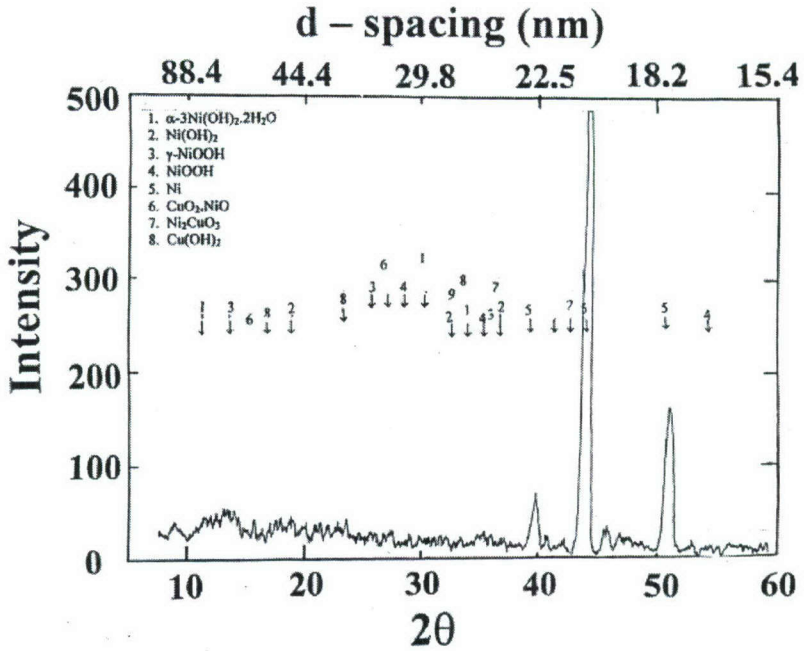

Figure 43. In-situ x-ray diffraction pattern obtained for 12.5 μm-thick (0.0005 in.) 90 - 10 Cu - Ni foil mounted on the electrochemical test cell, after exposure for 24 hours in seawater at +500 mV versus a Ni/NiO electrode.

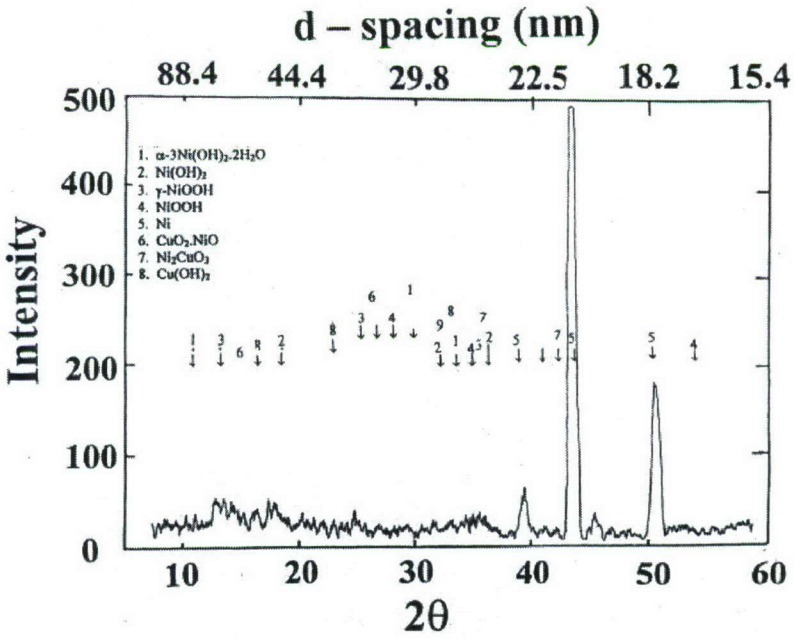

Figure 44. In-situ x-ray diffraction pattern obtained for 12.5 μm-thick (0.0005 in.) 90 - 10 Cu - Ni foil mounted on the electrochemical test cell, after exposure for 2 hours in seawater at +100 mV versus a Ni/NiO electrode.

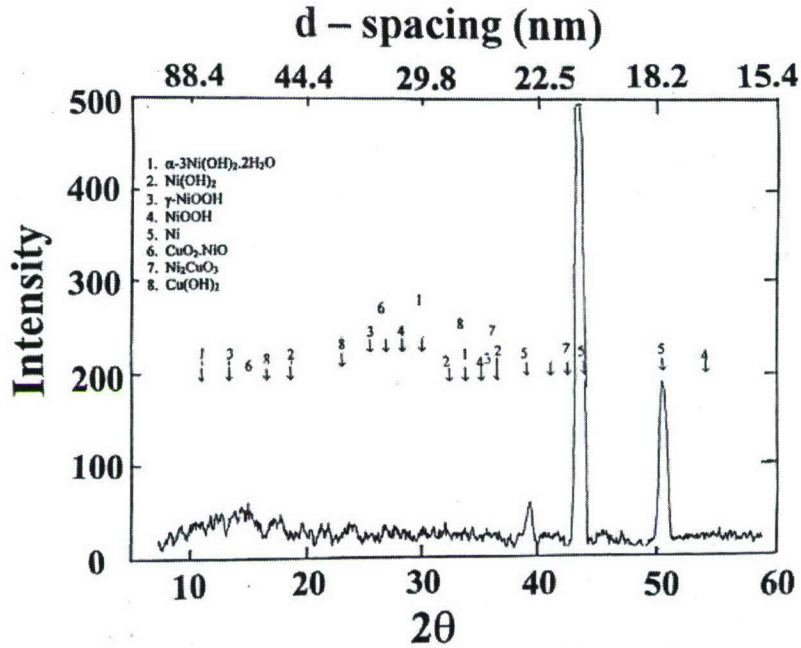

Figure 45. In-situ x-ray diffraction pattern obtained for 12.5 μm-thick (0.0005 in.) 90 - 10 Cu - Ni foil mounted on the electrochemical test cell, after exposure for 4 hours in seawater at +100 mV versus a Ni/NiO electrode.

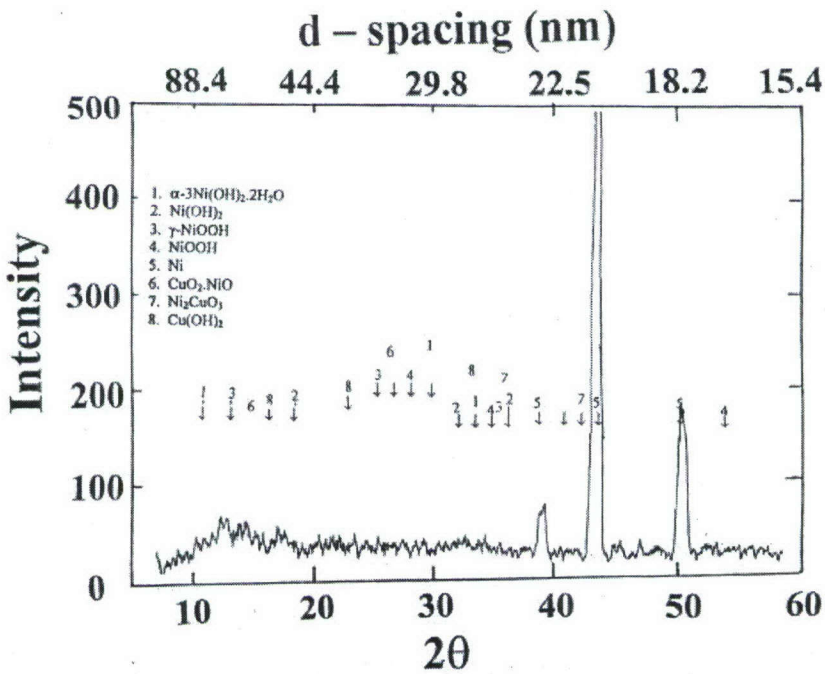

Figure 46. In-situ x-ray diffraction pattern obtained for 12.5 μm-thick (0.0005 in.) 90 - 10 Cu - Ni foil mounted on the electrochemical test cell, after exposure for 6 hours in seawater at +100 mV versus a Ni/NiO electrode.

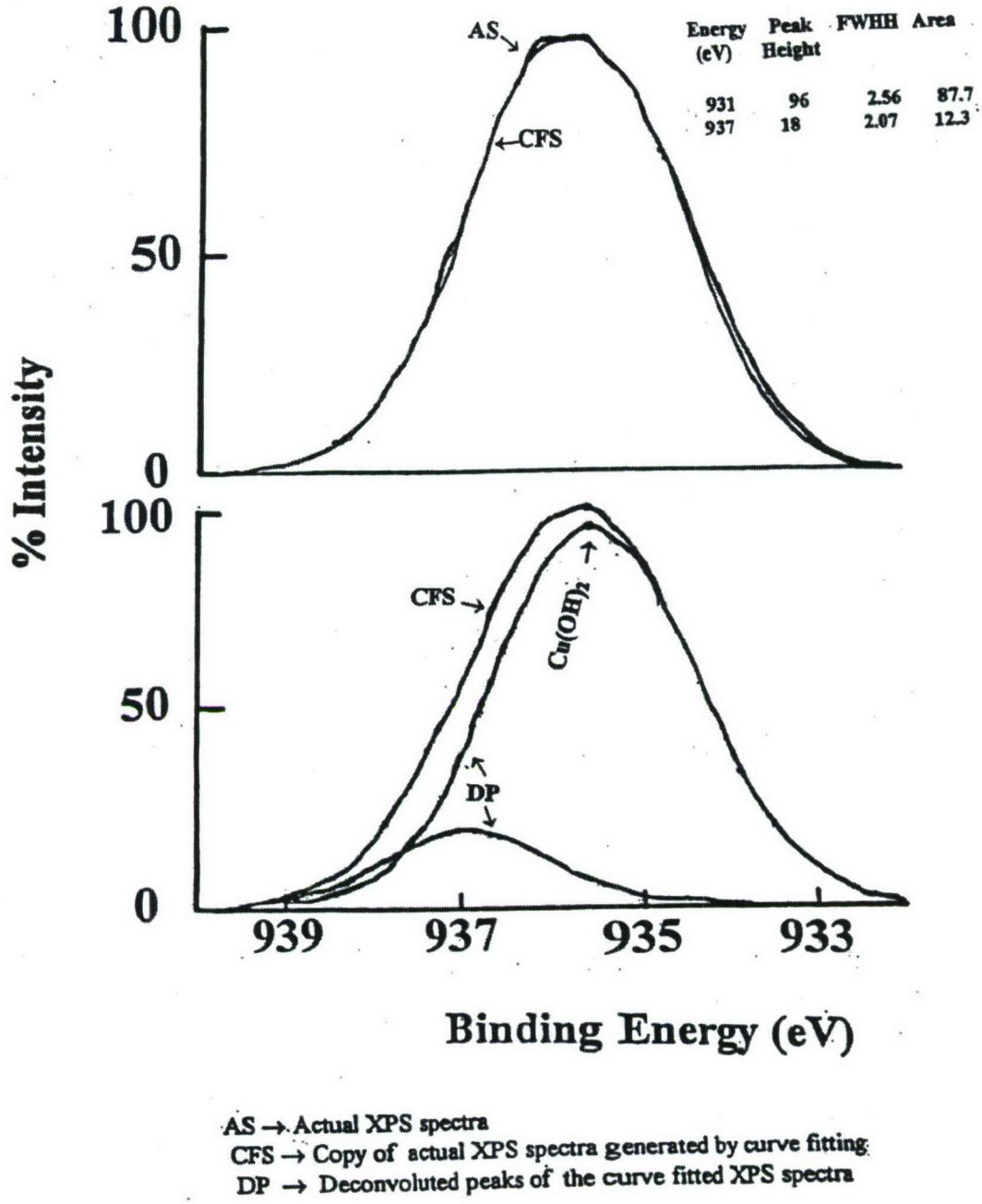

Figure 47. Copper peaks obtained from XPS analysis of 12.5 μm-thick (0.0005 in.) 90 -10 Cu - Ni foil surface exposed to the seawater at +500 mV for 24 hours.

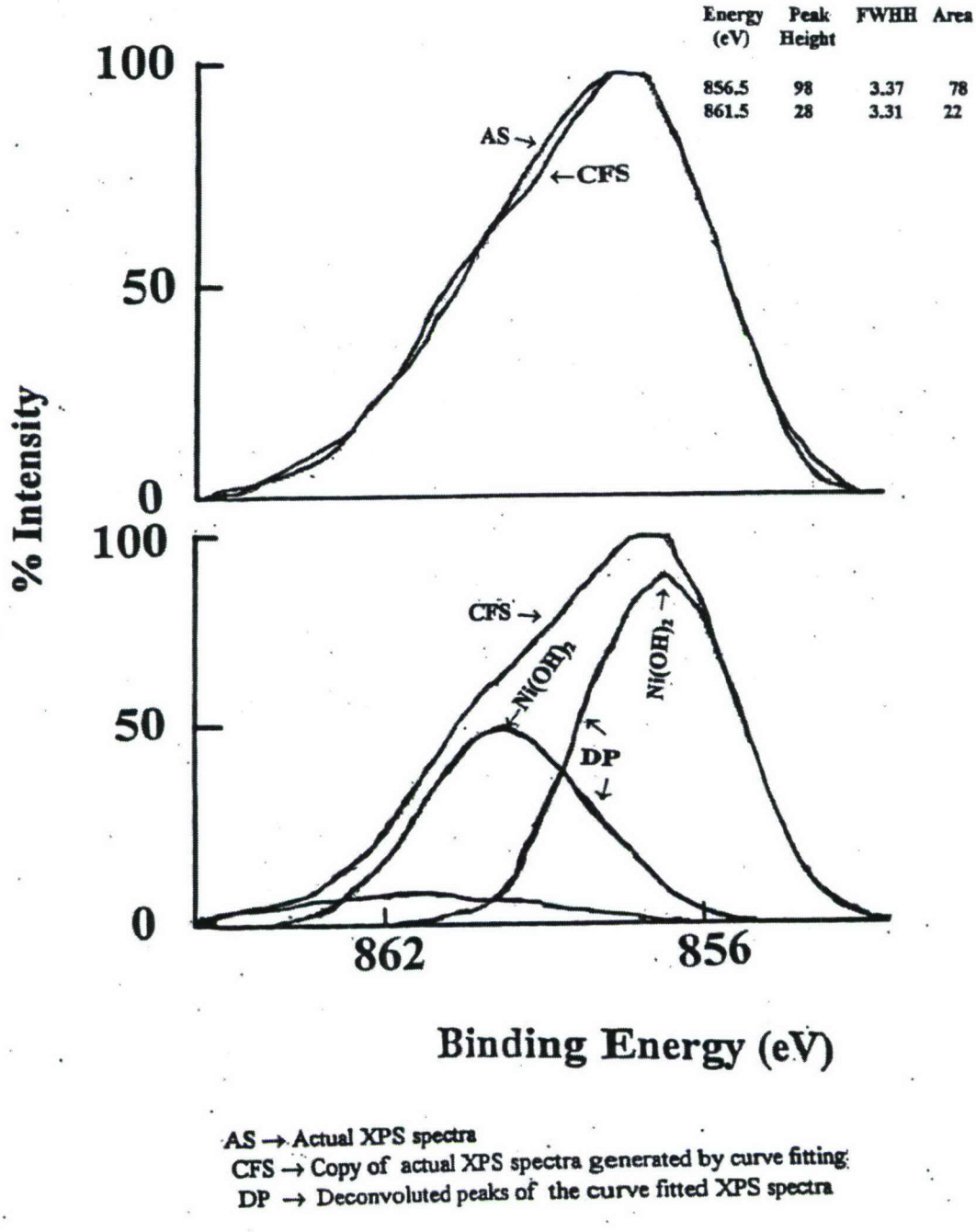

Figure 48. Nickel peaks obtained from XPS analysis of 12.5 μm-thick (0.0005 in.) 90 -10 Cu - Ni foil surface exposed to the seawater at +500 mV for 24 hours.

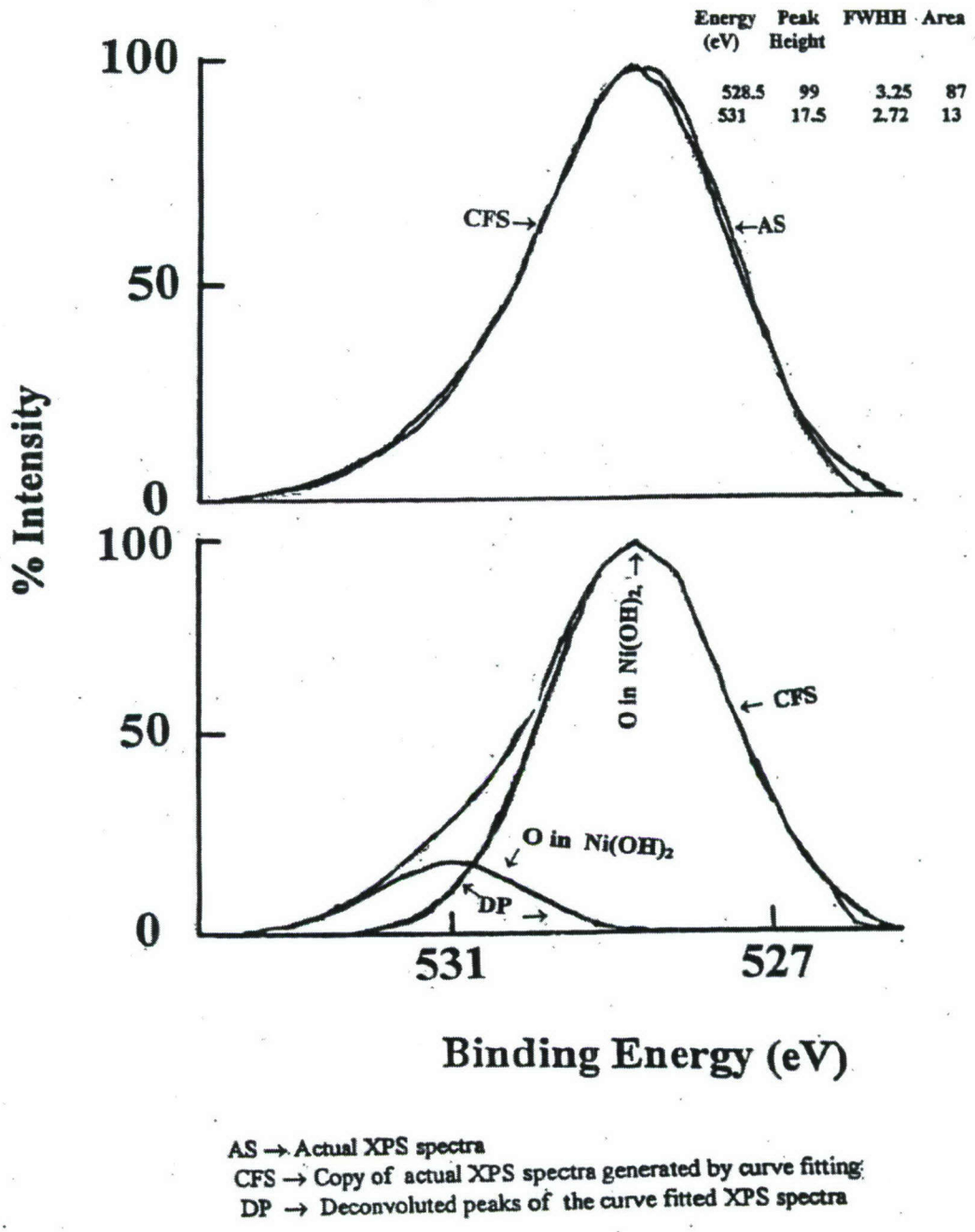

Figure 49. Oxygen peaks obtained from XPS analysis of 12.5 μm-thick (0.0005 in.) 90 - 10 Cu - Ni foil surface exposed to the seawater at +500 mV for 24 hours

70-30 Cu-Ni -Seawater System

Figure 50 shows a typical x-ray diffraction pattern obtained from a 12.5 m-thick (0.0005 in.) 70-30 Cu-Ni foil mounted on the test cell. The results suggest that the sample surfaces are not significantly oxidized.

Figure 51 shows a typical current versus applied potential plot of 70 - 30 Cu - Ni foil in seawater solution as it cycles once through from -1000 mV → +1000 mV → -1000 mV. The results (shown in Figure 51) suggest that the transition between a cathodic and anodic chemical reaction occurs over a very narrow potential range (-10 mV to +10 mV). The current remains independent of potential over the potential range investigated, i.e., 10 to 1000 mV and/or -10 to -1000 mV.

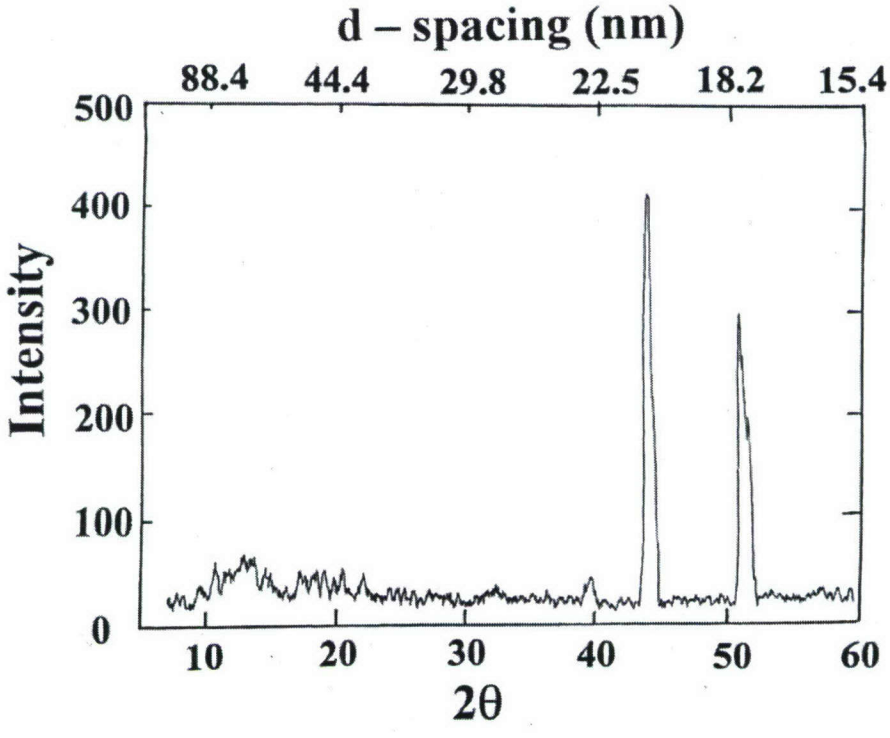

Figure 50. Typical x-ray diffraction pattern obtained from 70 % copper - 30 % nickel foil mounted on the electrochemical test cell.

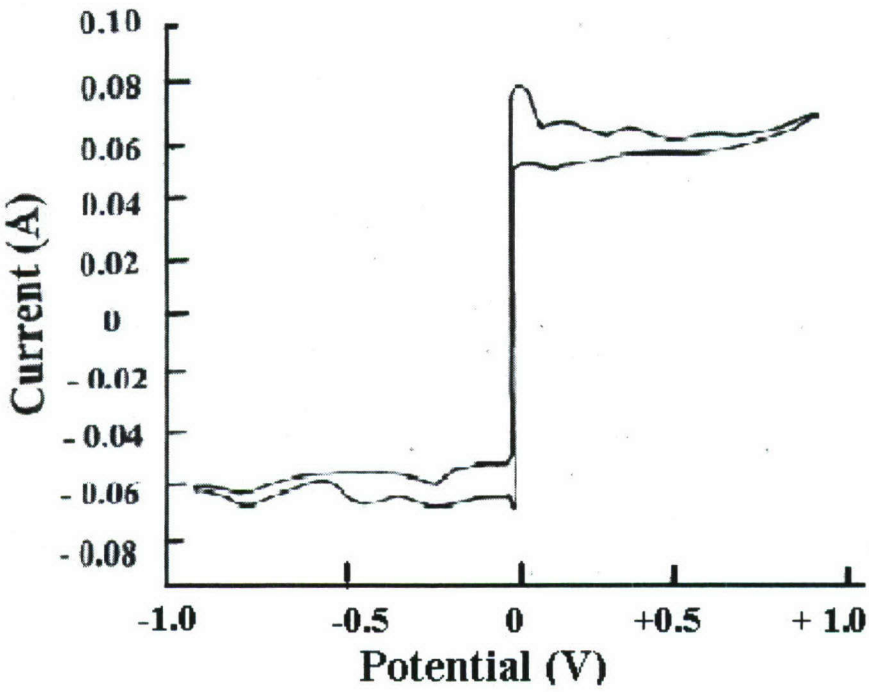

Figure 51. Current versus applied potential (versus reference potential) plot of 70 % copper - 30 % nickel/seawater system at room temperature.

XRD Results for Potentials of -500 mV and -100 mV

It was found that when a cathodic potential of either -500 mV or -100 mV was applied, during the first 60 minutes, no significant changes were observed in the diffraction pattern. After one hour, significantly measurable differences in the diffraction patterns were observed. Figures 52 thru 56 show typical x-ray diffraction patterns obtained after 1, 2, 4, 6, and 24 hours of exposure to a constant potential of - 500 mV, respectively. The diffraction patterns were analyzed. It was found that, apart from the initial hydrogen gas evolution (that was observed in all samples initially), the peaks for $Ni(OH)_2$ and CuO_2NiO underwent appreciable increase, while the peaks for NiOOH decreased with the exposure time. Figures 57 thru 60 show typical x-ray diffraction patterns obtained after 2, 4, 6 and 8 hours of exposure to a constant potential of -100 mV, respectively.

From the above x-ray diffraction results, a progression of the chemical reaction can be suggested. When a constant negative potential is applied (-500 mV or -100 mV), the cathodic reaction progresses with the accumulation of OH at the cathode and the interface reactions are:

$$Ni \Rightarrow Ni(OH)_2 \Rightarrow H_2 \uparrow$$

$$Cu \Rightarrow Cu(OH)_2 \Rightarrow H_2 \uparrow$$

$$H_2O \Rightarrow OH^- + \tfrac{1}{2} H_2 \uparrow$$

The x-ray diffraction results obtained during the present investigation indicate that at the negative potentials (- 500 and - 100 mV), the amount of NiOOH decreased with time. A similar electrochemical behavior, i.e. a decrease in the amount of NiOOH with time, was observed for nickel in Ni - KOH system [13-15].

The decrease in the concentration of NiOOH and an increase in the concentration of $Ni(OH)_2$, $Cu(OH)_2$ and $Cu_2O{\cdot}NiO$ can be explained only if one assumes that some NiOOH and CuO films were formed on the immersed metal/alloy surface even before the start of the electrochemical reaction. As soon as the negative potentials (-500 and -100 mV) were applied, the cathodic reaction began. As a result, the NiOOH and CuO were reduced to $Ni(OH)_2$ and $Cu(OH)_2$. Therefore, one can postulate that the electrochemical cathodic reaction for the 70-30 Cu-Ni in seawater at -500 mV and -100 mV to follow the typically expected steps:

For the nickel (and nickel oxide):

$$NiOOH \Rightarrow Ni(OH)_2 \Rightarrow H_2O \Rightarrow \tfrac{1}{2} H_2 \text{ gas} \uparrow + (OH)^-$$

$$Ni \Rightarrow Ni(OH)_2 \Rightarrow H_2O \Rightarrow \tfrac{1}{2} H_2 \text{ gas} \uparrow + (OH)^-$$

$$NiO \Rightarrow Ni(OH)_2 \Rightarrow H_2O \Rightarrow \tfrac{1}{2} H_2 \text{ gas} \uparrow + (OH)^-$$

and for copper (and copper oxide):

$$CuO \Rightarrow Cu(OH)_2 \Rightarrow H_2O \Rightarrow \tfrac{1}{2} H_2 \text{ gas} \uparrow + (OH)^-$$

$$Cu \Rightarrow Cu(OH)_2 \Rightarrow H_2O \Rightarrow \tfrac{1}{2} H_2 \text{ gas} \uparrow + (OH)^-$$

$$Cu_2O \Rightarrow Cu(OH)_2$$

$$Cu_2O + NiO \Rightarrow Cu_2O{\cdot}NiO$$

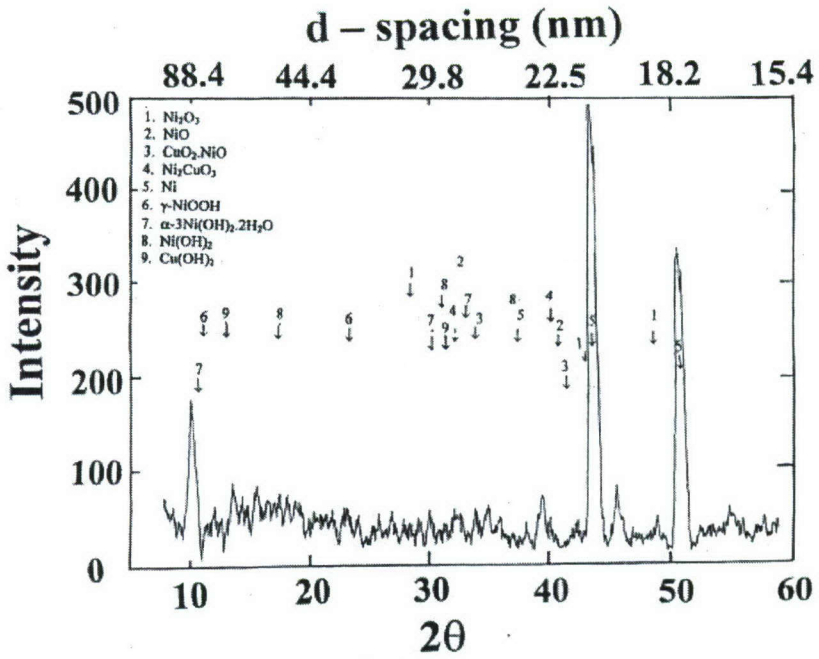

Figure 52. In-situ x-ray diffraction pattern obtained for 12.5 μm-thick (0.0005 in.) 70 - 30 Cu - Ni foil mounted on the electrochemical test cell, after exposure for 1 hour in seawater at -500 mV versus a Ni/NiO electrode.

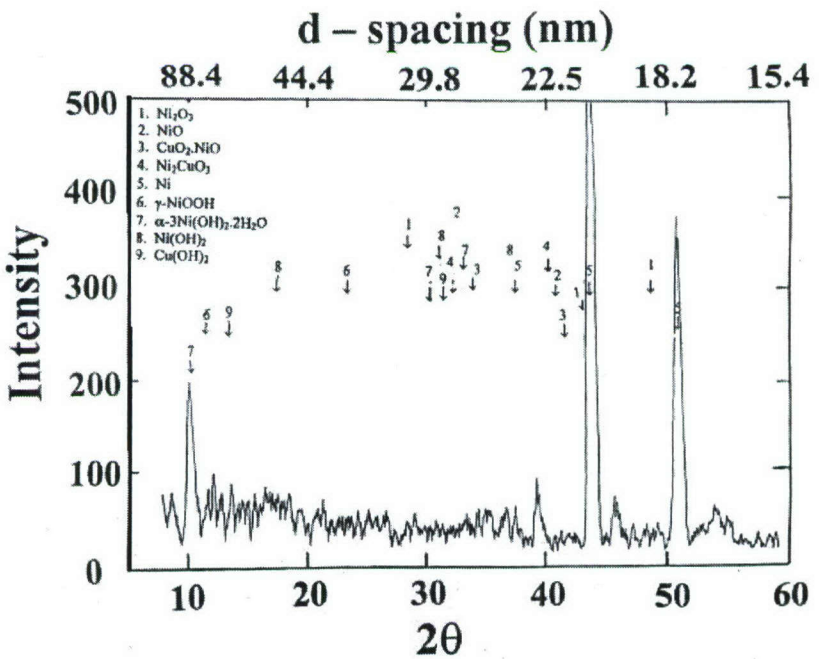

Figure 53. In-situ x-ray diffraction pattern obtained for 12.5 μm-thick (0.0005 in.) 70 - 30 Cu - Ni foil mounted on the electrochemical test cell, after exposure for 2 hours in seawater at -500 mV versus a Ni/NiO electrode.

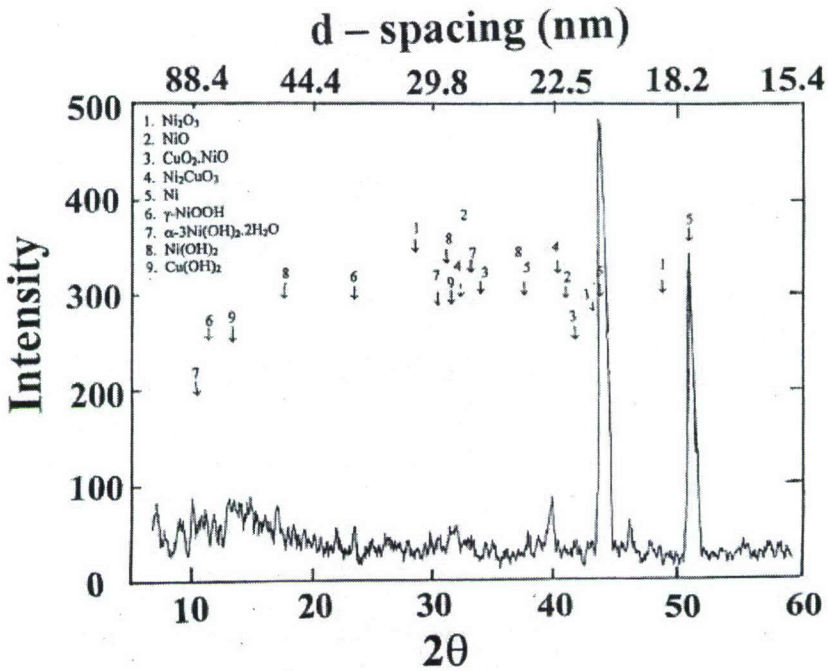

Figure 54. In-situ x-ray diffraction pattern obtained for 12.5 μm-thick (0.0005 in.) 70 - 30 Cu - Ni foil mounted on the electrochemical test cell, after exposure for 4 hours in seawater at -500 mV versus a Ni/NiO electrode.

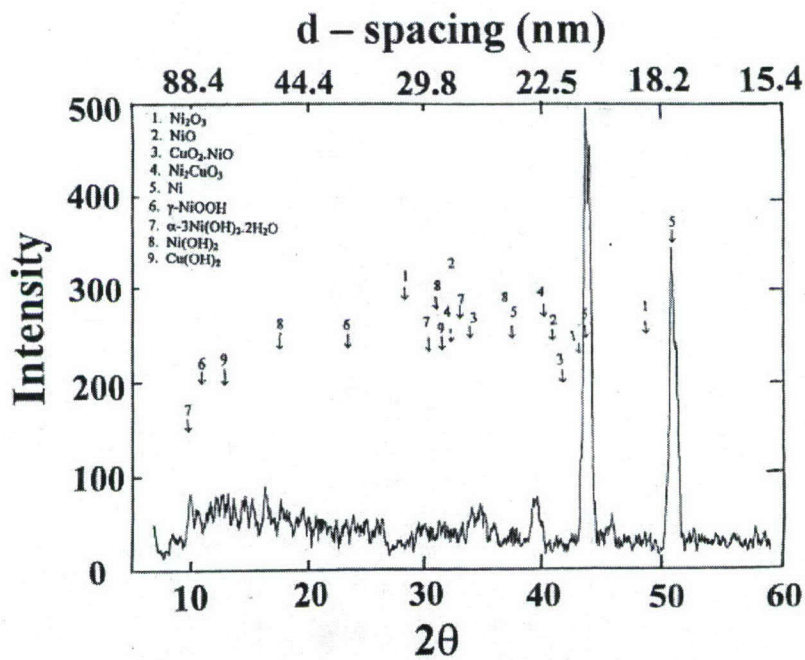

Figure 55. In-situ x-ray diffraction pattern obtained for 12.5 μm-thick (0.0005 in.) 70 - 30 Cu - Ni foil mounted on the electrochemical test cell, after exposure for 6 hours in seawater at - 500 mV versus a Ni/NiO electrode.

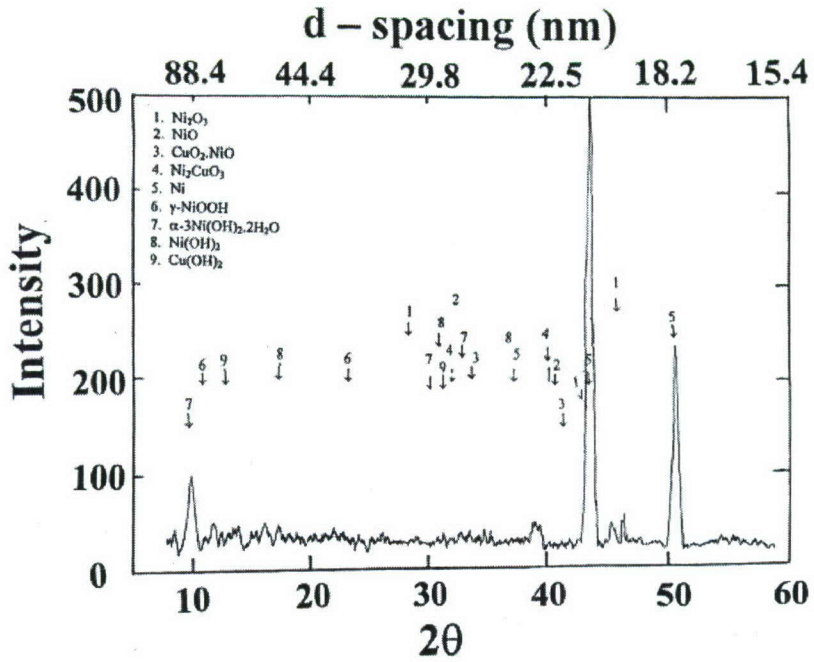

Figure 56. In-situ x-ray diffraction pattern obtained for 12.5 μm-thick (0.0005 in.) 70 - 30 Cu - Ni foil mounted on the electrochemical test cell, after exposure for 24 hours in seawater at - 500 mV versus a Ni/NiO electrode.

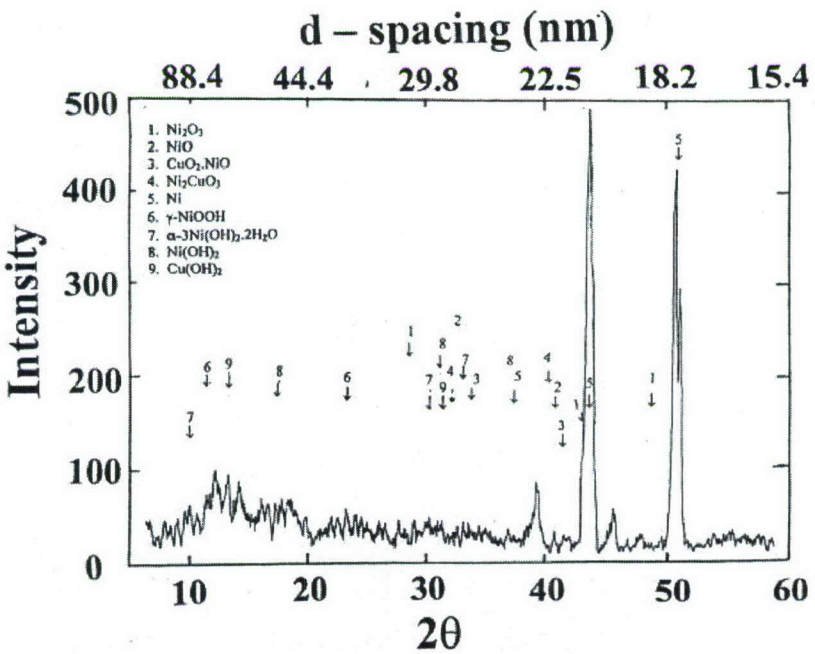

Figure 57. In-situ x-ray diffraction pattern obtained for 12.5 μm-thick (0.0005 in.) 70 - 30 Cu - Ni foil mounted on the electrochemical test cell, after exposure for 2 hours in seawater at -100 mV versus a Ni/NiO electrode.

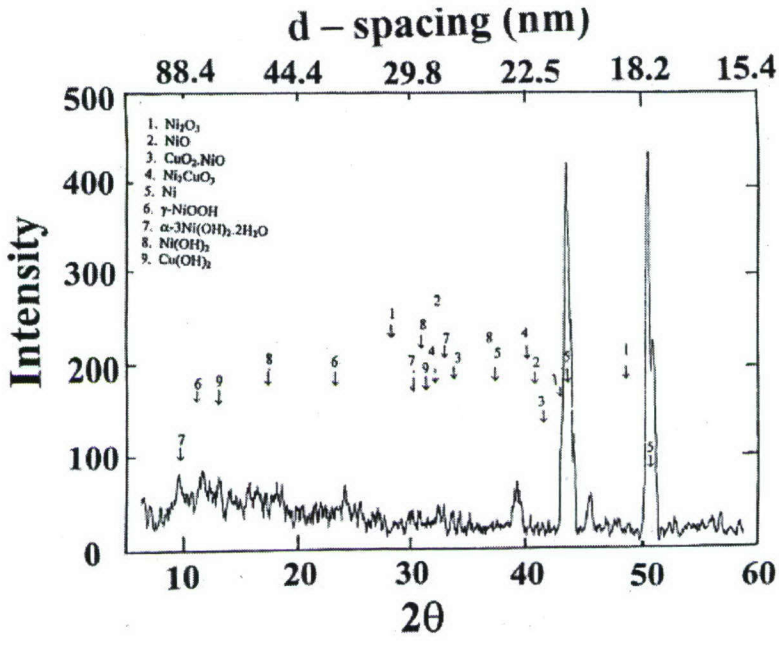

Figure 58. In-situ x-ray diffraction pattern obtained for 12.5 μm-thick (0.0005 in.) 70 - 30 Cu - Ni foil mounted on the electrochemical test cell, after exposure for 4 hours in seawater at - 100 mV versus a Ni/NiO electrode.

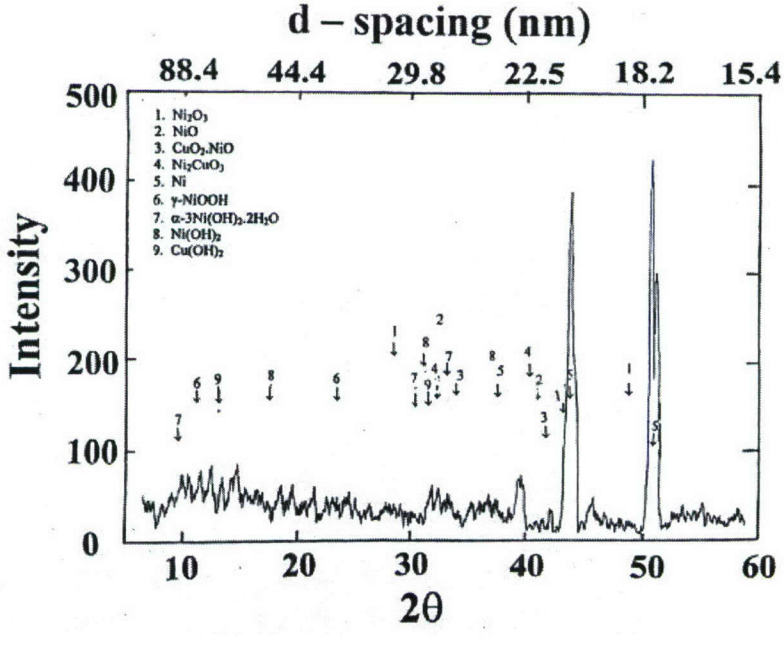

Figure 59. In-situ x-ray diffraction pattern obtained for 12.5 μm-thick (0.0005 in.) 70 - 30 Cu - Ni foil mounted on the electrochemical test cell, after exposure for 6 hours in seawater at -100 mV versus a Ni/NiO electrode.

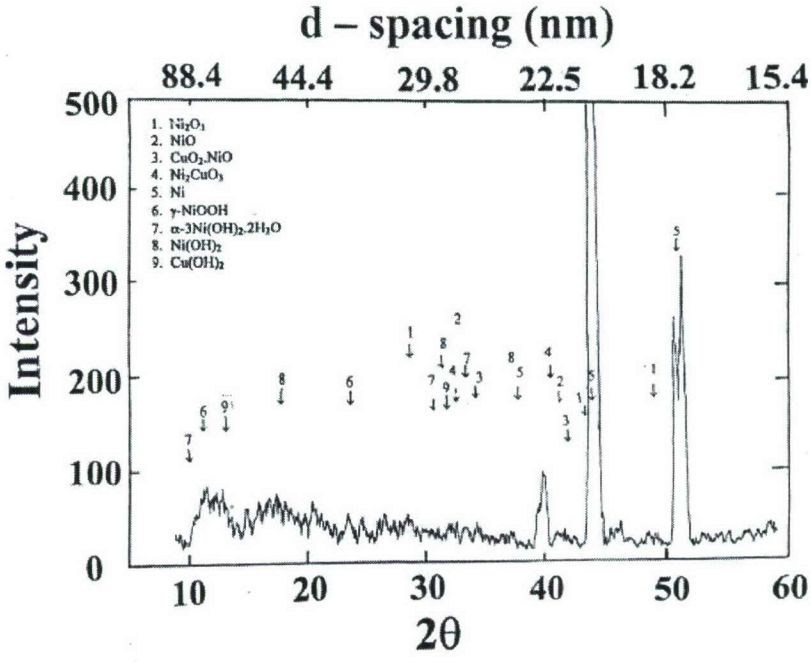

Figure 60. In-situ x-ray diffraction pattern obtained for 12.5 μm-thick (0.0005 in.) 70 - 30 Cu - Ni foil mounted on the electrochemical test cell, after exposure for 8 hours in seawater at -100 mV versus a Ni/NiO electrode.

XPS Results for Potential of - 500 mV

Figures 61, 62, and 63 show typical XPS spectra for copper, nickel, and oxygen, respectively, obtained from test foil subjected to - 500 mV in seawater solution. The results in Figures 61 and 62 suggest that $Cu(OH)_2$, CuO, and Ni_2O_3 are present in the outer passive layer. The detected structure of oxygen at 532 eV in Figure 63 corresponds to the oxygen associated with $Ni(OH)_2$.

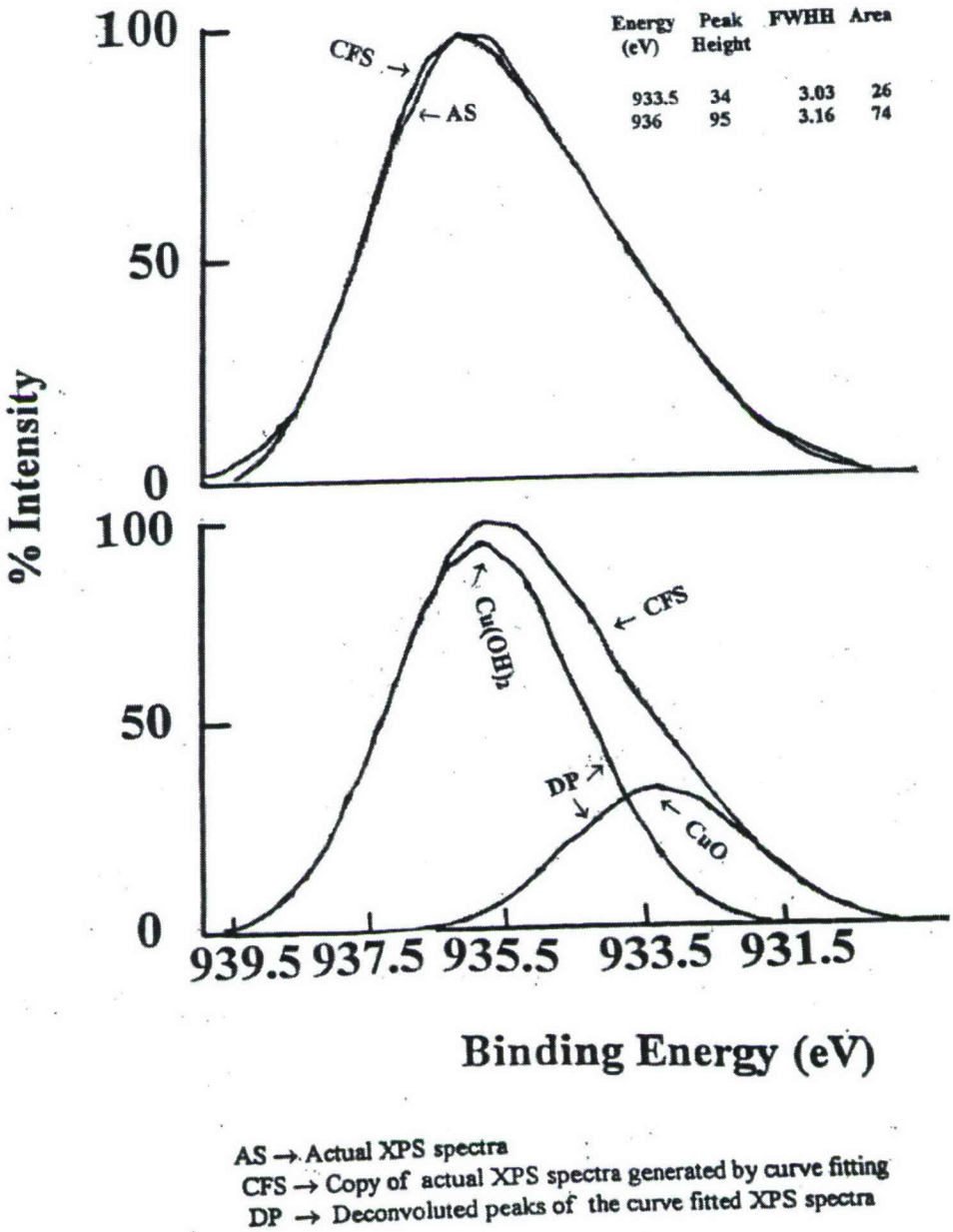

Figure 61. Copper peaks obtained from XPS analysis of 12.5 μm-thick (0.0005 in.) 70 - 30 Cu - Ni foil surface exposed to the seawater at -500 mV for 24 hours.

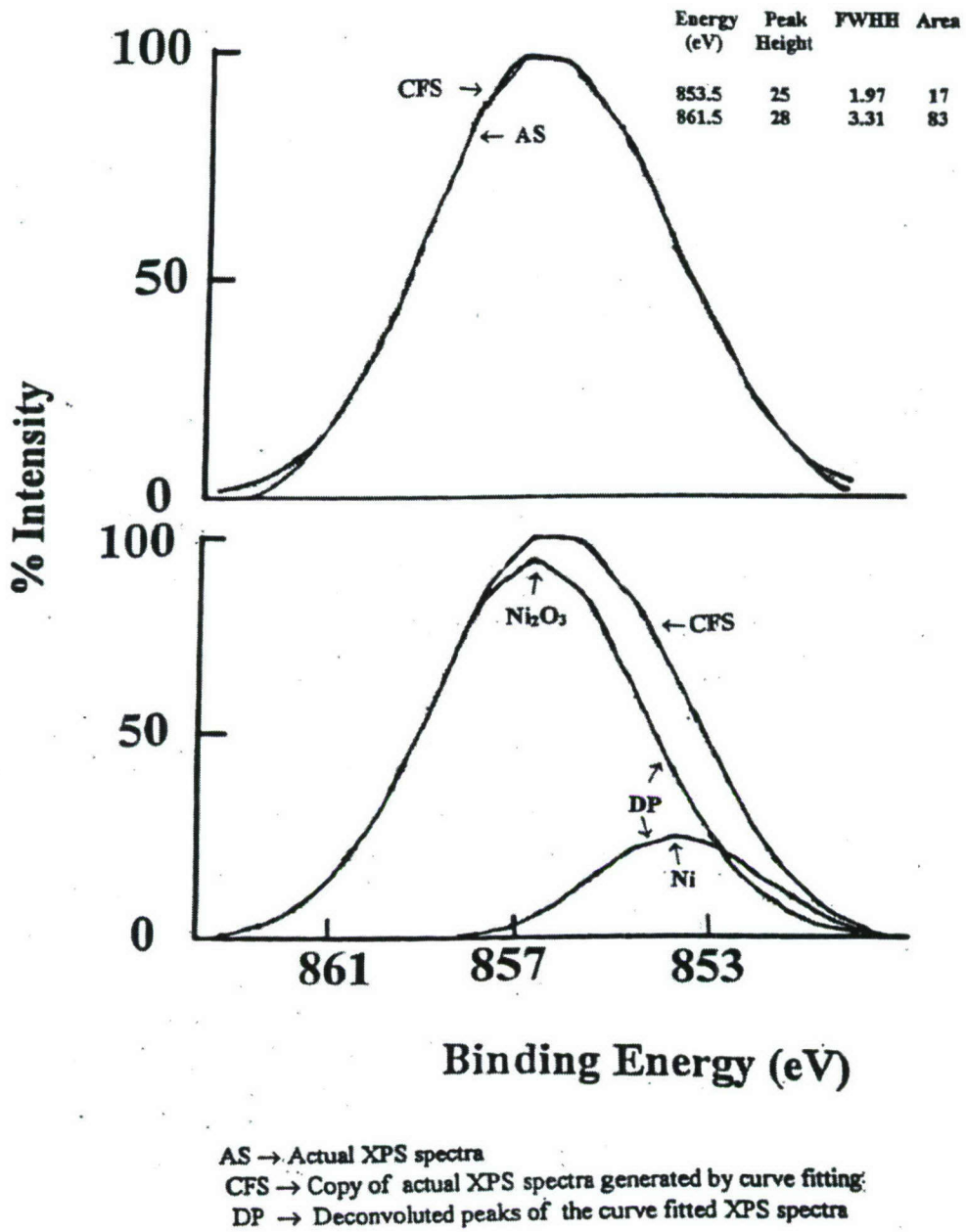

Figure 62. Nickel peaks obtained from XPS analysis of 12.5 μm-thick (0.0005 in.) 70 - 30 Cu -Ni foil surface exposed to the seawater at -500 mV for 24 hours.

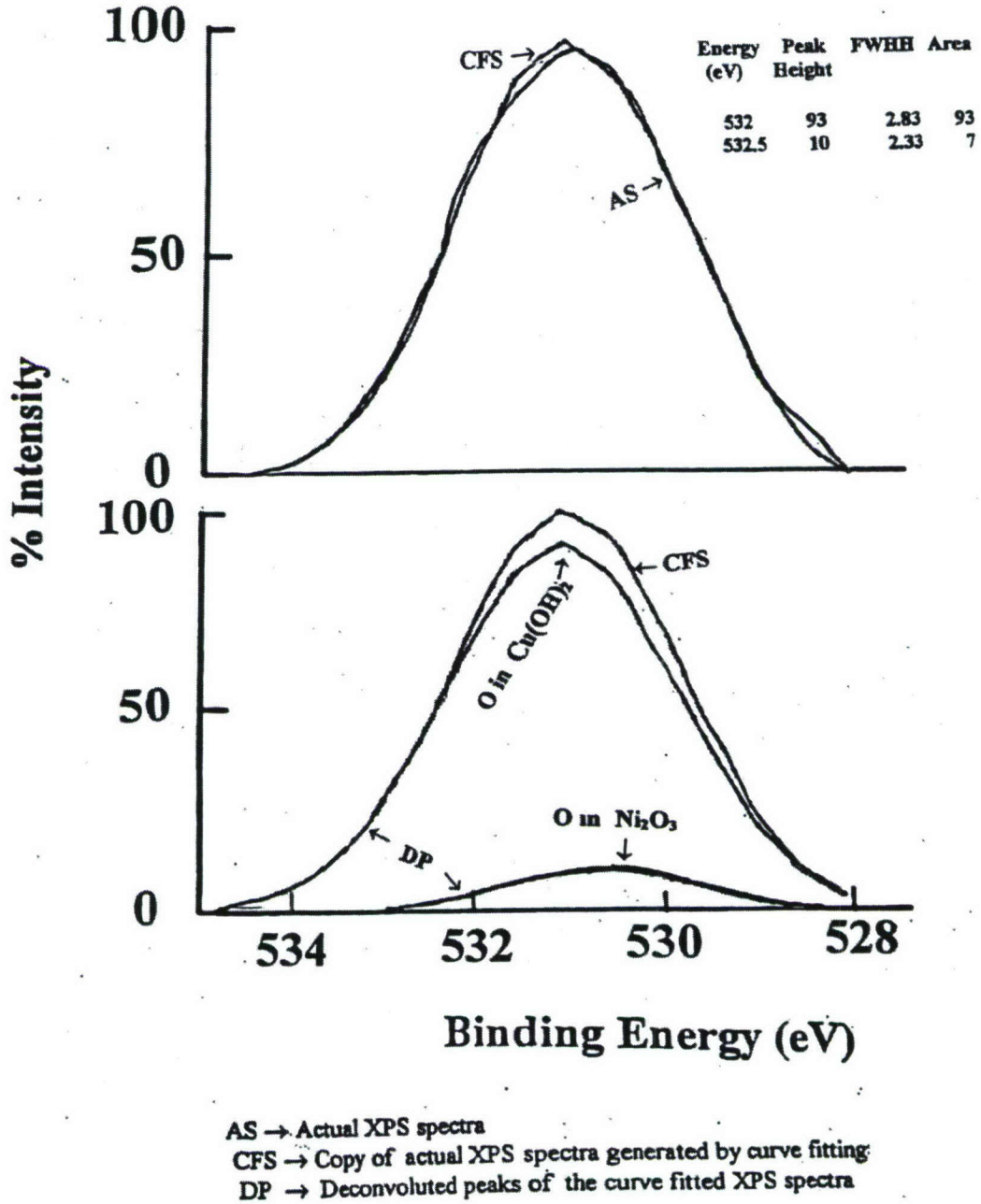

Figure 63. Oxygen peaks obtained from XPS analysis of 12.5 μm-thick (0.0005 in.) 70 - 30 Cu - Ni foil surface exposed to the seawater at - 500 mV for 24 hours.

XRD Results for Potentials of +500 mV and +100 mV

The x-ray diffraction results for 70-30 Cu-Ni foils subjected to + 500 mV are shown in Figures 64 thru 68. The figures correspond to the measurements made at time intervals of 1, 2, 4, 8, and 24 hours, respectively. Similarly, Figures 69 thru 71 show the x-ray diffraction patterns obtained from 70-30 Cu-Ni samples in seawater at +100 mV. The corresponding exposure times were 2, 4, and 6 hours, respectively. The x-ray diffraction results indicate that the interface of 70-30 Cu-Ni/seawater consists of NiO, Ni_2O_3, $Cu_2O{\cdot}NiO$, Ni_2CuO_3, NiOOH, $Ni(OH)_2$, α-$Ni(OH)_2{\cdot}2\ H_2O$, $Cu(OH)_2$, and CuO. These results suggest that the nickel and copper in 70-30 Cu-Ni foil are oxidized and both Ni^{+3} and Ni^{+2} states of nickel and Cu^{+1} and Cu^{+2} states of copper are present at the interface.

Therefore, one can postulate that the electrochemical anodic reaction for 70-30 Cu-Ni in seawater at +500 mV and +100 mV to follow the typical expected steps:

For nickel (and nickel oxide):

$$Ni \Rightarrow Ni(OH)_2 \Rightarrow Ni(OH)_2{\cdot}0.75\ H_2O \Rightarrow 3Ni(OH)_2{\cdot}2\ H_2O$$
$$\Rightarrow NiOOH \Rightarrow Ni_2O_3 \Rightarrow NiO$$
$$Ni \Rightarrow Ni(OH)_2 \Rightarrow NiOOH \Rightarrow Ni_2O_3 \Rightarrow NiO$$

and for copper (and copper oxide):

$$Cu \Rightarrow Cu(OH)_2 \Rightarrow CuO$$

$$Cu \Rightarrow Cu_2O \Rightarrow CuO$$

$$Cu_2O + NiO \Rightarrow Cu_2O{\cdot}NiO$$

$$CuO + 2NiO \Rightarrow Ni_2CuO_3$$

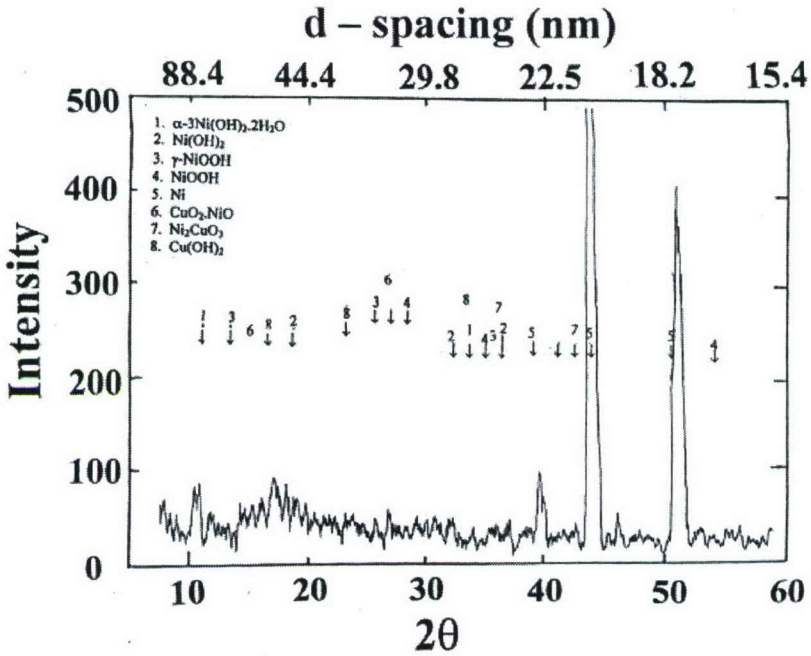

Figure 64. In-situ x-ray diffraction pattern obtained for 12.5 μm-thick (0.0005 in.) 70 - 30 Cu - Ni foil mounted on the electrochemical test cell, after exposure for 1 hour in seawater at + 500 mV versus a Ni/NiO electrode.

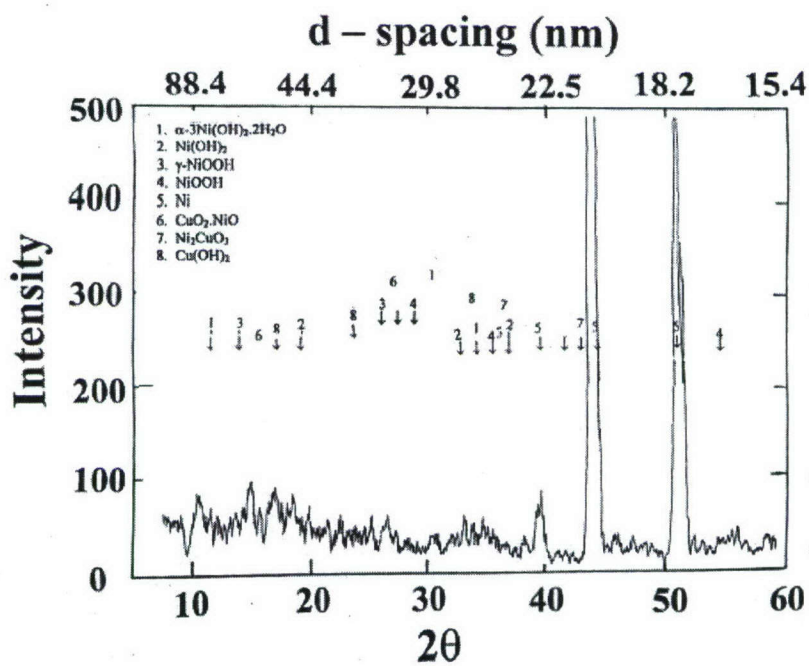

Figure 65. In-situ x-ray diffraction pattern obtained for 12.5 μm-thick (0.0005 in.) 70-30 Cu-Ni foil mounted on the electrochemical test cell, after exposure for 2 hours in seawater at + 500 mV versus a Ni/NiO electrode.

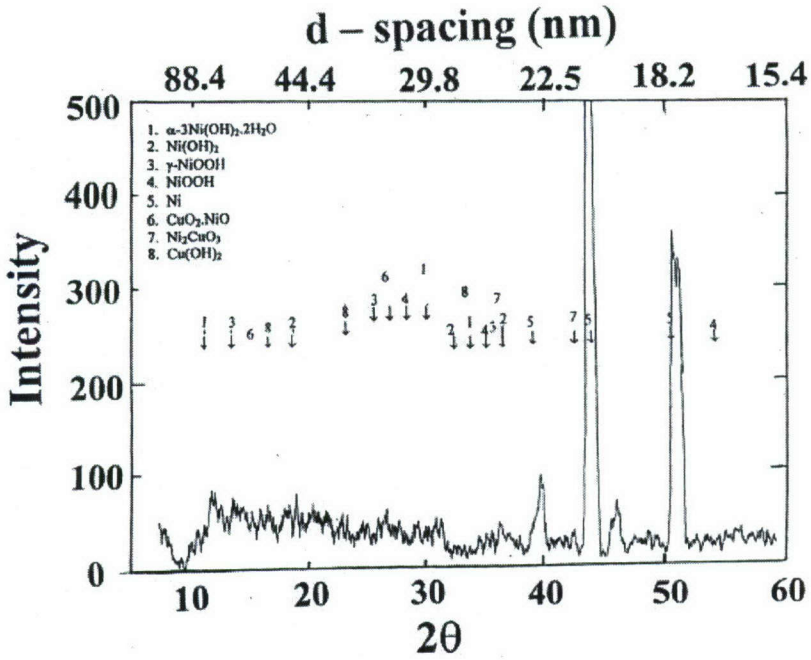

Figure 66. In-situ x-ray diffraction pattern obtained for 12.5 μm-thick (0.0005 in.) 70 - 30 Cu-Ni foil mounted on the electrochemical test cell, after exposure for 4 hours in seawater at + 500 mV versus a Ni/NiO electrode.

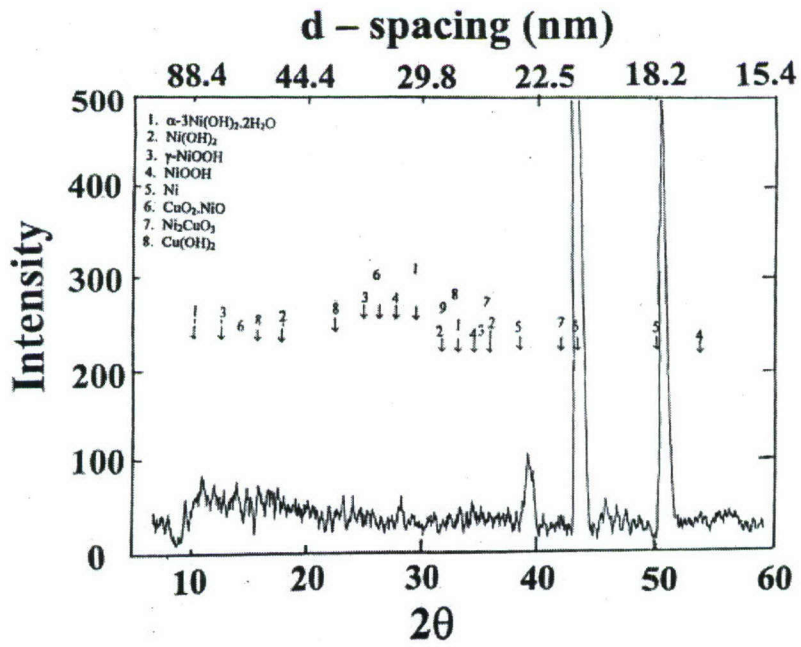

Figure 67. In-situ x-ray diffraction pattern obtained for 12.5 μm-thick (0.0005 in.) 70 - 30 Cu-Ni foil mounted on the electrochemical test cell, after exposure for 8 hours in seawater at + 500 mV versus a Ni/NiO electrode.

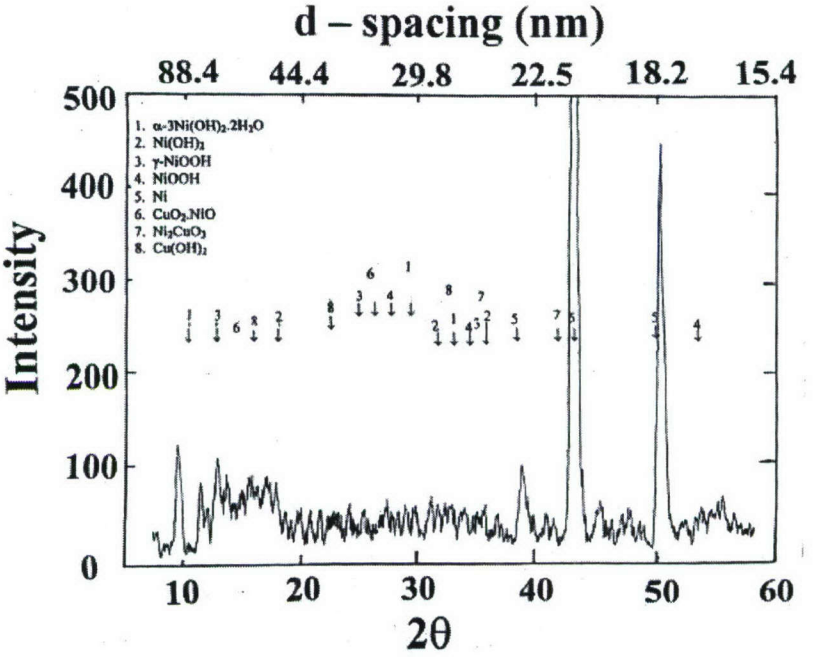

Figure 68. In-situ x-ray diffraction pattern obtained for 12.5 μm-thick (0.0005 in.) 70 - 30 Cu-Ni foil mounted on the electrochemical test cell, after exposure for 24 hours in seawater at + 500 mV versus a Ni/NiO electrode.

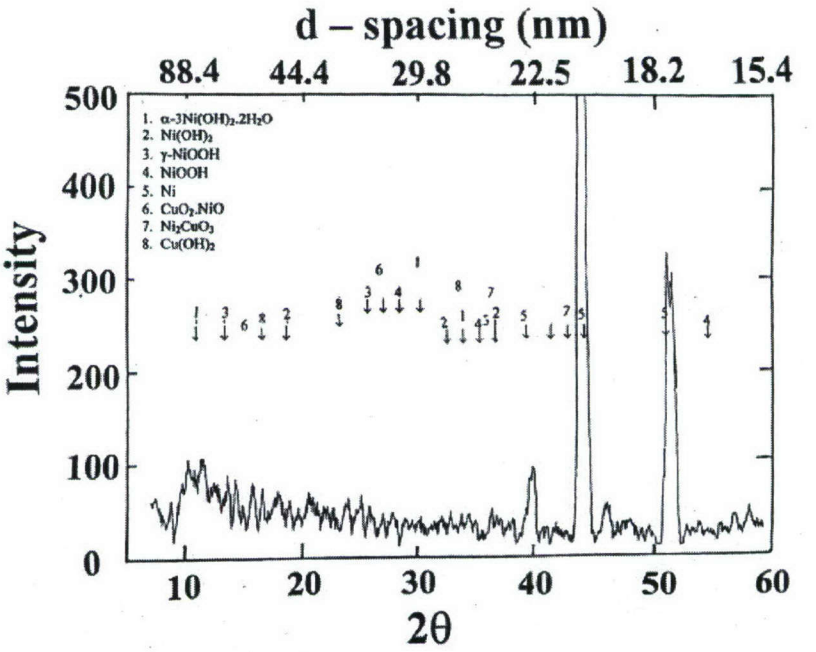

Figure 69. In-situ x-ray diffraction pattern obtained for 12.5 μm-thick (0.0005 in.) 70 - 30 Cu-Ni foil mounted on the electrochemical test cell, after exposure for 2 hours in seawater at + 100 mV versus a Ni/NiO electrode.

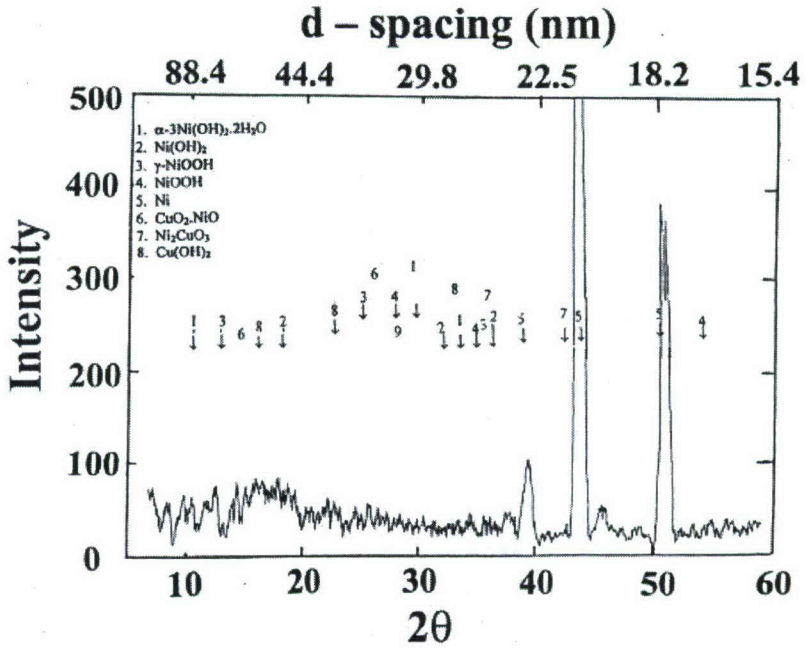

Figure 70. In-situ x-ray diffraction pattern obtained for 12.5 μm-thick (0.0005 in.) 70 - 30 Cu-Ni foil mounted on the electrochemical test cell, after exposure for 4 hours in seawater at +100 mV versus a Ni/NiO electrode.

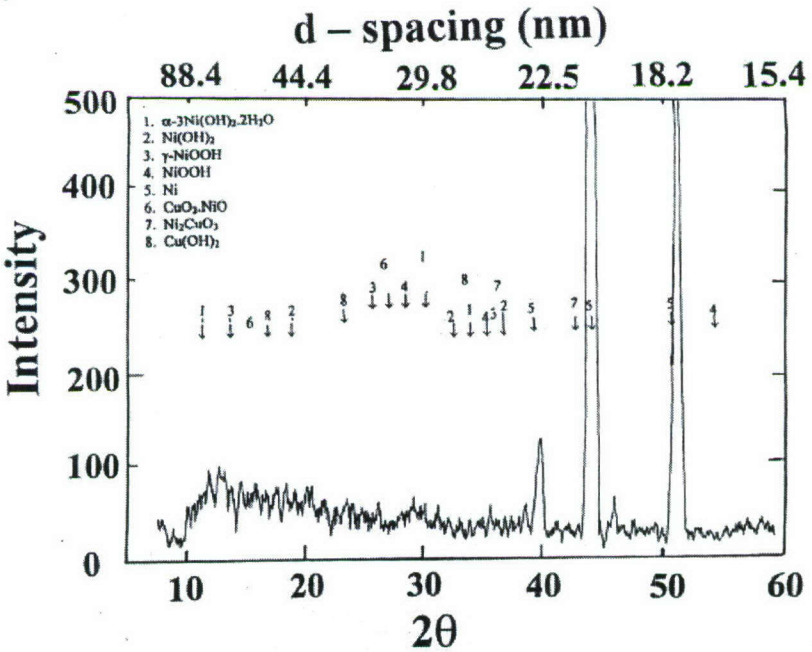

Figure 71. In-situ x-ray diffraction pattern obtained for 12.5 μm-thick (0.0005 in.) 70 - 30 Cu - Ni foil mounted on the electrochemical test cell, after exposure for 6 hours in seawater at +100 mV versus a Ni/NiO electrode.

XPS Results for Potential of +500 mV

Figures 72 thru 74 show XPS spectra for copper, nickel, and oxygen respectively, obtained from test foils after corrosion testing at + 500 mV in seawater solution for 24 hours. The results suggest that the 70-30 Cu-Ni foil involved in electrochemical reaction at + 500 mV in seawater for 24 hours is oxidized. The copper layers close to the surface are chemically transformed to $Cu(OH)_2$ and CuO. Similarly, the nickel layers close to the surface are chemically transformed into Ni_2O_3.

Discussion

Nickel -Seawater System

Based on classical electrochemical reaction mechanisms, it can be suggested that when a negative potential (-800 mV) is applied to nickel, the electrochemical cathodic reaction will be stimulated. The metal nickel will be reduced to form $Ni(OH)_2$ and other hydroxides with Ni^{+2} state. Furthermore, at this negative potential, the conversion of Ni(+2) to a Ni(+3) state and/or the formation of metal oxides (NiOOH, Ni_2O_3, NiO) are not anticipated.

Similarly, when a positive potential is applied (+ 450 mV) to nickel, the electrochemical anodic reaction should proceed. The metal nickel and its hydroxides (viz. $Ni(OH)_2$) will be oxidized to form hydroxides and or oxides (NiOOH, Ni_2O_3, NiO).

A careful examination of the present results indicate that the interface structure is very complex. However, by analyzing the data, one can suggest that the interface contains species that can be detected exclusively by x-ray diffraction, some can be detected by XRD and XPS and some components can be detected exclusively by the XPS. Since XPS detects only the components that are very close to the surface or outer layer, XPS analysis details the surface structure. If XRD cannot detect a species, it means that the concentration of that component is very small and below the detection capability of the XRD. A component that is detected only by XRD and not XPS means that the associated composition represents the inner passive layer.

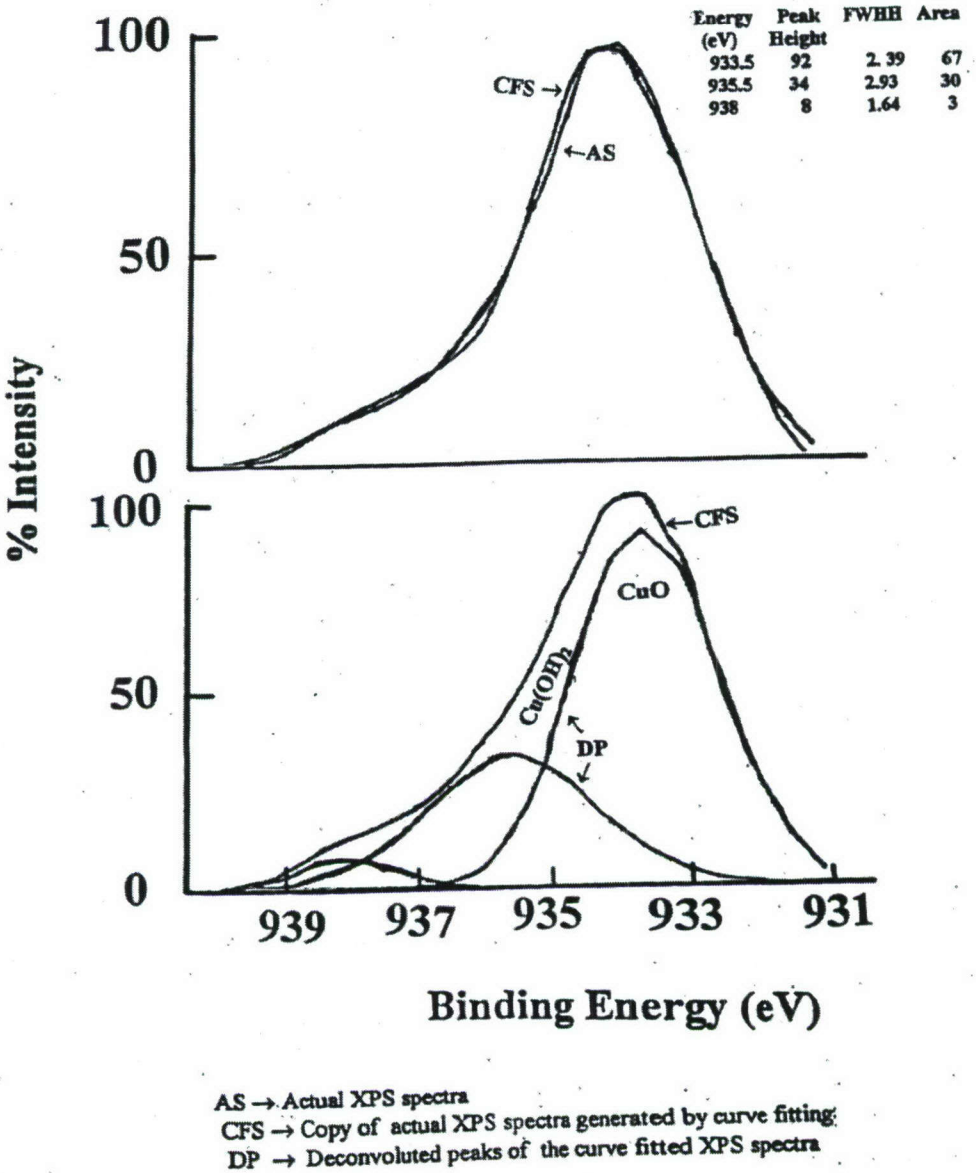

Figure 72. Copper peaks obtained from XPS analysis of 12.5 μm-thick (0.0005 in.) 70 - 30 Cu-Ni foil surface exposed to the seawater at + 500 mV for 24 hours.

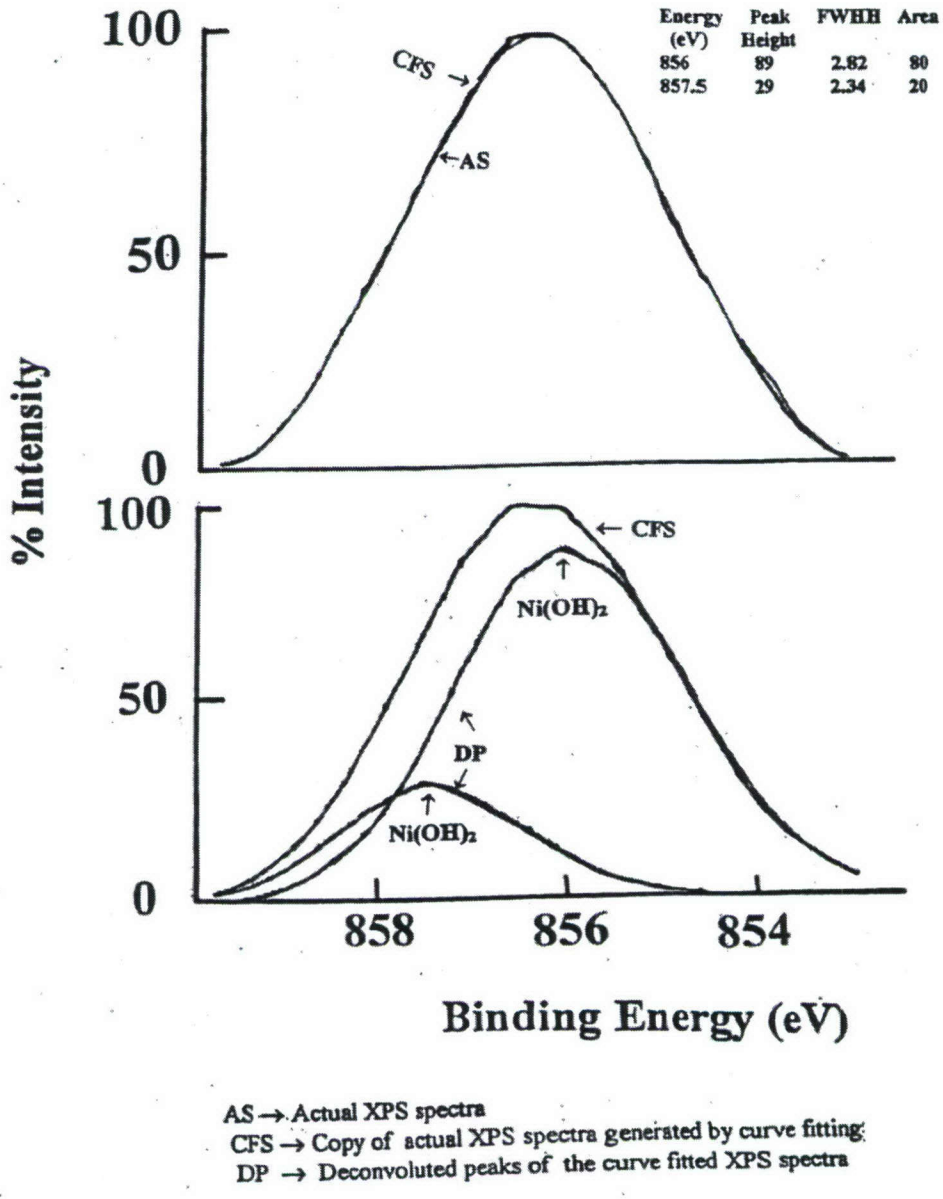

Figure 73. Nickel peaks obtained from XPS analysis of 12.5 μm-thick (0.0005 in.) 70 - 30 Cu-Ni foil surface exposed to the seawater at +500 mV for 24 hours.

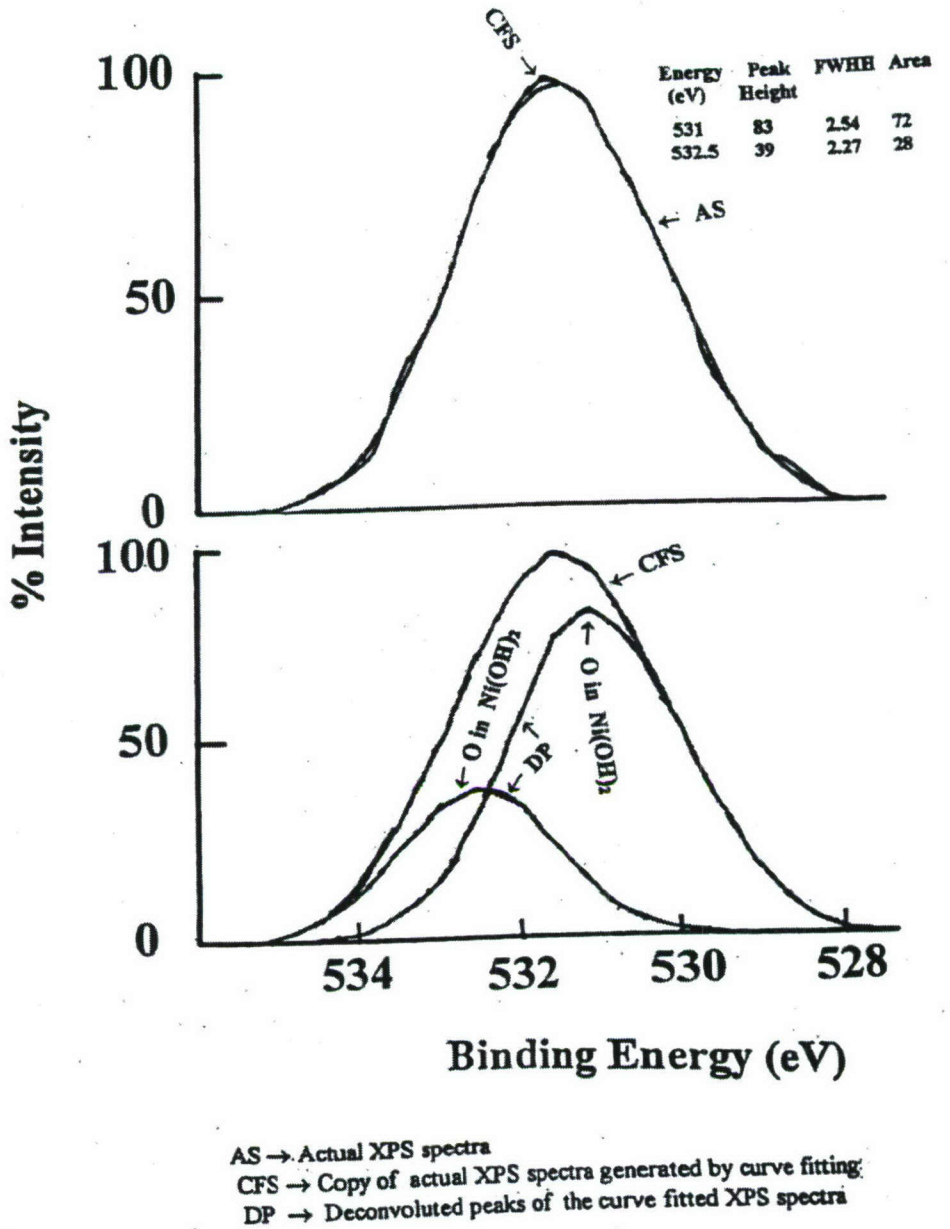

Figure 74. Oxygen peaks obtained from XPS analysis of 12.5 μm-thick (0.0005 in.) 70-30 Cu-Ni foil surface exposed to the seawater at +500 mV for 24 hours

Typical interface structure composition detected by the XRD, XRD/XPS, and XPS analysis for nickel/seawater system is given in Table 4. From the above anlysis it can be suggested that at -800 mV, the Ni/seawater interface constitutes NiOOH and $Ni(OH)_2$. The outer passive layer consists of $Ni(OH)_2$. The inner passive layer consists of primarily NiOOH. At +450 mV, the oxide layer consists of Ni_2O_3, NiO and $Ni(OH)_2$. The outer passive layer consists of NiO and $Ni(OH)_2$ and the inner passive layer consists of Ni_2O_3.

Table 4. Surface Films Detected by XRD and XPS
After Exposure to Seawater Solution.

Alloy	Potential Vs. (Ni/NiO) mV	Phases Detected By		
		XRD Only	Both XRD and XPS	XPS Only
Ni	-800	NiOOH	$Ni(OH)_2$	-
Ni	+ 450	NiO	NiO, $Ni(OH)_2$	Ni_2O_3
90-10 Cu-Ni	-500	NiOOH, CuO, $Cu_2O{\cdot}NiO$	$Ni(OH)_2$,$Cu(OH)_2$	-
90-10 Cu-Ni	-100	NiOOH, $Cu_2O{\cdot}NiO$	$Ni(OH)_2$,$Cu(OH)_2$	-
90-10 Cu-Ni	+100	$Cu_2O{\cdot}NiO$, Ni_2CuO_3	NiO, Ni_2O_3	-
90- 10 Cu-Ni	+500	$Cu_2O{\cdot}NiO$, NiOOH, Ni_2CuO_3	NiO, Ni_2O_3	$Ni(OH)_2$, $Cu(OH)_2$, CuO
70- 30 Cu-Ni	- 500	NiOOH, $Cu_2O{\cdot}NiO$	$Ni(OH)_2$, $Cu(OH)_2$	CuO
70-30 Cu-Ni	-100	NiOOH, $Cu_2O{\cdot}NiO$	$Ni(OH)_2$, $Cu(OH)_2$	-
70-30 Cu-Ni	+100	$Cu_2O{\cdot}NiO$, Ni_2CuO_3	NiO, Ni_2O_3	-
70-30 Cu-Ni	+ 500	$Cu_2O{\cdot}NiO$, Ni_2CuO_3	NiO, Ni_2O_3	$Cu(OH)_2$, CuO

90-10 and 70-30 Cu-Ni -Seawater System

Based on classical electrochemical reaction mechanisms, it can be suggested that when a negative potential (-500 mV or -100 mV) is applied to nickel and copper, the electrochemical cathodic reaction will be stimulated. The metals nickel and copper will be reduced to form $Ni(OH)_2$ and $Cu(OH)_2$ and other hydroxides with Ni(+2) and Cu(+2) states. Furthermore, at these negative potentials, the conversion of Ni(+2) to a Ni(+3) state and/or the formation of metal oxides (NiOOH, Ni_2O_3, CuO·NiO) are not anticipated.

Similarly, when a positive potential is applied (+500 mV or +100 mV) to nickel and copper, the electrochemical anodic reaction should proceed. The metals nickel and copper and their hydroxides (viz. $Ni(OH)_2$ and $Cu(OH)_2$) will be oxidized to form hydroxides and or oxides (NiOOH, Ni_2O_3, NiO, CuO) with Ni(+3) and Cu(+2) states.

It can be argued that the anodic reaction(s) (oxidation) may still occur when the metal is cathodically polarized; but it will be occurring at a much reduced rate compared with cathodic reaction. Similarly, when the metal is anodically polarized, a cathodic reaction may occur at a much reduced reaction rate.

The XRD results suggest that when +500 and +100 mV were applied in seawater, the 90-10 Cu-Ni alloy structure shows the presence of some $Ni(OH)_2$ and $Cu(OH)_2$ and significant Ni_2O_3, NiO, and CuO (with Ni(+3) and Cu(+2) states). The XPS results indicate that at the 90-10 Cu-Ni/seawater interface the outer alloy layers that are in contact with the seawater are transformed into $Ni(OH)_2$, Ni_2O_3, NiO, $Cu(OH)_2$ and CuO (with Ni^{+3} and Cu^{+2} states). Therefore, it is possible that Ni_2O_3, NiO, and CuO (with Ni(+3) and Cu(+2) state) phases are present as the inner passive layer of the alloy.

Summary

From the present investigation, the following conclusions can be made.

Nickel-Seawater System

1. The experimental technique described here can successfully determine the structure of the passive layer at the metal-solution interface during an electrochemical process.

2. During the electrochemical reaction of the nickel/seawater system, at -800 mV, significant $Ni(OH)_2$ and NiOOH are formed at the interface. From XRD and XPS analysis of the structure of the interface, it is possible to suggest that $Ni(OH)_2$ is present at the outer passive layer and NiOOH is present at the inner passive layer.

3. At + 450 mV the interface (inner and outer passive layers) structure consists of NiO, Ni_2O_3, $Ni(OH)_2$, and NiOOH. The inner passive layer is composed of NiOOH and the outer passive layer is comprised of Ni_2O_3.

90-10 Cu-Ni Alloy - Seawater System

1. During the electrochemical reaction of the 90-10 Cu-Ni/seawater system, at -500 mV, significant $Ni(OH)_2$, NiOOH, $Cu(OH)_2$, $Cu_2O{\cdot}NiO$, and CuO are formed at the interface of the 90-10 Cu-Ni foil and the seawater solution.

2. From XRD and XPS analysis of the structure of the interface, it is possible to suggest that at -500 mV, both $Ni(OH)_2$, $Cu(OH)_2$ and CuO are present at the outer passive layer and NiOOH and $Cu_2O{\cdot}NiO$ are present at the inner passive layer.

3. At +500 mV, the interface (inner and outer passive layers) structure of the 90-10 Cu-Ni foil and the seawater solution consists of NiO, Ni_2O_3, Ni_2CuO_3, $Ni(OH)_2$, NiOOH, $Cu_2O{\cdot}NiO$, and CuO.

70–30 Cu-Ni-Seawater System

1. During the electrochemical reaction of the 70-30 Cu-Ni/seawater system, at -500 and -100 mV, significant $Ni(OH)_2$, NiOOH, $Cu(OH)_2$ and $CuO_2 \cdot NiO$ are formed at the interface.

2. From XRD and XPS analysis of the structure of the interface, it is possible to suggest that at -500 mV, both $Ni(OH)_2$ and $Cu(OH)_2$ are present at the outer passive layer and NiOOH and $CuO_2 \cdot NiO$ are present at the inner passive layer.

3. At +500 mV the interface (inner and outer passive layers) structure consists of NiO, Ni_2O_3, $Ni(OH)_2$, NiOOH, $Cu(OH)_2$ and $CuO_2 \cdot NiO$. The inner passive layer comprises $Ni(OH)_2$, $Cu_2O \cdot NiO$ and Ni_2CuO_3. The outer passive layer icomprises NiO, Ni_2O_3, CuO, and $Cu(OH)_2$.

References

1. Ross, P. N. and Wagner, F. T., "The Application of Surface Physics Techniques to the Study of Electrochemical Systems," *Advances in Electrochem*, 13, 69 (1985).

2. Flischmann, M. and Hill, I. R., "Surface Enhanced Raman Spectroscopy," eds. Chang, R. K. and Furtak, T. 5., *Plenum Pub.*, New York, 275 (1982).

3. Bewick, A. and Pons, B. S., "Advances in Infra-red and Raman Spectroscopy," edt. Clark, R. J. H. and Hester, RE., Pub., Wiley Heydon, New York 12, Chap. 1(1985).

4. Bomchil, O. and Rekel, C., " Neutron Diffraction Study of the Electrochemical Passivation of Nickel Powder," *Electro Anal. Chem.,* 101, 133 (1979).

5. Lang, G. G., Kruger, J., Black, D. R. and Kuriyama, M., "Structure of Passive Films on Iron Using a New Surface–EXAFS Technique," *J. Electrochem. Soc.*, 130, 240 (1983).

6. Bosio, L., Cones, R. and Froment, M., "Reflection EXAFS Studies of Protective Oxide Formation on Metal Surfaces," Proc. 3rd Int. EXAFS Conf., Stanford, CA (1984).

7. Marra, W. C., Elsenberger, P. and Cho, A. Y. J., " x-ray Total External Reflection Bragg Diffraction: A Structural Study of Gallium Arsenide-Aluminum Interface," *Appl. Phys*, 50, 6927 (1979).

8. Cowan, P. L., Goloychenko, J. A. and Robbins, M.F., " X-ray Standing Waves at the Crystal Surface," Phys. Rev. Lett., 44, 1680 (1980).

9. Golovchenko, J. A., Patel, S. W., Kaplan, D. R., Cowan, P. L. and Bedzyk, P., "Solution to the Surface Registration Problem Using x-Ray Standing Waves," *Phys. Rev. Lett.*, 49, 560 (1982).

10. Pandya, K. I., O'Grady, W. E. Corrigan, D. A., Mc Breen, J. and Hoffman, R. W., "In-situ x–Ray Adsorption Spectroscopic Studies of Nickel Oxide Electrodes," *J. Phys. Chem,* 94, 21(1990).

11. Rommel, H. E. G., *Time Dependent Energy Efficiency Losses at Nickel Cathodes in Alkaline Water Electrolysis Systems*, MS Thesis, Johns Hopkins University, Baltimore, MD 1982.

12. Moran, P. J. and Guanti, R. S., "Measurement of Electrolyte Conductivity in Highly Conducting Solutions," *161st Electrochem. Soc., Meeting*, Montreal, Canada, 1982.

13. A. Srinivasa Rao and J. N. Murray, *Characterization of Surface Film Growth During the Elecrochemical Process: Part I (Nickel-KOH System),* NSWCCD-61-TR-98/17, Jun 1998.

14. A. Srinivasa Rao, *Characterization of Surface Film Growth During the Elecrochemical Process: Part II (90% Copper-10% Nickel -KOH System*), NSWCCD -61-TR-98/21, Sept. 1998.

15. A. Srinivasa Rao and J. N. Murray, *Characterization of Surface Film Growth During the Elecrochemical Process: Part III (70% Copper-30% Nickel -KOH System),* NSWCCD-61-TR-98/24 Oct 1998.

Distribution

DoD - CONUS	copies
CHIEF OF NAVAL RESEARCH ATTN 332 (AIRAN J. PEREZ) CORROSION PROGRAM MANAGER 875 N. RANDOLPH STREET ARLINGTON VA 22203-1995	1
COMMANDER NAVAL SEA SYSTEM COMMAND ATTN SEA 05M (KAZNOFF) 1333 ISAAC HULL AVE SE STOP 5130 WASHINGTON NAVY YARD DC 20376-5130	1
COMMANDER NAVAL SEA SYSTEMS COMMAND ATTN SEA 05M1 1333 ISAAC HULL AVE SE STOP 5132 WASHINGTON NAVY YARD DC 20376-5132	1
COMMANDER NAVAL SEA SYSTEMS COMMAND ATTN SEA 05M2 1333 ISAAC HULL AVE SE STOP 5132 WASHINGTON NAVY YARD DC 20376-5132	1
DEFENSE TECH INFORMATION CENTER 8725 JOHN KINGMAN ROAD SUITE 0944 FORT BELVOIR VA 22060-6218	1

INTERNAL		copies
CODE 0115		1
CODE 0112		1
CODE 60		1
CODE 60	(SUDDUTH)	1
CODE 61		1
CODE 612	(RAO)	4
CODE 611		1
CODE 612		1
CODE 612	(CZYRYCA)	1
CODE 612	(FIELDER)	1
CODE 612	(GAIES)	1
CODE 612	(HAYDEN)	1
CODE 612	(MOUSSOUROS)	1
CODE 612	(PURTSCHER)	1
CODE 612	(ROE)	1
CODE 612	(STILES)	1
CODE 612	(SUTTON)	1
CODE 612	(SYLVESTER)	1
CODE 612	(WONG)	1
CODE 612	(ZHANG)	1
CODE 612	(BRANDEMARTE)	1
CODE 613		1
CODE 614		1
CODE 615		1
CODE 616		1
CODE 617		1
CODE 62		1
CODE 63		1
CODE 64		1
CODE 65		1
CODE 66		1
CODE 3442	(TIC – PDF ONLY)	1

This page intentionally left blank

Carderock Division